National Library of Canada
Acquisitions and Bibliographic Services Branch
395 Wellington Street
Ottawa, Ontario
K1A 0N4

Bibliothèque nationale du Canada
Direction des acquisitions et des services bibliographiques
395, rue Wellington
Ottawa (Ontario)
K1A 0N4

Your file Votre référence

Our file Notre référence

NOTICE

The quality of this microform is heavily dependent upon the quality of the original thesis submitted for microfilming. Every effort has been made to ensure the highest quality of reproduction possible.

If pages are missing, contact the university which granted the degree.

Some pages may have indistinct print especially if the original pages were typed with a poor typewriter ribbon or if the university sent us an inferior photocopy.

AVIS

La qualité de cette microforme dépend grandement de la qualité de la thèse soumise au microfilmage. Nous avons tout fait pour assurer une qualité supérieure de reproduction.

S'il manque des pages, veuillez communiquer avec l'université qui a conféré le grade.

La qualité d'impression de certaines pages peut laisser à désirer, surtout si les pages originales ont été dactylographiées à l'aide d'un ruban usé ou si l'université nous a fait parvenir une photocopie de qualité inférieure.

Canada

Separation and Purification of Gases with Molecular Sieves

Robert Triebe

A thesis submitted to the School of Graduate Studies and Research

in partial fulfillment of the requirements for the degree of

M. A. Sc. in Chemical Engineering

Department of Chemical Engineering

University of Ottawa

ISBN 0-315-95995-9

UNIVERSITÉ D'OTTAWA
UNIVERSITY OF OTTAWA

Abstract

Equilibrium adsorption constants were determined for CO, CO_2, NO, N_2, CH_4, C_2H_4, and C_2H_6 on various molecular sieves between 233 and 523 K. The molecular sieves tested for adsorption of these gases were 4A and 5A zeolite, 13X and a CaX zeolite, H- mordenite, a natural clinoptilolite and a carbon molecular sieve. The gas chromatographic method was used for all equilibrium measurements.

Upon choosing the promising CO / N_2 / clinoptilolite system for further studies, kinetic (diffusion) characteristics of each of these pure gases in the clinoptilolite pores was examined between 323 and 423 K using the gas chromatographic method.

Pure gas and binary gas adsorption isotherms for the CO / N_2 / clinoptilolite system were determined up to 1 atmosphere pressure at 303 K using the gas chromatographic method. Pure isotherms were fit with the Langmuir and Vacancy Solution Theory models. Pure gas modelling results were used to predict and compared to the experimentally determined binary gas isotherms.

Separation of polar compounds from non - polar compounds was facilitated by inclusion of divalent cations in the zeolite micropores. Clinoptilolite showed great promise for various separations. The chromatographic method for measuring adsorption isotherms is limited in the measurement of rectangular isotherms, yielding errors dependant upon the accuracy of the gas blending system. The Wilson form of the VST accurately predicts the binary adsorption data.

Acknowledgement

The author would like to express his sincere appreciation of the guidance and support offered by Dr. F. H. Tezel. Thank you for providing the basis for a very interesting and rewarding two years at the University of Ottawa. The input you provided was invaluable and the space and freedom you allowed me in my studies was priceless in helping me develop excellent research skills.

The work would not have been completed without the aid of Mr. J. Gasperetti, Mr. L Tremblay, and Mr. A. Bonaldo. I thank you all for your time, patience and advice. I would further like to thank my fellow graduate students. It is they who criticized and discussed my work with me to eventually mold this final product.

Table of Contents

List of Tables

List of Figures

Nomenclature

A_i	regression coefficients of equation 25
a_i	standard state molar area of component i
B_i	regression coefficients of polynomial equation 22
b	initial slope of adsorption isotherm (Langmuir & VST models)
C_i	polynomial fit coefficents for equation 23
C	sorbate concentration in bulk phase
c	sorbate concentration in macropores
D_0	pre exponential factor in equation 48
D_c	micropore diffusivity
D_K	Knudsen diffusivity
D_L	axial dispersion coefficient
D_M	molecular diffusivity
D_p	macropore diffusivity
E_a	diffusional activation energy
ΔG_i^0	standard state free energy of adsorption of pure component i
$-\Delta \bar{H}_0$	limiting heat of adsorption
K_0	pre exponential factor in vant Hoff equation
K_c	dimensionless equilibrium constant based on sorbate concentration in zeolite crystal
K_p	dimensionless equilibrium constant based on sorbate concentration in zeolite pellet
K_p'	apparent equilibrium constant based on sorbate concentration in zeolite pellet
k	external film mass transfer coefficient
L	sorbent bed length

M	molecular mass
M_z	mass of zeolite
n_m	number of moles adsorbed
n^{inf}	maximum total number of moles in surface phase excluding vacancy
n_m^s	total number of moles of mixture in surface phase
$n_m^{s,inf}$	maximum total number of moles of mixture in surface phase
P	total pressure
P_i^0	spreading pressure, or partial pressure of adsorbed phase
p_i	partial pressure of component i
Q	local sorbate concentration in pellet
$\overline{Q}$	average sorbate concentration in pellet
q	local sorbate concentration in zeolite crystal
$\overline{q}$	average sorbate concentration in zeolite crystal
q_i	adsorbed phase concentration of component i
q_m	ultimate monolayer capacity (Langmuir model)
R	radial coordinate for pellet
R_g	ideal gas constant
R_M	macropore radius
R_p	radius of zeolite pellet / particle
Re	Reynolds number
r	radial coordinate for zeolite crystal
r_b	radius of zeolite bed
r_c	radius of zeolite crystal
Sc	Schmidt number
Sh	Sherwood number
T	temperature
t	time

$-\Delta U_o$	internal energy change of adsorption
V_b	volume of zeolite bed
v	interstitial velocity
x	number of H_2O molecules in zeolite unit cell
x_i	mole fraction of i in vacancy free adsorbed phase (VST model)
x_i^*	mole fraction of i in adsorbed phase vacancy solution (VST model)
y_i	mole fraction of i in vacancy free vapour phase (VST model)
Y_i	mole fraction of component i in total gas phase

Greek Letters

α_{iv}	species interaction parameter (Flory Huggins VST)
β	regression coefficient (equation 25)
γ_i^*	activity coefficient of component i in adsorbed phase
$\delta(t)$	pulse function
ε	void fraction of bed (porosity)
θ	void fraction of pellet
θ_i	fractional coverage of component i
ρ_b	bed density
ρ_p	pellet density
ϕ_i	fugacity coefficient of component i
Λ_{ij}	species interaction parameter (Wilson VST)
υ	interstitial velocity
σ^2	variance (second moment of response peak)

μ	mean (first moment of response peak)
τ	tortuosity factor
ω	volume fraction of zeolite crystal to total solid in pellet

1. Introduction

The use of molecular sieve zeolites for gas separation and purification in industry continues to increase, largely due to the tremendous versatility of these adsorbents. Over 85 different synthetic and natural zeolite structures have been identified [Meier & Olson (1992)], each with characteristic pore diameters and structures. Furthermore each alumino - silicate in this group (numbering over 60) offers a variety of ionic forms, each with a different pore size and unique adsorptive properties. Given the flexibility offered by zeolitic ion exchange and by the number of natural and synthetic zeolitic structures available, many successful combinations may be found for virtually any gas separation or purification application. Therefore further understanding of zeolitic adsorption properties is crucial if the best adsorbent is to be efficiently found for the many gas separations and purifications necessary in industry today. Some of these applications include air drying, air separation and purification, flue gas purification and the separation, drying and sweetening of natural gases [Breck (1973)].

Of the many separations possible with molecular sieve zeolites, two types were chosen for study. Many major environmental problems such as acid rain, photochemical smog, and the thinning of the ozone layer have been attributed to various common industrial emissions. A large fraction of these contaminants are products of the massive amounts of combustion processes involved in power production. For this reason it was decided to examine a number of molecular sieve zeolites for the separation of CO, CO_2, and NO from N_2. The majority of this combustion for power production is that of non renewable resources such as coal and oil. As these resources are depleted, natural gas is becoming a larger and larger fraction of the world's remaining non renewable energy sources. The harnessing of the energy available from natural gas in underground deposits has therefore become an important issue. Methane can be used to produce methanol which is being widely considered as an alternative fuel. In the processing of methane obtained from natural deposits, common separations include the removal of alkenes, CO, and CO_2 from the natural gas streams. Therefore zeolites were also screened for the potential separation of C_2H_4 from

CH_4 and C_2H_6. Combining the data with that from the air purification study provided insight into other separations of interest such as CH_4 from N_2 and CO and CO_2 from CH_4.

1.1 Separation of CO, CO_2, and NO from N_2

As environmental regulations justifiably become more stringent, industry must consider economically viable means of reducing contaminant emissions to acceptable levels. Major common contaminants such as CO, CO_2 and NO can presently be removed from a variety of sources via temperature swing or pressure swing adsorption. Such adsorptive separation processes have become commonplace in air bulk separations and purification applications in favour of the more expensive cryogenic distillation and gas absorption systems. Large scale pressure swing adsorption is used in the steel industry in Italy to produce pure O_2 by successive adsorptive removal of H_2O, N_2 and CO_2 from air by use of a variety of adsorbents, yielding 150 tonnes / day of 93% pure O_2 at 15 atmospheres [Labrousse (1989)]. N_2 production by adsorptive separation of O_2, H_2O and CO_2 on a confidential adsorbent is also in large scale operation in France, where 6000 Nm^3/h of 95% N_2 (5% O_2) are produced in a Gaz de France plant [Thorogood et al. (1989)]. Lee and Stahl report that 5A zeolite can selectively adsorb N_2 from air so as to yield 95% O_2 in a properly designed PSA process [Lee & Stahl (1973)]. Kasuya and Tsuji detail a process for production of high purity CO gas (used as a raw material in some chemical production processes) from air rich in CO using a copper impregnated activated alumina adsorbent [Kasuya & Tsuji (1991)]. Applications of PSA in air purification are equally well established. A general review of the possibilities and limits of dry sorbents for industrial flue gas purification in Germany has been published [Michele (1987)], and many more specific studies have been conducted.

The air purifications of primary interest in the present study are the removal of CO_2, CO and NO_x from an N_2 stream at near ambient conditions. Some synthetic zeolites have already been tested for possible separation of these compounds. Giacobbe reports on production of high purity O_2 using 5A and 13X zeolites, successfully removing trace levels of CO_2 (from 50 ppm in feed to 25 ppb in product)

[Giacobbe (1989, 1991)]. CO_2 adsorption on modified A, X and Y zeolites was studied by Coughlan et al. [Coughlan et al. (1975)]. Haq and Ruthven studied adsorption of CO_2, CH_4, O_2, and N_2 on 4A and 5A zeolites [Haq & Ruthven (1986 a, b)], and Ruthven studied single and binary gas behaviour of CO, CH_4, O_2, and N_2 adsorption on 5A zeolite [Ruthven (1976)]. Adsorption of CO_2, NO, NO_2, and SO_2 on natural and synthetic mordenites and on 5A and 13X zeolites was studied by Ma and Mancel [Ma & Mancel (1972)], and NO adsorption on a large variety of metal impregnated and untreated activated carbons and zeolites was examined by Kaneko and Inouye [Kaneko & Inouye (1988)]. Separation of NO_x from nitric acid plant tail gas on 13X and Norton 200 zeolites was examined by Joithe [Joithe et al. (1972)]. Anderson has taken part in studies of CO, CO_2, O_2, and N_2 on 4A zeolite [Eagan & Anderson (1975), Harper et al. (1969)], and Danner, Wenzel, and Dorfman studied various CO - N_2 - O_2 systems on 5A and 10X zeolites [Danner & Wenzel (1969), Dorfman & Danner (1975)]. The vast amount of data available on these systems (CO, CO_2, NO and N_2 adsorption on common zeolites) demonstrates their significance in air purification applications. However, natural zeolites have not been examined in such great detail due to industrial disadvantages such as inconsistency of composition and cost of possible purifications and modifications. A study of adsorption of CO_2 on various natural (mordenite, ferrierite, clinoptilolite and chabazite) and synthetic zeolites showed chabazite to be a more promising adsorbent for CO_2 separation from N_2 than 4A and 5A zeolites [Inui et al. (1988)]. Adsorption of CO_2, SO_2 and NH_3 on Hungarian clinoptilolites and mordenites has been studied by Kallo [Kallo et al. (1982)], and an excellent review of the general structural and adsorptive properties of ion exchanged clinoptilolites has also been published [Ackley et al. (1992), Ackley & Yang (1991 a)]. These articles include experimental results comparing ion exchanged clinoptilolites to 4A zeolite for the separation of CH_4 from N_2. Again the natural zeolites showed great promise and versatility for the specified separation. Despite such promising results, the data available on natural zeolite adsorption properties is scarce relative to that for synthetic zeolites. The advantages of natural zeolites can only be realized through detailed studies of their adsorption properties and of the roles played by various exchangeable cations in gas adsorption.

In this study, the molecular sieves chosen for potential separation of CO, CO_2, and NO from N_2 were 4A and 5A zeolites (for comparison with literature), a synthetic H - Mordenite, a natural Turkish clinoptilolite and a high surface area activated carbon. The gas chromatographic method was used to determine the Henry's Law constants of each system over various temperature ranges between 243 and 473 K. The separation factors (ratios of Henry's Law constants) for NO, CO and CO_2 from N_2 on each molecular sieve were then calculated and compared to determine a favorable molecular sieve for these common separations. On finding a promising system and conditions, pure component and binary gas adsorption isotherms were measured.

1.2 Separation of C_2H_4 from CH_4 and C_2H_4 from C_2H_6

Much research has also been done on the utilization of adsorptive processes for various light hydrocarbon separations. Applications in removal of CO_2 from light natural gases with molecular sieves have recently been examined by many authors including Sircar [Sircar (1988 a, b)], Dexin and Youfan [Dexin & Youfan (1988)], and Hart and Thomas [Hart & Thomas (1991)]. Further applications in separations of alkenes from alkanes have been studied by Schoellner and Mueller [Schoellner & Mueller (1986)] on various 4A zeolites, Hampson and Rees [Hampson & Rees (1992)] on NaY and Silicalite - 1, and Kaul [Kaul (1987)] on 13X and activated carbon. Adsorption of C_2H_4 and C_2H_6 on 13X zeolite has been studied extensively by Danner, Hyun and Choi [Hyun & Danner (1985, 1982 a, b), Danner & Choi (1978)]. Further work has been done on the adsorption of light hydrocarbons, particularly C_2H_4, on various cation exchanged X zeolites [Habgood (1964), Carter et al. (1966)]. Exxon and UOP have also registered patents for alkene / hydrocarbon separations on various modified sodium X and Y zeolites [Carter et al. (1967), Kimberlin & Judson (1958), Neuzil & Rosback (1977), Rosback (1973, 1975)]. Traditionally many light hydrocarbon separations are done by cryogenic distillation, involving expensive high pressure units. Temperature or pressure swing adsorption processes offer a viable alternative as separation conditions are likely less extreme. Such processes also offer potential for separation at high temperatures which is usually advantageous, as natural light gases are often recovered above room

temperature, making low temperature separation costly. It is this type of alkene / alkane separation that is of primary interest in this study, specifically the separation of C_2H_4 from CH_4. CH_4 adsorption on various molecular sieves has been well documented by Haq and Ruthven [Haq & Ruthven (1986 a, b)], Yucel and Ruthven [Yucel & Ruthven (1980)], and Tezel and Apolonatos [Tezel & Apolonatos (1993)], and these existing results were used to verify some of the results obtained in this study. Having gained confidence in the experimental method, various zeolites were screened for the C_2H_4 / CH_4 separation in the present study. Adsorption of C_2H_6 on some zeolites was also examined. It should be noted that the zeolites studied will also have a greater affinity for most common light gas impurities such as CO_2 and H_2S than for CH_4 due mainly to the strength of their quadropole moments [Sircar (1988 a, b)]. Thus there is potential for removal of low levels of common impurities along with the alkene. The zeolites chosen for study of potential separation of C_2H_4 from CH_4 were 4A, 5A, 13X, a Calcium - X zeolite, H - mordenite and a natural Turkish clinoptilolite. Separation of C_2H_6 from CH_4 was also studied on 4A and 5A zeolites and on the natural clinoptilolite.

1.3 Adsorption Measurement Techniques

In gas adsorption studies, two key parameters are commonly measured. Firstly, the capacity (amount of gas adsorbed per unit mass of adsorbent) of a molecular sieve under given conditions can be calculated by allowing a gas and a molecular sieve to come to equilibrium and measuring the amount adsorbed. Secondly, the diffusivities of gases in molecular sieves (in units of area per unit time) can also be evaluated through dynamic experiments. Determination of these parameters involves measurement of the adsorbent - adsorbate system response to a change in conditions. The measured capacities and diffusivities can be used to predict selectivities, and to choose and design adsorption processes. Both types of measurements may be done by a variety of methods, the most common of which are the volumetric, gravimetric (equilibrium methods) and gas chromatographic (dynamic) methods.

The volumetric method involves measuring the pressure change in a known volume of gas subjected to an adsorbent sample. As the gas is adsorbed and allowed to come to equlibrium the measured decrease in the closed system pressure yields the amount of gas adsorbed under the given conditions. This method has been used extensively to determine adsorption isotherms and measure diffusivities, from the original Brunauer Emmet and Teller apparatus [Brunauer et al. (1938)] to a more complicated and versatile modern volumetric apparatus [Kaul (1987)]. Schematics and precise descriptions of other similar modern volumetric apparatus are easily found [Schalles & Danner (1988), Huang & Fair (1988), Miller (1987)]. Volumetric systems have the advantage of being able to be combined with other methods. However, often the time to reach equilibrium can be large making experiments slow, and furthermore very sensitive pressure measurement equipment is required.

Gravimetric determination of adsorption properties operates on an equally simple priciple. A molecular sieve sample is placed on a highly sensitive balance and exposed to the adsorbate gas at the desired conditions. The change in weight is measured to determine the weight of gas adsorbed. By measuring the weight change with time, diffusivities can also be calculated. The gravimetric method has also been used regularly for experimental determination of capacity and diffusivity, and examples of such apparatus are found in literature [Hayhurst & Lee (1983), Kaneko & Inouye (1988)]. The gravimetric method has the distinct advantage that the amount of gas adsorbed or desorbed is measured directly. The main disadvantage is that coupled with the required sensitivity of the balance is the difficulty of mounting and maintaining such a balance to be independent of any interference that may arise. Furthermore, as with the volumetric method, in the examination of binary systems the gravimetric method becomes complicated as simultaneous measurements of gas phase and adsorbed phase compositions are required [Ruthven & Kumar (1980)]. The two equilibrium methods are therefore favored for systems with relatively slow diffusion and moderate conditions (temperature and pressure).

The gas chromatographic method is a dynamic method of conducting common adsorption measurements. It depends on following the response of a chromatographic column to a pulse or step perturbation in adsorbate concentration. The first and second moments of the response peak produced by a pulse or step perturbation in carrier concentration may indirectly yield the capacity and the diffusivity for

any given system. Such methods have recently been used in many studies for determination of zeolitic capacities and diffusivities, and detailed descriptions of chromatographic methods appear in various articles [Ruthven & Kumar (1979, 1980), Shah & Ruthven (1977), Van der Vlist & Van Der Meijden (1973), Hyun & Danner (1985, 1982 a, b), Haynes & Sarma (1973), MacDonald & Habgood (1972), Eberly (1969), Sarma & Haynes (1974), Suzuki & Smith (1971)]. The gas chromatographic method, although indirectly measuring the adsorption parameters, has been shown to agree well with previous gravimetric and volumetric data [Ruthven & Kumar (1979, 1980), Shah & Ruthven (1977), Hyun & Danner (1985)]. For pure component systems, the volumetric and gravimetric methods are simple and straightforward and the gas chromatographic method offers no real advantages. By contrast, the determination of binary isotherms by equilibrium methods is more difficult due to the required simultaneous measurement of gas phase and adsorbed phase compositions. Thus for the determination of binary isotherms the gas chromatographic method is simpler and quicker. It also offers the advantage of being easily adapted to the high temperature and pressure conditions common to adsorptive and catalytic applications. The chromatographic method was used exclusively in this study and is described in full detail in section 4.

Another method of measuring adsorption constants is the dynamic method in which a column of adsorbent is exposed to a gas mixture. The gas is pumped through the column until equilibrium is reached (ie, when the effluent composition and flow from the column are constant). The column is then separated and degassed, the resulting gas yielding the amount and composition of the gas adsorbed at experimental conditions. This method is effective for binary system as it avoids the problems of the gravimetric and volumetric methods. Application of dynamic apparatus is quite common, and examples can be found in literature [Danner & Wenzel (1969), Reich et al. (1980)]. A new, less developed method of measuring adsorption properties is the zero length column (ZLC) method, which has small sample size and quick measurements as advantages [Ruthven et al. (1991)].

1.4 Scope of Research

The purpose for this research was to screen various adsorbents for potential application in the separations of alkenes from alkanes (hydrocarbon separation) and of CO, CO_2, and NO from N_2 (air purification). Information concerning other separations involving the gases studied was also examined. On finding a suitable adsorbent and conditions for either type of separation, pure gas isotherms for each component were determined under these conditions. These conditions were dictated by the conditions under which the respective separations would likely take place in practical applications - high temperature (50 to 250 °C) for the hydrocarbon separation, and lower temperatures (ambient to 100 °C) for the air purification (typical flue gas conditions). As the research progressed it was discovered that a natural Turkish clinoptilolite examined showed great promise for many separations, and the CO - N_2 - Clinoptilolite system was chosen for further study. Pure gas isotherms were determined for this system at 30 °C and atmospheric pressure. Having determined the pure gas isotherms for the two gases involved in the separation, various models were applied to predict the binary isotherm for the system in question. Then the binary isotherm was determined experimentally and the models evaluated. Diffusivity experiments were also conducted for the selected CO - N_2 - clinoptilolite system.

2. Theory

This section discusses the theory behind the gas chromatographic method and presents the various models which were used to describe the experimental data. First, general column theory is reviewed, followed by the theory behind determination of capacities and diffusivities from gas chromatographic methods. Then the mathematical models which were used to fit the experimental pure gas isotherms and to predict the binary isotherms are presented.

2.1 Model of a Molecular Sieve Column

The response of a molecular sieve column subjected to a pulse injection of adsorbate at the inlet at time zero may be described by the following equations [Shah & Ruthven (1977)], which are formally similar the model of Haynes and Sarma [Haynes & Sarma (1973)] for diffusion in bidisperse structured catalysts. There are three sets of equations representing zeolitic (micropore) diffusion, macropore diffusion and column diffusion:

Zeolitic diffusion:

$$D_c\left(\frac{\partial^2 q}{\partial r^2}+\frac{2}{r}\frac{\partial q}{\partial r}\right)=\frac{\partial q}{\partial t} \tag{1}$$

$$q(r_c,t)=K_c c(R,t) \tag{2}$$

$$\frac{\partial q}{\partial r}(0,t)=0 \tag{3}$$

$$\bar{q}=\frac{3}{r_c^3}\int_o^{r_c} r^2 q\,dr \tag{4}$$

Macropore diffusion:

$$\theta D_p\left(\frac{\partial^2 c}{\partial R^2}+\frac{2}{R}\frac{\partial c}{\partial R}\right)=\omega(1-\theta)\frac{\partial \bar{q}}{\partial t}+\theta\frac{\partial c}{\partial t} \tag{5}$$

$$\frac{3k}{R_p}[C(z,t)-c(R_p,t)] = \frac{\partial \overline{Q}}{\partial t} \tag{6}$$

$$\frac{\partial c}{\partial t}(0,t) = 0 \tag{7}$$

$$\overline{Q} = \frac{3\omega(1-\theta)}{R_p^3}\int_o^{R_p} \overline{q}R^2 dr + \frac{3\theta}{R_p^3}\int_o^{R_p} cR^2 dR \tag{8}$$

Column Diffusion:

$$D_L\frac{\partial^2 C}{\partial z^2} - \upsilon\frac{\partial C}{\partial z} - \left(\frac{1-\varepsilon}{\varepsilon}\right)\frac{\partial \overline{Q}}{\partial t} = \frac{\partial C}{\partial t} \tag{9}$$

$$C(z,0) = c(R,o) = q(r,0) = 0 \tag{10}$$

$$C(0,t) = C_o\partial(t) \tag{11}$$

$$C(\infty,t) = 0 \tag{12}$$

The passage of the sorbate pulse through the sorbent filled column is characterised by three separate modes of transport corresponding to the three markedly different sizes of passages in a packed column. Thus the mass transfer parameters are the axial dispersion coefficient D_L, the mass transfer coefficient k, and the effective macropore (D_p) and micropore (D_c) diffusivities.

Implicit in the derivation of these equations are a number of assumptions. Firstly it is assumed that the adsorption is instantaneous and reversible and that the isotherm is linear [Haynes & Sarma (1973)]. Adsorption isotherms are linear at low concentrations (Henry's law region) so this condition can be achieved by ensuring that a small sorbate pulse size is used. A pulse size which maintains surface coverages of less than a few per cent of monolayer is suggested. However, since there is a rapid decline in sorbent concentration once the pulse enters the column, higher pulse concentrations may also be tolerable [Schneider & Smith (1968 a, b)]. Secondly it is assumed that the pressure drop along the length of the column is negligible, ensuring consistent adsorption conditions throughout the column. This condition can be met by keeping gas velocities relatively low and by using large enough adsorbent particles so as not to excessively obstruct flow. Pressure drop can easily be measured during experiments to confirm this

condition. A third assumption is that the sorbate micropore diffusivity is independent of concentration (Fickian diffusion). Again a dilute sample can help ensure this condition, as concentration - independent diffusion is most likely when the system is only slightly disturbed from its steady state concentration [Haynes (1975)]. However it is noted for certain systems [Eberly (1969)] that within the Henry's law region the micropore diffusivity is inversely related to the sorbate concentration. This generally occurs when the critical diameter of the sorbate is small in comparison to the pore size of the sorbent. When sorbent pore size and sorbate critical diameter are similar, the diffusivity is normally independent of concentration in the Henry's law region [Shah & Ruthven (1973), Ruthven & Derrah (1972 b)]. If the diffusivity is inversely related to the concentration, the precise value of the micropore diffusivity determined experimentally will depend upon the pulse size. The fourth assumption is that any deviations from plug flow in the column are adequately described by axial dispersion. The topic of axial dispersion as a source of nonideality in chromatography has been well discussed [Van Deemter et al. (1956)].

A rigorous solution to this set of equations (1 through 12) is not provided. Instead the relationship between the mass transfer parameters and the moments of the response curve can be determined. This is done by transforming equations 1, 5 and 9 into the Laplace domain with respect to t and solving the resulting ordinary differential equations with the transformed boundary conditions, as detailed by Suzuki & Smith [Suzuki & Smith (1971)]. The moments of the chromatogram are easily related to the mean and variance (μ and σ^2) of the response peak which are given as [Shah & Ruthven (1977)]:

$$\mu = \frac{L}{\upsilon}\left[1 + \left(\frac{1-\varepsilon}{\varepsilon}\right)K_p\right] \tag{13}$$

$$\frac{\sigma^2}{2\mu^2} = \frac{D_L}{\upsilon L} + \left(\frac{\varepsilon}{1-\varepsilon}\right) \bullet \left(\frac{\upsilon}{L}\right) \bullet \left(\frac{R_p}{3k} + \frac{R_p^2}{15\theta D_p} + \frac{r_c^2}{15 D_c K_p}\right) \tag{14}$$

Here it is assumed that $K_p >> 1$, otherwise the equation includes another term [Haynes & Sarma (1973)]. These equations relate the experimentally determinable mean and variance of the response peak to the Henry's law constant (K_p), the axial dispersion coefficient (D_L), the external film mass transfer coefficient

(k), and the micropore and macropore diffusivities (D_c and D_p). Through these relationships various capacity and diffusivity data can be obtained by calculating the mean and variance of gas chromatograph response peaks resulting from a sorbent column being exposed to a pulse of sorbate gas.

2.2 Determination of Henry's Law Constants

In using the gas chromatographic method to learn about zeolitic capacity the actual capacity under given conditions must be calculated indirectly. This results from equation 13 yielding only the slope of the isotherm K_p from the experimental mean of the response peak. If a small pulse of sorbate at minimal partial pressure were passed through the column, the calculated slope would be the initial slope of the isotherm (the Henry's law constant). Most isotherms exhibit linear behaviour at low pressures, and the isotherms under these conditions are simply described by the relationship:

$$\bar{q} = K_p P \tag{15}$$

The temperature dependance of the Henry's Law constant can be described by an Arrhenius type equation:

$$K_p = K_0 \exp^{\frac{-\Delta U_0}{R_g T}} \tag{16}$$

The initial heat of sorption, $-\Delta H_0$, is then easily calculated from the internal energy change of sorption ($-\Delta U_0$ from equation 16), as $-\Delta H_0 = -\Delta U_0 + R_g T$. It is easy to determine Henry's law constants at various temperatures for many gases and adsorbents, allowing determination of the pre exponential factor K_0 and the internal energy change of adsorption ΔU_0. These values may then be used to calculate equilibrium separation factors, which are the ratios of the Henry's law constants. The values of the these factors are useful in prediction of promising separations and separation conditions.

2.3 Determination of Pure Gas Isotherms

The slope of the isotherm can easily be determined with the gas chromatographic method. By obtaining the slope of the isotherm at a variety of partial pressures, the isotherm can be constructed as the integral of the experimental slope - partial pressure relationship. This is done practically by using a mixed carrier gas consisting of helium (a non adsorbing inert gas) and the sorbate. Then the resulting chromatographic peak represents the response of a column at the sorbate partial pressure in the carrier. The slope can thus be calculated at chosen carrier partial pressures to obtain a complete isotherm [Schneider & Smith (1968), Shah & Ruthven (1977), Ruthven & Kumar (1980), Hyun & Danner (1982 a, 1985)]. For a mixed carrier system the first moment of the response peak is redefined as:

$$\mu = \frac{L}{\upsilon}\left[1 + \left(\frac{1-\varepsilon}{\varepsilon}\right) \bullet K_p'\right] \tag{17}$$

Where K_p' is the slope of the combined carrier isotherm which contains contributions from the adsorption of both components:

$$K_p' = (1 - Y)\frac{dq_1}{dp_1} + Y\frac{dq_2}{dp_2} \tag{18}$$

The second component (helium) is assumed to be non adsorbing and dq_2/dp_2 is therefore a constant. It may be determined experimentally from equation 18 as Y (the mol fraction of the adsorbing component) approaches 1. Thus by rearranging and integrating equation 18, the capacity (q_1) may be found as a function of the adsorbate partial pressure (p_1) yielding the desired pure component isotherm from the experimental K_p' vs Y relationship.

2.3.1 Pure Gas Adsorption Isotherm Models

A wide variety of pure gas adsorption models are available. Various models have been compared at length in literature [Suwanayuen & Danner (1980 a, b), Miller et al. (1987), Miller (1987), Cochran et al. (1985 a, b), Schalles & Danner (1988)] and summaries of numerous models and comparisons thereof are contained in two texts [Yang (1987), Ruthven (1984)]. Some of the more common models for pure gas isotherms which have seen regular use include the BET Isotherm [Brunauer et al. (1938)], the Langmuir isotherm (and extensions thereof), the Statistical Thermodynamic Model [Ruthven et al. (1973 a), Derrah et al. (1972)] and the Vacancy Solution Theory (VST) [Suwanayuen & Danner (1980 a, b)]. The BET Isotherm applies to the adsorption of gases approaching their vapour pressures (ie, $0.05 < P/P_o < 0.35$) and was therefore not applicable to the systems studied here. Although the Statistical Thermodynamic Model generally provides isotherm fits as good as or better than those provided by the Langmuir and the Ideal Adsorbed Solution Theory (IAST) models, is much more computationally complex, particularily for binary systems, and was not applied here. The models chosen for modelling pure isotherms in this study were the Langmuir isotherm and the VST, as both facilitate predicition of binary adsorption equilibrium from pure gas adsorption data. Details of various models not mentioned here are available in literature [Yang (1987), Ruthven (1984)].

The Langmuir isotherm simply describes the adsorption capacity of a zeolite as a function of its pressure with the initial slope of the isotherm (b) and the ultimate monolayer capacity of the zeolite (q_m) as constants:

$$\frac{1}{q} = \frac{1}{q_m} + \frac{1}{bq_m}\frac{1}{P} \qquad (19)$$

By plotting 1/P against 1/q, values of b and q_m can be calculated, yielding the Langmuir isotherm. This model includes the assumption of a local idealized monolayer. The Langmuir model is best suited for simple type I isotherms which do not exhibit excessively rectangular behaviour [Yang (1987)].

The VST [Suwanayuen & Danner (1980 a, b)] is a more versatile and complicated model for gas adsorption. The isotherm relationship includes terms representing the initial slope of the isotherm and the ultimate capacity, and is not limited to monolayer coverage. Also included in the VST model are terms (Λ_{1v} and Λ_{v1}) accounting for the different interactions between the vacant surface and the sorbate molecules:

$$P = \frac{q^{\infty}}{b_1}\left[\Lambda_{1v}\frac{1-(1-\Lambda_{v1})\theta_1}{\Lambda_{1v}+(1-\Lambda_{1v})\theta_1}\right]\frac{\theta_1}{1-\theta_1}\exp\left[\frac{-\Lambda_{v1}(1-\Lambda_{v1})\theta_1}{1-(1-\Lambda_{v1})\theta_1}-\frac{(1-\Lambda_{1v})\theta_1}{\Lambda_{1v}+(1-\Lambda_{1v})\theta_1}\right] \quad (20)$$

The exact form of the VST isotherm equation depends upon the definition of the activity coefficients. The above relationship uses the Wilson equation to calculate activity coefficients. Using the Flory - Huggins definition for the activity coefficients yield a simpler (three coefficient) and usually equally accurate VST relationship [Cochran et al. (1985 a, b)]:

$$P = \frac{q^{\infty}}{b_1}\left(\frac{\theta_1}{1-\theta_1}\right)\exp\left(\frac{\alpha_{1v}^2\theta_1}{1+\alpha_{1v}\theta_1}\right) \quad (21)$$

Both forms of the VST were chosen for the modelling of pure gas isotherms. In the case of an ideal adsorbed phase the vacancy - sorbate interaction parameters equal unity and the VST reduces to the Langmuir Isotherm.

2.4 Determination of Binary System Isotherms

Binary isotherms are obtained in a manner similar to that used for obtaining pure gas isotherms. The key difference is that instead of using a non adsorbing gas as the second sorbate, two competing sorbates are mixed in the carrier gas and dq_2/dp_2 is no longer constant. The two derivatives in equation 18 represent the slopes of the individual isotherms. The apparent equilibrium constant K_p' is determined

experimentally at various mixed carrier compositions with equation 17 and the required derivatives are expressed as polynomial functions of the gas phase composition:

$$\frac{dq_1}{dp_1} = B_0 + B_1 Y_1 + B_2 Y_1^2 ... + B_{k-1} Y_1^{k-1} \tag{22}$$

$$\frac{dq_2}{dp_2} = C_0 + C_1 Y_1 + C_2 Y_1^2 ... + C_{k-1} Y_1^{k-1} \tag{23}$$

and the measured equilibrium constants $K_p^{'}$ are also fitted to a polynomial function of Y_1:

$$K_p^{'} = A_0 + A_1 Y_1 + A_2 Y_1^2 ... + A_k Y_1^k \tag{24}$$

Adding to this system of the equations the "end points" of the isotherms (ie, the values of q_1 and q_2 at Y_1=1 and Y_2=1, respectively) which are easy to acquire experimentally from the pure gas isotherms, the system of equations may be solved for k=3 and the B_k and C_k coefficients may be determined from the known values of the A_k coefficients [Van der Vlist & Van der Meijdan (1973), Ruthven & Kumar (1980)].

Tezel [Tezel (1986)] details another route for calculating the unknown coefficients. If the polynomial fit does not provide the required good fit of the K'_p vs. Y data, an alternative to the polynomial expression is

$$K'_p = A_{-1}(Y+\beta) + A_0 + \frac{A_1}{(Y+\beta)} + \frac{A_2}{(Y+\beta)^2} \tag{25}$$

where the slopes of the individual gas adsorption isotherms in the mixed system are given by:

$$\frac{dq_1}{dp_1} = B_0 + \frac{B_1}{(Y+\beta)} + \frac{B_2}{(Y+\beta)^2} \tag{26}$$

$$\frac{dq_2}{dp_2} = C_0 + \frac{C_1}{(Y+\beta)} + \frac{C_2}{(Y+\beta)^2} \tag{27}$$

These B and C coefficients can be solved for by using the A coefficients obtained in the non linear regression fit of equation 25 to the experimental data in the following system of equations:

$$A_{-1} = C_0 - B_0 \tag{28}$$

$$A_0 = B_0(1+\beta) - B_1 - C_0\beta + C_1 \tag{29}$$

$$A_1 = B_1(1+\beta) - B_2 - C_1\beta + C_2 \tag{30}$$

$$A_2 = B_2(1+\beta) - C_2\beta \tag{31}$$

$$q_1 = P\left[B_0 Y + B_1 \ln\frac{(Y+\beta)}{\beta} + \frac{B_2 Y}{\beta(Y+\beta)}\right] \tag{32}$$

$$q_2 = P\left[C_0(1-Y) - C_1 \ln\left(\frac{Y+\beta}{1+\beta}\right) + \frac{C_2(1-Y)}{(1+\beta)(Y+\beta)}\right] \tag{33}$$

with the boundary conditions

$$q_1(binary) = q_1(pure) \quad @ \quad Y = 1.0 \tag{34}$$

$$q_2(binary) = q_2(pure) \quad @ \quad Y = 0.0 \tag{35}$$

where the values of $q_1(pure)$ and $q_2(pure)$ are taken from the end points (at P = 1 atm) of the pure gas isotherms. The isotherms are then defined by equations 32 and 33.

Thus by fitting the experimental binary adsorption K_r values to a non linear model the coefficients of the gas mixture isotherm equations can be calculated and the isotherms plotted by either of the two methods [Van der Vlist & Van der Meijdan (1973), Ruthven & Kumar (1980), Tezel et al. (1992)].

2.4.1 Binary Gas Adsorption Isotherm Models

Extensions of the models described for pure gas adsorption exist for the prediction and modelling of binary adsorption data, and these were also applied in this study. A thermodynamic based model, the Ideal Adsorbed Solution Theory (IAST) of Myers & Prausnitz [Myers & Prausnitz (1965)] was also used to predict binay isotherms from pure gas isotherm data. The basic theory of each approach is described hereafter.

Extended Langmuir Model

The extended Langmuir equation [Yang (1987), Ruthven (1984)] for multicomponent adsorption is based on the assumption of an ideal localized monolayer, as is the Langmuir isotherm for pure gases. Given the partial pressure P_i and the fractional coverage q_i for each component i in an n component mixture, the extended Langmuir equation may be expressed as:

$$\theta_t = \sum_{i=1}^{n} \theta_i = \frac{\sum B_i P_i}{1 + \sum_{j=1}^{n} B_j P_j} \tag{36}$$

This relationship allows prediction of multicomponent isotherms from the Langmuir fits of pure component adsorption data.

Ideal Adsorbed Solution Theory

The IAST of Myers & Prausnitz is a thermodynamic treatment of an adsorption system considered to be a mixed sorbate forming an ideal solution with the gas phase. The fundamental equations

for liquids are applied to the gas phase. For a binary sorbate mixture to be in equilibrium the spreading pressures of both components must be equal, and a simple thermodynamic treatment of the system yields the equations:

$$\int_0^{P_1^0} \frac{q_1}{P} dP = \int_0^{P_2^0} \frac{q_2}{P} dP \tag{37}$$

$$PY_1 = P_1^0 X_1 \tag{38}$$

$$PY_2 = P_2^0 X_2 = P_2^0 (1 - X_1) \tag{39}$$

These three equations define the adsorbed mixture. Given the pure gas isotherms the binary isotherm may be predicted. Equation 37 may be solved either by direct integration of simple isotherm relationships or by graphical integration of the pure gas data. This model provides a good fit for a wide variety of data, but it falls short in that it assumes an ideal adsorbed phase. Yang [Yang (1987)] makes some interesting points concerning the fact that the IAST does not take into account strong surface - sorbate interactions. In some cases the adsorbed mixture treated as a liquid displays ideal behaviour when the bulk liquid would not. Simply taking into account activity coefficients and treating the system as a non ideal one is not necessarily the solution, as the validity of treating the adsorbed phase as a liquid is in question due to the potentially strong surface - sorbate interactions. An attempt to compensate for this shortcoming by treating an unoccupied adsorption site as a thermodynamic entity called a *vacancy*.

Vacancy Solution Theory

The Vacancy Solution Theory (VST) , as applied to pure gases, attempts to incorporate this interaction between the vacancy and the sorbate gases. For multicomponent systems the final equilibrium equations using the Wilson and Flory - Huggins activity coefficients, respectively, are [Cochran et al. (1985 a, b), Suwanayuen & Danner (1980 a, b)]:

$$y_i \phi_i P = \gamma_i^s x_i \frac{n_m^s}{n_m^{s,\infty}} \exp\left(\frac{\Delta G_i^0}{R_g T}\right) \exp\left(\frac{\pi a_i}{R_g T}\right) \tag{40}$$

$$y_i \phi_i P = \gamma_i^s x_i \frac{n_m}{n_m^\infty} \frac{n_i^\infty}{b_i} \left[\frac{\exp \alpha_{iv}}{1 + \alpha_{iv}} \right] \exp \left\{ \left[\left(\frac{n_i^\infty - n_m^\infty}{n_m} \right) - 1 \right] \ln \gamma_v^s x_v^s \right\} \quad (41)$$

Combining this with the Wilson or Flory - Huggins definition of activity coefficients and an equation defining the ultimate total sorbate adsorbed (n_i^{inf}), the binary isotherms may be predicted by simultaneous iterative solution of the equilibrium equation for each species. The precise step by step method of calculation is given by Suwanayuen & Danner [Suwanayuen & Danner (1980 a, b)], and the required equations for solving the Flory - Huggins version of the VST are given and discussed in a series of articles [Cochran et al. (1985 a, b), Danner (1983)]. The FORTRAN program used for this calculation is included in the appendix.

The value of modelling binary isotherms from pure gas data is tremendous as pure gas data is available in abundance while binary and ternary data are far more scarce. By discovering which models predict multicomponent adsorption equilibrium the best by comparison with experimental data, one can extend these models to obtain multicomponent adsorption information without multicomponent system data. This can help better and more efficiently apply the information available concerning the adsorption of various gases on molecular sieves, and aid in prediction of promising sorbents for a given gas separation before any multicomponent experiments are conducted.

2.5 Determination of Micropore Diffusivity

As discussed in the introduction, in the study of adsorption we are often interested in equilibrium capacity and zeolitic diffusivity. Zeolitic diffusivity can be measured by the gas chromatographic method from the second moment of the response peak (equation 14). Diffusion in zeolites by chromatography has been studied and modelled in depth [Schneider & Smith (1968 a, b), Eberly (1969), Suzuki & Smith (1971), Macdonald & Habgood (1972), Ma & Mancel (1972, 1973), Hashimoto & Smith (1973), Haynes & Sarma (1973), Shah & Ruthven (1977), Ruthven & Kumar (1979), Sarma & Haynes (1974), Ruthven (1984 a), Ruthven et al. (1991)]. The task is to evaluate the various contributing mass transfer resistances in equation 14.

The external film mass transfer coefficient is approximated by the correlation [Bird et al. (1960)]:

$$Sh = \frac{2R_p k}{D_M} = 2 + 1.45(Sc)^{\frac{1}{3}}(Re)^{\frac{1}{2}} \tag{42}$$

Which is applicable for Reynolds' numbers less than 100. At low Reynolds' numbers this reduces to $kR_p=D_M$ [Schneider & Smith (1968 a, b)] and equation 14 reduces to:

$$\frac{\sigma^2 L}{2\mu^2 \upsilon} = \frac{D_L}{\upsilon^2} + \frac{\varepsilon}{1-\varepsilon}\left(\frac{R_p^2}{3D_M} + \frac{R_p^2}{15\theta D_p} + \frac{r_c^2}{15D_c K_p}\right) \tag{43}$$

The relative contributions from the three mass transfer resistances and axial dispersion must then be evaluated.

The axial dispersion may be calculated one of three ways. It may be determined experimentally by executing "blank" runs on columns filled with non - porous particles equal in size to the sorbent particles used [Sarma & Haynes (1974)]. Another method of estimating the axial dispersion is through a simple correlation. There are two main mechanisms which contribute to axial dispersion in a uniformly packed bed. These are molecular diffusion and turbulent mixing, dominant at low and high velocities, respectively. The correlation given is [Langer et al. (1978)]:

$$D_L = 0.7D_M + \upsilon R_p \tag{44}$$

The axial dispersion may also be calculated by plotting experimental values of $(\sigma^2 L/2\mu^2\upsilon)$ against $(1/\upsilon^2)$ [Schneider & Smith (1968 a)]. Equation 43 shows that the slope of this graph will yield the value of D_L, the axial dispersion, under the given conditions. The plot will be linear at low velocities when turbulence is minimal. This graphical method was used in the present study.

The macropore diffusivity, which is a combination of molecular diffusivity (diffusion controlled by other gas molecules) and Knudsen diffusivity (diffusion controlled by collisions with the macropore walls) must also be evaluated. The molecular diffusivity, which is generally dominant when the mean free

path of the diffusing molecule is less than the macropore diameter, may be calculated via a number of empirical correlations [Reid et al. (1977)]. The Knudsen diffusivity, which controls when the mean free path is significantly greater than the macropore radius, may be defined as:

$$D_K = 9700 R_M \sqrt{\frac{T}{M}} \tag{45}$$

Where R_M is expressed in cm. The total macropore diffusivity may therefore be represented as a sum of the resistances:

$$\frac{1}{D_p} = \frac{1}{D_M} + \frac{1}{D_K} \tag{46}$$

Thus the macropore diffusivity D_p can be calculated given the molecular diffusivity of a gas in macropores of known radius under any given conditions. The macropore diffusivity may also be calculated experimentally [Hashimoto & Smith (1973)]. This is done by plotting experimental values of $(\sigma^2 L/2\mu^2 \upsilon)$ against $(1/\upsilon^2)$ for a system in which micropore (zeolitic) diffusion is negligible. Then the last term in equation 43 is neglected and the macropore diffusivity may be obtained from the intercept of the plot.

Having solved for the axial dispersion, the molecular diffusivity and the macropore diffusivity, the micropore diffusivity may be calculated experimentally from equation 43. This method works well, but many thing must be considered before the chromatographically obtained micropore diffusivities can be considered reliable. The range of micropore diffusivities which may be measured chromatographically is limited. Very high micropore diffusivities cannot be calculated, as if D_c is too high, axial dispersion or another mass transfer resistance will control the diffusion. Excessively low micropore diffusivities result in the sorbate bypassing the micropores entirely and the response peak representing diffusion through the macropores [Shah & Ruthven (1977)]. Such limits have been studied in depth. Mathematically these limits for zeolitic diffusivity measurements by gas chromatography may be written as:

$$\frac{D_M}{R_p^2} >> 15K_p\frac{D_c}{r_c^2} \tag{47}$$

This condition is shown to be met in the appendix. Habgood & MacDonald [Habgood & MacDonald (1970)] have studied conditions under which determination of micropore diffusivities by chromatography are possible. Arbitrary limits were chosen for relative response peak width and graphical correlations were presented for easy verification of feasible experimental conditions. By checking these suggested boundary conditions for determination of micropore diffusivity by chromatography, one can gain greater confidence in knowing that the response peak represents zeolitic diffusion, not macropore diffusion or axial dispersion. A detailed review of zeolitic diffusivity determination via a number of experimental methods and results obtained by such methods are well summarized by Ruthven [Ruthven (1984 a)]. Diffusivity determination is an important part of understanding gas - sorbent interactions, and experiments conducted for measurement of micropore diffusivities in common molecular sieves by a variety of methods are abundant in literature [Habgood (1958, 1964), Costa et al. (1985), Yeh & Yang (1989), Loughlin & Ruthven (1972), Yucel & Ruthven (1980), Ruthven & Derrah (1972 a, b), Rees et al. (1991)].

3. Properties of Materials

There are two essential materials used for this study, those being the gases (sorbates) and molecular sieves (sorbents). The gases are briefly discussed and characterized below. The zeolites used are discussed in varying detail, more information being provided for the natural clinoptilolite as it is not as well defined in literature as type A and X zeolites. Sources and physical properties of all gases and molecular sieves used are detailed below for complete reproducibility of experimental results.

3.1 Gases

All sorbate gases were obtained from Air Products or Matheson Gas Products. Carrier gases and fuel gases (for the flame ionization detector) were chosen according to the GC manufacturer's specifications. It is critical that any gas used as a carrier be extremely pure whereas the sample gas (introduced as a small volume pulse) purity is not as critical. In measuring pure gas and binary isotherms a mixed carrier was used and the carrier gas filter (provided with the GC) upstream of the column was removed, as the zeolite packed filter would drastically increase the time to reach equilibrium between runs. Thus the carrier gas purity became a greater issue in these experiments and high cost gases had to be used. Impurities in this unfiltered carrier gas, particularly oxygen, slowly contribute to the fouling of the thermal conductivity detector. Each gas, its manufacturer and manufacturer's specifications and grade name, along with the use of each gas, is summarized in the table below. For any gas calculations, such as determination of molecular diffusivity, properties were taken from Reid, Prausnitz and Sherwood's *Properties of Gases and Liquids* [Reid, Prausnitz & Sherwood (1977)].

Table 3.1 : Purity, Sources & Uses of Gases

Gas	Purity	Grade	Source	Use
Helium	99.999%	Ultra High Purity	Matheson	Carrier
Methane	99.0%	Chemically Pure	Air Products	Sample
Ethane	99.0%	Chemically Pure	Air Products	Sample
Ethylene	99.5%	Chemically Pure	Air Products	Sample
Nitric Oxide	49.6% in Helium	Mixed Gas	Air Products	Sample
Carbon Dioxide	99.8%	Bone Dry	Matheson	Sample
Carbon Monoxide	99.3%	Chemically Pure	Air Products	Sample
Nitrogen	99.998%	Zero Gas	Matheson	Sample
Carbon Monoxide	99.99%	Matheson Purity	Matheson	Carrier
Nitrogen	99.998%	Ultra High Purity	Air Products	Carrier
Air	19.5 - 23.5% O_2	Breathing Quality	Air Products	FID fuel51
Hydrogen	99.9%	High Pressure	Air Products	FID fuel

3.2 Molecular Sieves

The molecular sieves used require significantly more detailed descriptions, for the different qualities of these materials determine thier adsorptive properties. Key qualities include the size of the pores (for activated carbon and zeolites) and the ions present (for zeolites only). A general description of zeolites is given here; the specific zeolites studied and the activated carbon used are then discussed in greater detail in the appropriate sections below.

Zeolites (as formed in nature or synthesized) are crystalline, hydrated aluminosilicates of group I and group II elements, in particular sodium, calcium, potassium, magnesium, strontium and barium [Breck (1973)]. Higher polyvalent ions may be introduced by ion exchange. Structurally the zeolites have rigid framework extending in all directions consisting of AlO_4 and SiO_4 tetrahedra linked through shared oxygen atoms. Different methods of linking the tetrahedra lead to a large variety of rigid zeolite structures. Zeolites as used in industry commonly consist of pure crystals of these tetrahedra bound in a clay matrix. These bound zeolite crystals are generally between 0.1 and 100 microns in size, creating a secondary porous structure consisting of the paths between the crystals themselves and clay binder

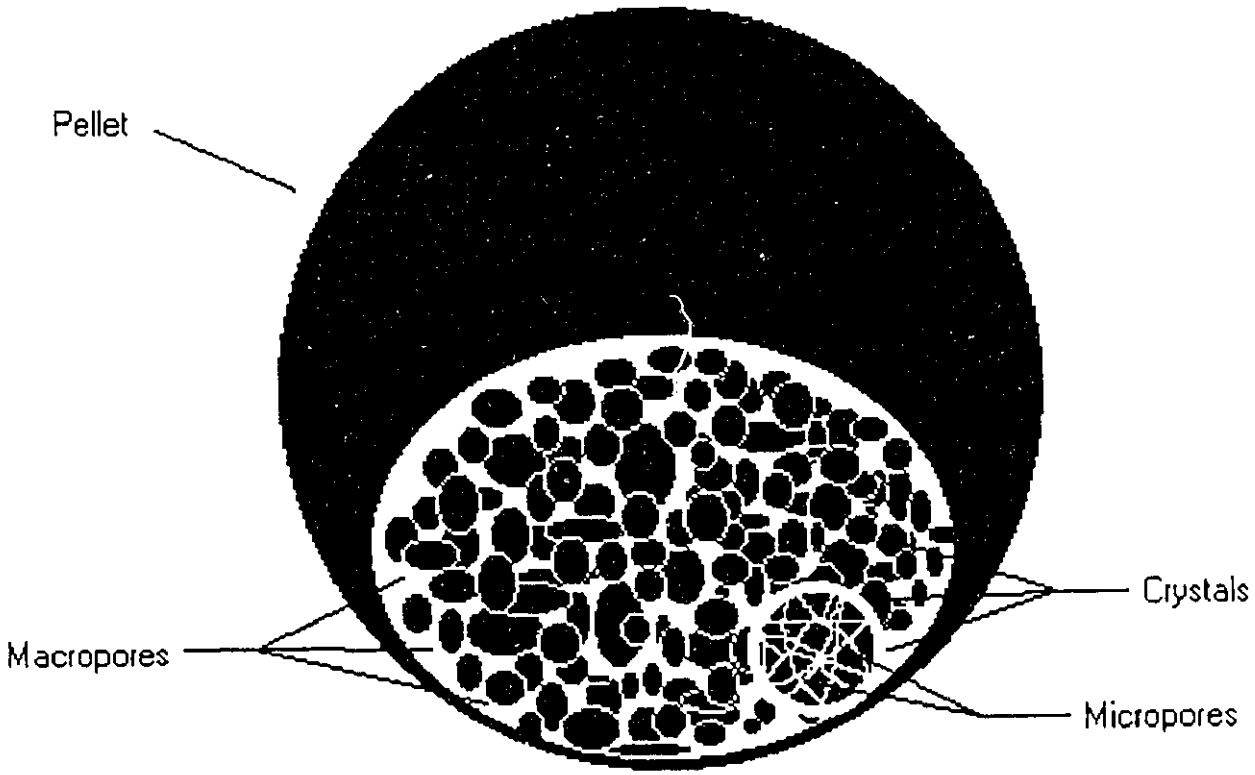

Figure 3.1 : Schematic representation of the bidisperse pores in zeolite pellets

(macropores), as demonstrated in figure 3.1. Thus adsorption occurs only after the gas has traversed the macropores to reach the zeolite crystals. As mentioned above, the key factors in determining the adsorptive properties of a zeolite are the pore opening size and the cations present. The type of zeolite structure (one, two or three dimensional channel networks) also influences adsorptive properties. How these qualities dictate adsorptive properties of a zeolite warrants further discussion [Davis (1991)].

If in a given binary gas separation one molecule can pass into the pores of a chosen molecular sieve and another cannot, then separation will be simple, as one gas is retained and the other rejected. If both gases can pass into the pores but at significantly different rates, a kinetic separation may be possible. Clearly pore size will influence the diffusion rates of the gases in the micropores. It should be noted that since molecules in general are not spherical and since the molecules and the crystal lattice vibrate, a simple comparison of kinetic diameter is not enough to determine whether a given molecule will enter the micropores of a given zeolite. In many cases a molecule with kinetic diameter greater than the pore diameter may enter the zeolite pores.

In the case of zeolites, when ions are present in the micropores, diffusion through these pores can also be heavily influenced by their interaction with the surface. For every alumina tetrahedron in the zeolite structure, a positive charge is required to make the entire structure neutral. Thus the lower the silica : alumina ratio, the greater the number of cationic charges in the crystal. This silica : alumina ratio varies from about 1 to infinity (as in silicalite). Cations present in the zeolite structure interact with the electrical field of the sorbate molecule. When strong cation sites are present molecules with strong dipoles or quadropoles will likely be slow diffusing through the zeolite cages [Derrah et al. (1972), Ma & Mancel (1972, 1973), Kallo et al. (1982), Hampson & Rees (1992), Schoellner & Mueller (1986)]. Furthermore the type, number and location of ions in a given zeolitic structure influences the pore opening size as ions may block the pore openings to varying degrees. Examples in literature of ion exchange drastically affecting adsorption properties of a given zeolitic structure include completely reversing a zeolite's selectivity for a given separation [Ackley & Yang (1991 a), Tsitsishvili and Andronikashvili (1971)] and dramatically varying capacity for pure gases [Ackley et al. (1992), Sirkecioglu et al. (1993), Schoellner & Mueller (1986)]. Given that most zeolites can be ion exchanged to yield partially or completely different cation

content, and given that natural zeolites normally have a large variety of ions present, it is clear that the influence of the cations (by affecting pore size and through sorbate - sorbent interactions) is an extremely important factor in determining a zeolite's adsorption properties.

As mentioned above, the silica and alumina tetrahedra can be linked a variety of ways to form a wide variety of zeolite framework structures. The most common structures and details concerning composition and dimensions are well summarized in literature [Breck (1973), Meier & Olson (1992)]. The channels accessible to the gas molecules may run in a one, two or three dimensional fashion. This will also effect adsorption properties. Slower diffusion and greater potential for pore blockage is expected with a one dimensional structure. A three dimensional channel structure, on the other hand, may allow access to the zeolite cages through multiple pores, facilitating mass transport in the micropores and freely exposing cations to the sorbate gas. Thus the type of channel structure also has an effect on the adsorption properties of any given zeolite.

In addition to adsorption capacity and diffusivity considerations, selecting a zeolite for a given application requires that many practical problems be considered. These include thermal, hydrothermal and chemical stability, possible catalytic activity, physical strength, attrition resistance, and ability to be regenerated and reused. Zeolitic capacity and diffusivity, and to some extent, reversibility, are considered in this report. Other physical parameters such as strength and attrition resistance can be found in literature, but in general zeolites are very stable under high temperature and pressure conditions [Breck (1973)]. The adsorption conditions examined in this paper (up to 1 atmosphere pressure, from -40 to 200 °C) in no way

Table 3.2 : Suppliers & Characteristics of Molecular Sieves

Adsorbent Type	Source	Supplied as	Packed as
4A	Linde	1/8" pellets	20-42 mesh particles
5A	Linde	1/8" pellets	20-42 mesh particles
10X	Strem Chemicals Inc.	1/16" pellets	20-42 mesh particles
H - Mordenite	Norton Zeolon 900H	1/8" pellets	20-42 mesh particles
Clinoptilolite	Bigadic, Turkey	25-40 mesh particles	25-40 mesh particles
Activated Carbon	Supelco	20-45 mesh spheres	20-45 mesh spheres

threaten the stable structure of the zeolites used. [Koyama & Takeuchi (1977), Federova & Aliev (1966)]. The zeolites used are summarized in table 3.2 along with their respective suppliers and particle sizes and forms. This leads to a more detail discussion of the specific zeolites used in this study.

3.2.1 Type A

One of the most commonly used and studied zeolites is the type A zeolite, which does not occur naturally. In commercial production since 1954 it has been used in a variety of practical applications including the separation, drying and purification of gases. Three common ionic forms of A zeolite exist, these being the potassium (3A), sodium (4A) and calcium (5A) forms. The chemical formula for a Linde 5A zeolite cage, which contains sodium (Na^+) and calcium (Ca^{++}) ions, is [UOP (1990)]:

$$Ca_{4.5}Na_3[(AlO_2)_{12}(SiO_2)_{12}] \bullet xH_2O$$

These cages form a uniform three dimensional pore structure. The formula for 4A zeolite is the same except that the 4.5 Ca^{++} are replaced with 9 more Na^+ for a total of 12 Na^+ ions per cage. For 3A zeolite the formula is the same except that some Na^+ ions from the 4A form are exchanged with K^+ ions. The structure of type A zeolite is shown in figure 3.2, showing eight cages connected to form one zeolite unit cell from two slightly different perspectives. Each corner is an Al or Si atom, and each line represents an O atom between them. Specific locations of the ions in the type A zeolite cage are well known [Breck (1973), Ruthven (1984 b)] but are not given in the diagram to avoid confusion. As given in the formula, each cell in the diagram contains 12 Al and 12 Si. The Si : Al ratio of type A zeolite is 0.7 to 1.2, indicating a high cation content relative to most other zeolites. The pore size of type A zeolite depends upon the ions present, but all pores in all directions are equivalent. The effect of ions causing pore blockage is well demonstrated by A zeolite, as 4A has an effective diameter of 3.8 A whereas 5A, which contains fewer ions in different locations, has a pore opening of 4.4 A. Of course the presence of ions will also influence the free volume available for adsorption within the unit cell, which for A zeolites is approximately 900 A^3.

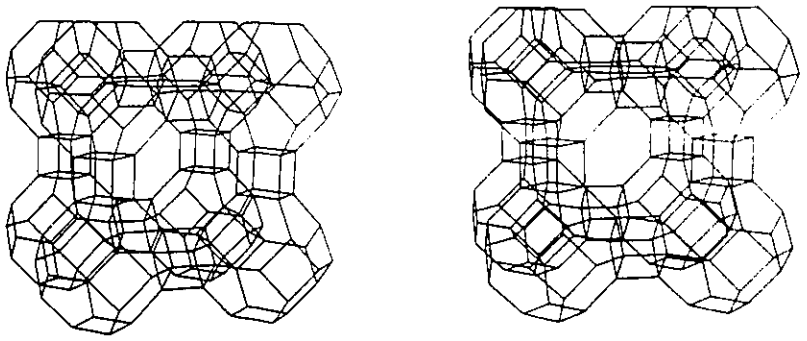

Figure 3.2 : Schematic representation of zeolite A structure

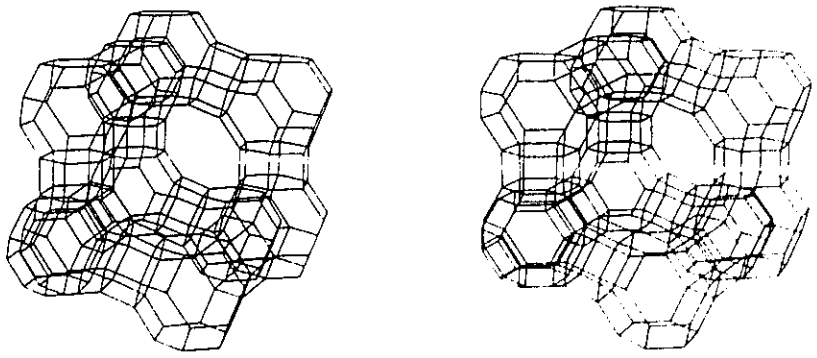

Figure 3.3 : Schematic representation of zeolite X structure

Studies of physical and adsorptive properties of A zeolites have been done extensively, making it a favorable zeolite to choose for comparison of experimental results with literature. Once the experimental method is verified by comparison with existing results, further experiments can be conducted with greater confidence. Papers dealing with the kinetic and equilibrium adsorption properties of light hydrocarbons and / or of NO_x and CO_x on the A zeolites examined are common [Danner & Wenzel (1969), Eagan & Anderson (1975), Eberly (1969), Habgood (1958), Haq & Ruthven (1986 a, b), Harper et al. (1969), Hashimoto & Smith (1973), Inui et al. (1988), Kondis & Dranoff (1971), Loughlin & Ruthven (1972), Miller et al. (1987), Ruthven & Derrah (1972 a, 1975), Ruthven & Kumar (1979, 1980), Ruthven (1984 a, 1976), Schalles & Danner (1988), Tezel & Apolonatos (1993), Yeh & Yang (1989), Yucel & Ruthven (1980 a, b), Ruthven et al. (1991), Brandt & Rudloff (1965), Emesh & Gay (1985), Ma & Mancel (1972), Kaneko & Inouye (1988), Giacobbe (1989), Dexin & Youfan 1988), Hart & Thomas (1991), Ruthven & Loughlin (1973 a, b, 1971), Tsitsishvili and Andronikashvili (1971), Schoellner & Mueller (1986), Derrah et al. (1972)]. An excellent general review of A zeolite crystal structure and use is also given by Breck [Breck (1973)].

3.2.2 Type X

Type X zeolite is a synthetic zeolite with identical structure to the natural zeolite faujasite. Type X is also identical to type Y zeolite with the exception that type Y zeolite has a higher Si : Al ratio (1.5 - 3.0 as compared to 1.0 - 1.5) and thus fewer cations [Ruthven (1984 b)]. Only type X zeolite was used in the present study, so only the type X form of the faujasite structure is discussed further. The chemical formula for Strem Chemicals sodium type X zeolite (13X zeolite) may be written as [Strem Chemicals Inc. (1990)]:

$$Na_{86}[(AlO_2)_{86}(SiO_2)_{106}] \bullet xH_2O$$

The three dimensional channels and cage structure of type X zeolite are shown in figure 3.3 [Meier & Olson (1992)]. There are many ionic forms of type X zeolite, one of the more common being the calcium exchanged version (10X zeolite), which contains approximately 40 Ca^{++} and 6 Na^{+} ions per cage [Ruthven (1984 b)]. Strontium, barium and potassium have also been used in various ionic combinations. The location of ions in the large faujasite cage has been well documented [Breck (1973), Ruthven (1984 b)], and these locations depend upon the nature and number of ions, and on the presence of trace quantities of moisture. The faujasitic structure demonstrates extreme versatility in gas separations and catalysis applications through ion exchange and metal impregnation. The 8.4 A pore openings in type X zeolite are the largest of the common commercially produced zeolites, and therefore generally allow quick diffusion into the pore structure. The large 192 tetrahedra unit cells have a void volume of approximately 7500 A^3. The pore volume and diameter are therefore affected relatively less by ion exchange than those of type A zeolite (from a 34% difference between type 3A and 5A zeolite channel diameters to a maximum 5% difference between common cationic forms of type X zeolite). Therefore with small gases the many ionic forms may be used freely without worry of significant pore blockage due to the various ion sizes and locations. The adsorptive properties of type X zeolites have been studied in some depth [Kaneko & Inouye (1988), Tsitsishvili and Andronikashvili (1971), Ma & Lee (1977), Ma & Mancel (1972), Ruthven et al. (1991), Ruthven (1984 a), Miller (1987), MacDonald & Habgood (1972), Kaul (1987), Inui et al. (1988), Hyun & Danner (1985, 1982 a, b), Danner & Wenzel (1969), Joithe et al. (1972), Giacobbe (1991)]. A detailed review of faujasitic structure and ion location is given by Breck [Breck (1973)].

3.2.3 Mordenite

Mordenite occurs naturally and may be synthesized, commonly coming in Na^{+} and H^{+} cationic forms. The Si : Al ratio of both natural and synthetic mordenites is approximately 5. The chemical formula for the synthetic Zeolon 900 H - Mordenite (H^{+} cationic form of mordenite), which was used in this study, may be written as [Ruthven (1984 b)]:

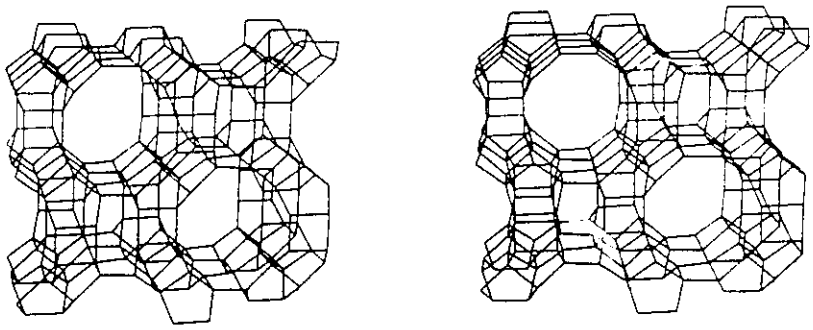

Figure 3.4 : Schematic representation of mordenite crystal structure

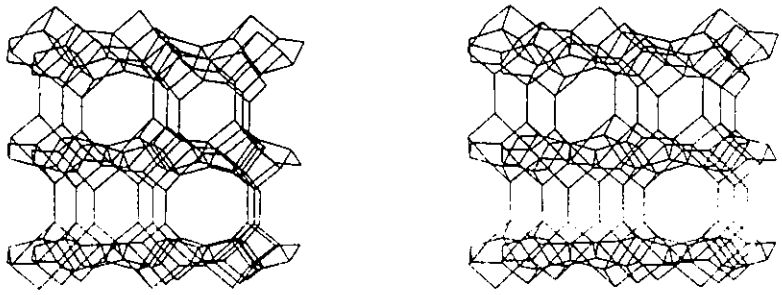

Figure 3.5 : Schematic representation of clinoptilolite crystal structure

$$H_8[(AlO_2)_8(SiO_2)_{40}] \bullet 24H_2O$$

For diffusion of very small molecules mordenite has a two dimensional channel structure, but for larger molecules the channel structure is one dimensional, as shown in figure 3.4 [Meier & Olson (1992)]. The one dimensional structure makes mordenite very susceptible to pore blockage due to the presence of extraneous material (in natural mordenite) and due to fouling (eg. coking when dealing with hydrocarbons). The location of ions in mordenite has been determined to some degree [Breck (1973)]. It should be noted that although the main mordenite channels have nominal pore diameters of 6.7 to 7 A, small molecules such as CH_4 and C_2H_6 are slowly adsorbed which is inconsistent with this large pore size. It is accepted that extraneous matter in the natural zeolite partially blocks the pores, causing the mordenite to behave as a small port zeolite [Ruthven (1984 b)]. A synthetic type of mordenite known as "large port" mordenite has been prepared and it is apparently free of this extraneous material, displaying the adsorption characteristics expected for a 7 A pore size [Breck (1973)]. The unit cell void volume of mordenite has been determined to be approximately 800 A^3. Adsorption on natural and synthetic mordenites has been studied by numerous authors [Ma & Mancel (1973, 1972), Kallo et al. (1982), Kaneko & Inouye (1988), Tezel & Apolonatos (1993), Hayhurst & Lee (1983), Eberly (1969), Ruthven et al. (1984)] and the structural properties of mordenite have also been well summarized [Breck (1973), Ruthven (1984 b)].

3.2.4 Clinoptilolite

Clinoptilolite, a structural isomer of the natural zeolite heulandite, is the most abundant natural zeolite [Ackley & Yang (1992)]. Clinoptilolite has a Si : Al ratio between 4 and 5, the most common naturally occuring counter balancing cations being Ca^{++}, Na^{+}, Mg^{++} and K^{+}. A mix of these ions will be found in a clinoptilolite deposit, but ion exchange allows for modification to a large variety of fully and partially exchanged clinoptilolites. The unit cell of the clinoptilolite used in this study may be represented as:

$$(K_2, Ca, Mg)_3[(AlO_2)_6(SiO_2)_{30}] \bullet xH_2O$$

Where Na^+ is also present to a small degree. The two dimensional channel structure of clinoptilolite is shown in figure 3.5 [Meier & Olson (1992)]. The major ion locations in clinoptilolite and the effects of different ion locations and sizes on aperture diameters have been determined [Koyama & Takeyuchi (1977)]. The large channels in clinoptilolite have dimensions of 7.2 by 4.4 A, and the smaller parallel channels have dimensions of approximately 4.7 by 4.1 A. The channels running perpendicular to the main channels in the two dimensional clinoptilolite structure have dimensions of 5.5 by 4 A. The clinoptilolite unit cell has a void volume of approximately 700 A^3. Despite its excellent potential for various gas separations, clinoptilolite has not been studied extensively due to the low cost and availability of synthetic zeolites and due to purity and composition variation inherent in natural clinoptilolite. A better understanding of clinoptilolite's adsorption properties and how they are affected by ion exchange must be achieved if they are to be successfully applied in industry. Studies of the adsorptive and ion exchange properties of natural clinoptilolites can be found [Ackley et al. (1992), Ackley & Yang (1991 a, b), Ames (1961 a, b), Sirkecioglu et al. (1992), Barrer & Makki (1964), Barrer & Townshend (1976), Minato (1985), Minato & Utada (1971), Kallo et al. (1982), Ruthven et al. (1984), Inui et al. (1988)] and excellent reviews of the clinoptilolite structure and composition are available [Gottardi & Galli (1985), Sand & Mumpton (1978), Breck (1973)].

3.2.5 Carbon Molecular Sieves

Carbon may be formed into a molecular sieve, but it is not a zeolite as it contains no silica or alumina. It consists of elementary graphite microcrystallites which are stacked together in random orientation, and the spaces between these crystals form the micropores. This difference in composition leads to distinct differences in adsorption properties. The carbon contains no cations in its structure and is thus essentially nonpolar (and hydrophobic), and the framework is not perfectly uniform. Thus there are

no strongly charged adsorption sites, nor is there a rigid pore or cage size. Adsorption on a carbon molecular sieve depends more on the sorbate species size than its charge, whereas adsorption on high alumina zeolites generally depends very strongly on the polarity of the sorbate species. The non uniform pore structure leads to a pore size distribution rather than a distinct pore size. By careful selection of carbon molecular sieve synthesis and treatment conditions, pore sizes can be tailored to some degree, achieving a micropore size distribution from 4 to 9 A. The carbon molecular sieve used in this study had a listed micropore size distribution between 3 and 40 A. The existence of a micropore size distribution means that molecular sieving selectivity of a carbon molecular sieve seldom approaches the near perfect separation that may be provided by zeolites under favorable conditions. However relatively high kinetic separation factors can be attained with a well prepared carbon sieve [Ruthven (1984 b)]. Adsorption studies on carbon molecular sieves are extremely common, and activated carbons are presently applied in air separations and have potential for nuclear off gas scrubbing and hydrogen production. Some of the more recent studies of the adsorption of the sorbate gases chosen for this project on carbon sieves were reviewed [Kaul (1987), Reich et al. (1980), Myers & Ou (1983), Huang & Fair (1988), Hart & Thomas (1991), Costa et al. (1985, 1981)]. As technology for synthesis of carbon sieves advances, more applications will likely come forth as they approach the versatility offered by zeolites.

4. Experimental

The equipment used in all experiments is described followed by descriptions of the different methods for regenerating the column and for determining pure and mixed gas isotherms. The processing of experimental data is then reviewed so that all steps in arriving at the final data presented in the results are clearly defined.

4.1 Apparatus

A Varian 3400 gas chromatograph (GC) equipped with a flame ionization detector (FID) and a thermal conductivity detector (TCD) was used for all experiments. The zeolite column was fully contained in the GC oven for accurate temperature control. The sampling valve introduced a 0.25 cc pulse at atmospheric pressure into the carrier stream. Gas sampling and the monitoring and analysis of response peaks were automatically controlled through the use of a Viewdac data acquisition system (DAS) from Keithley MetraByte installed on an Akran 486 computer, ensuring accurate marking of sample introduction time. First and second moments of the response peak were calculated and, along with the raw data, were written to a Lotus 123 file, which allowed further data analysis and printing of the experimental results. All information pertinent to the run, including GC detector settings and gas flowrates, were recorded along with the response peak data. In mixed gas experiments a Gow Mac thermal conductivity cell, a Gow Mac model 40 - 200 power supply & control unit, and a Series 5000 Fisher Recordall chart recorder were used to measure mixed gas composition.

For experiments conducted at temperatures other than ambient, the carrier gas was preheated in a coil contained in the GC oven before passing through the sampling valve, thus ensuring that gases entering the column were at the designated temperature. Gas velocities were kept low to ensure negligible pressure drop in the column. Column pressure drop was measured with an Ashcroft pressure gauge during all experiments and was found to be negligible. Carrier and reference gas velocities were controlled with the Varian 3400 digital flow controllers accurate to within 3% of setting and flowrates were verified with

bubble meter measurements. For mixed gas experiments component gas flows were metered through Matheson E100 rotameter tubes accurate to 5% of full range. Rotameters were individually calibrated for each gas studied using bubble flow meters with supply gases provided at 40 psi, regulated by Matheson dual stage regulators. Tubing was in general 1/8", but all tubing between sample injection and column and between column and detector was kept to minimal length and diameter (1/16") to reduce dead volume. Dead volumes between sampling port and detectors were calculated at room temperature by measuring the mean of the response curve produced when a gas sample pulse was passed through the GC tubing at a known flow rate with the adsorption column removed. All experimental means of the adsorption column response curves were corrected by subtracting the corresponding dead time (calculated from the dead volume and the gas flowrate).

Sample specifications for a column packed with 5A zeolite particles are given in table 4.1. The particle size (and therefore the porosity) and bed density were not constant for all runs due to differences in molecular sieves (see table 3.2). Porosity inside the column was calculated from the bed mass and the

Table 4.1 : Column Specifications

Particle mesh size	20 - 42
Average particle diameter	602.5 μm
Bed density	.93 g/cm^3
Bed porosity	0.37
Inside diameter	0.51 cm
Bed length	10 cm

apparent density of the zeolite particles. Bed density was indirectly determined for each hydrated and dehydrated sieve by weight measurement on a Fisher Scientific Company Gram-atic balance. Sample calculations are provided in the appendix.

4.2 Experimental Method

Precise descriptions of methods for zeolite ion exchange, column regeneration, and for pure and mixed carrier gas experiments are given below. Schematics showing set up of the equipment detailed above are provided and discussed.

4.2.1 Zeolite Ion Exchange

Ion exchange was performed on an industrial NaX zeolite to partially exchange the Na^+ ions with Ca^{++} ions. The exchange was conducted in the following manner, as described by Khulbe [Khulbe et al. (1993)]. Ten grams of Strem NaX zeolite pellets were crushed and screened to produce a 20 - 42 mesh partcle size range, as used in the experimental column. These particles were dried at 110 °C for 3 hours. The dried zeolite was then placed in a twin flask constructed of two 250 ml Erlenmeyer flasks, as shown in figure 4.1. The flask was then evacuated to remove air from the pores. After evacuation the vacuum line was closed and the impregnation solution was slowly introduced into section B of the flask, taking care not to allow any air into the system through splashing of the solution. The impregnation solution used was 100 ml of 1 molar $CaCl_2$ solution. The twin flask was then turned to drop all the zeolite into the impregnation solution. Once the zeolite particles were completely immersed, air was slowly bled into the flask to return the system to atmospheric pressure. The slurry was left for 24 hours with occasional stirring. The slurry was then filtered, washed 4 times with distilled water, and dried at room temperature for 2 days. The resultant CaX zeolite was regenerated as described in section 4.2.2. Analysis of the original and ion exchanged zeolite for determination of the degree of exchange was done by direct current plasma spectroscopy after leaching the zeolites with aqua regia.

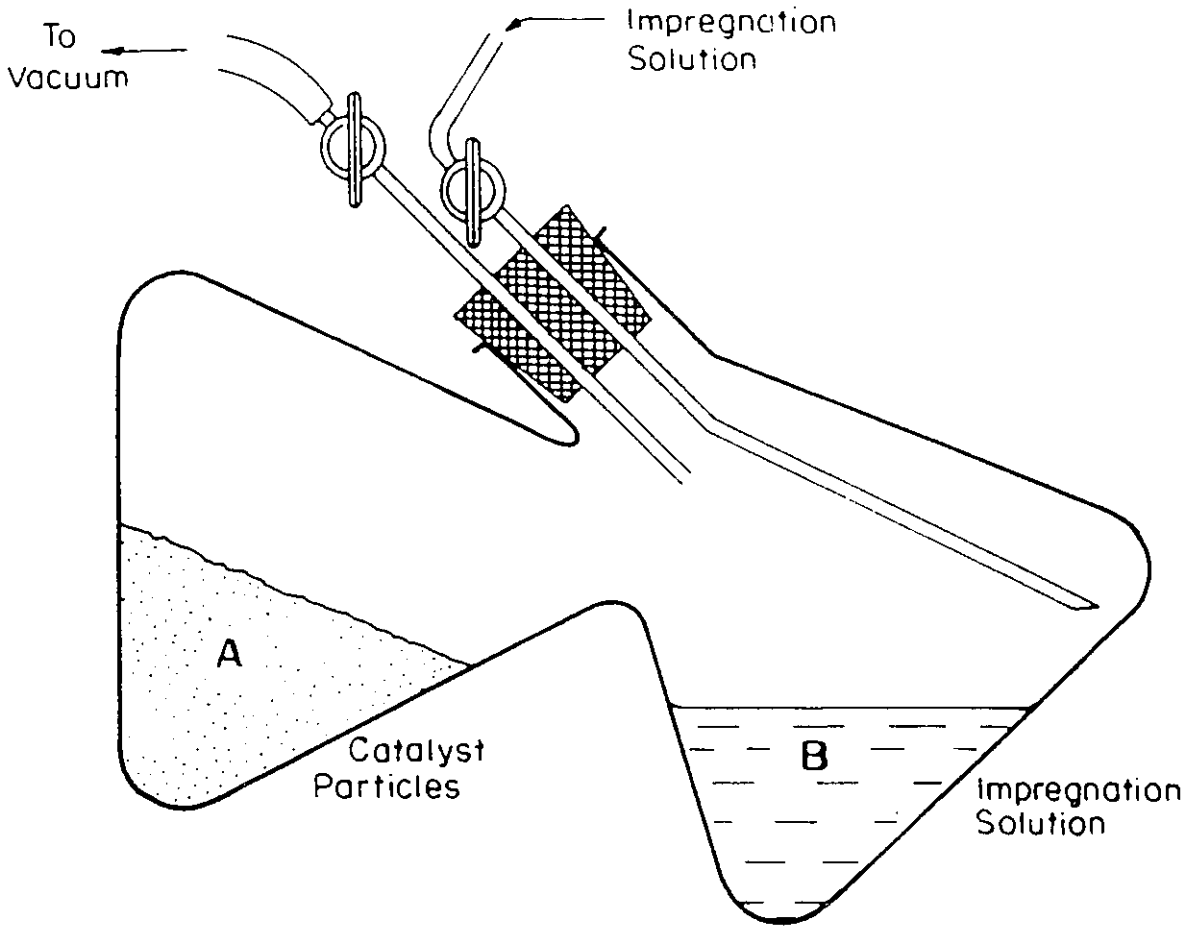

Figure 4.1 : Twin flask apparatus for ion exchange

4.2.2 Sorbent Regeneration

All molecular sieves were regenerated identically before any adsorption experiments were done to ensure removal of trace impurities and moisture from the micropores. The process involved running He through the column at approximately 5 cc/min, first at 373 K for 2 hours to remove excess moisture and then at 623 K for 24 hours to remove any further impurities. Naturally the presence of any moisture or impurities in the sorbent micropores would influence adsorption capacity and diffusion rates in the sieve. The regeneration temperature of 350 °C was selected for many reasons. Various regeneration conditions have been examined and relatively high temperatures are required if the zeolite is to fully recover its adsorption properties [Federova & Aliev (1966)]. Furthermore it has been shown that structural changes in A zeolites occur at temperatures above 700 K. The zeolite regeneraton temperatures used in the various studies found in literature generally range from 250 to 400 °C. It should be noted that adsorption properties can be influenced significantly by regeneration conditions, and thus comparison of the present study's results should be done with literature studies reporting similar or identical regeneration procedures.

The column was not regenerated after each pure gas experiment, as the column was only exposed to a small sample pulse, and it was continuously purged with He carrier between experiments. In cases where the some sample may become chemisorbed or otherwise trapped in the micropores, the effect may be seen in successive experiments as a decreasing capacity and the results would become less valid as more of the sorbent surface is covered with each experiment. Fortunately by simply repeating experiments under identical conditions this situation could be detected. For mixed carrier experiments, the sorbent in the column was replaced and regenerated with each change in carrier gas.

4.2.3 Pure Carrier Gas Experiments

In determination of Henry's law constants for adsorbent screening a pure He carrier gas was used at a flowrate of 15 or 30 cc/min, depending upon the strength of adsorption. The set up of the apparatus used in these experiments is shown in figure 4.2. The regulated carrier gas was supplied at 40 psi to allow

proper flow control with the valves in the GC. The carrier passed through a Varian Gas Purifier (for removal of trace O_2), into the GC oven through the preheater (a coiled 2 m length of 1/8" copper tubing), through the digital flow controller and into the sampling loop. The sample gas was run at low flows to ensure the sample was introduced at atmospheric pressure. The sample valve was triggered automatically by the DAS and data recording and the GC run were simultaneously initiated. The sample containing carrier then passed trough the 1/16" stainless steel tubing to the column and out through the TCD and FID linked in series. Thus two different dead volumes were calculated, one each for the TCD and FID. The detector outlets then led through two bubble meters and into the atmosphere. Although both the TCD and FID signals were recorded for each run, only the clearer peak (that with the stronger signal and better defined baseline) was processed. For runs at sub ambient temperatures liquid N_2 was used to provide the required cooling.

4.2.4 Mixed Carrier Gas Experiments

In determining pure or binary gas adsorption isotherms, a mixed carrier is required to allow measurement of the slopes of the isotherms at various sorbate partial pressures. This required a different experimental setup than those with a pure carrier, as shown in figure 4.3. Rotameters were used to meter gas flows through a Gow Mac TCD cell which was connected to a chart recorder. The recorder was calibrated for each gas mixture (He-N_2, He-CO, and CO-N_2) before determining the respective isotherm. Thus the carrier gas composition was set with the rotameters and monitored with the TCD cell during all mixed carrier experiments. The mixed gas then passed through the reference side of the TCD cell, through the sample introduction valve, and into the zeolite column. The exit of the column was connected to the detector side of the TCD cell and then vented. Thus instead of splitting the carrier stream as was done in pure carrier experiments, the same carrier stream was passed through both sides of the TCD. Only the TCD was used for the isotherm experiments as it offered much higher sensitivity to CO and N_2 than the FID.

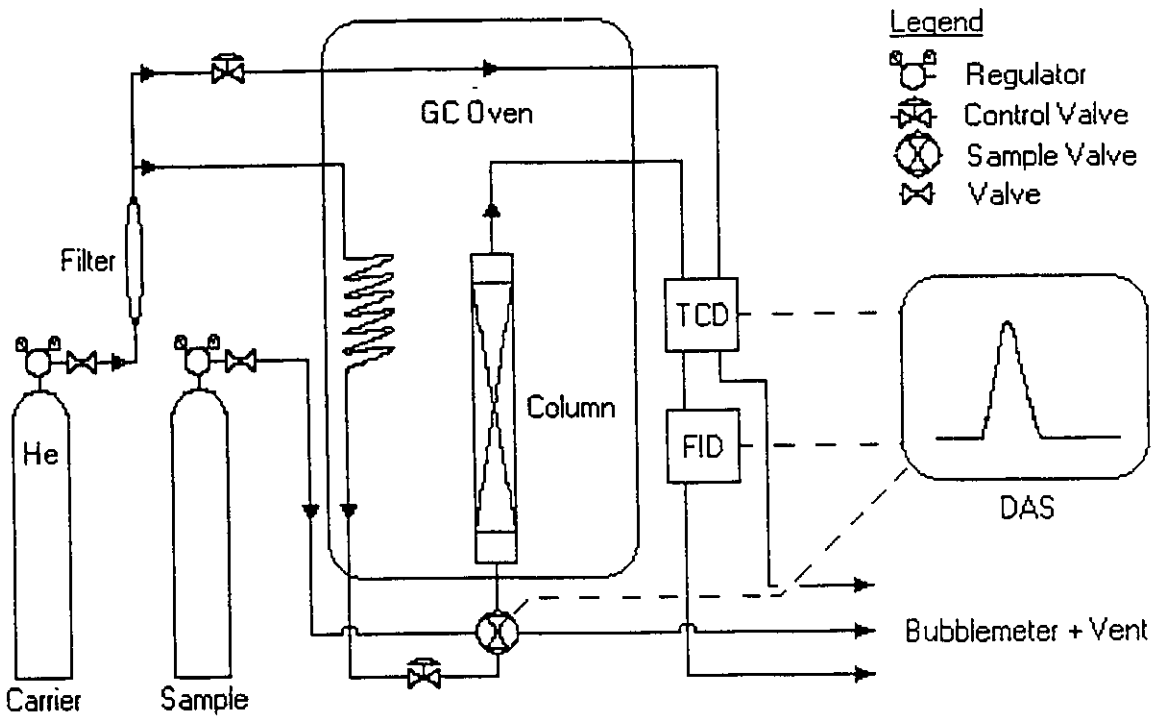

Figure 4.2 : Experimental apparatus for pure carrier gas experiments

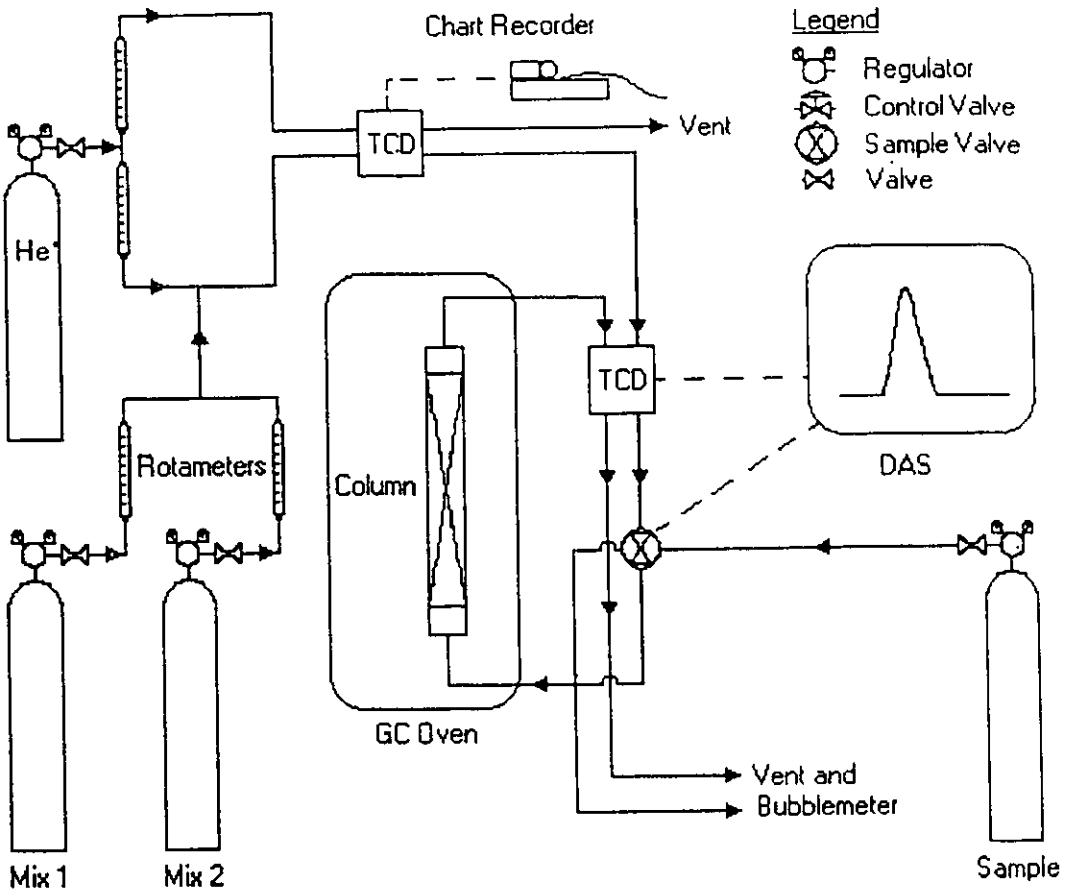

Figure 4.3 : Experimental apparatus for mixed carrier gas experiments

Other differences include the bypassing of the digital flow controllers and the removal of the carrier gas filter. The flow controllers contained in the GC were not used as they would introduce a variable pressure drop downstream of the rotameters, and due to the fact that the supply pressure after passing through the rotameters was not high enough for proper operation of the flow controllers. The filter was removed for convenience, but this could also lead to problems. In changing the carrier composition during experiments, the zeolite column in the oven needed time to reach equilibrium. In some cases, for the approximately two grams of adsorbent in the column the time to reach equilibrium exceeded 24 hours. The gas purifier contained more than ten times the mass of sorbent in the column and would have led to excessive waiting for equilibrium conditions. Furthermore the purifier was designed to remove O_2 from relatively weakly adsorbed gases including He and N_2, but not CO. Thus with CO in the carrier the supplied Varian gas purifier was not applicable. The problem here is that the recommended carrier purity is 99.999%, and that the filter should further remove 99% of trace O_2. Since high purity CO is very expensive, only 99.99% purity was attainable, and this led to accelerated oxidation of the TCD filaments. Other than these changes in apparatus, the DAS set up was the same and data was recorded and processed the same as for pure carriers with the exception that the carrier gas composition was also documented.

4.3 Data Analysis

Methods of data treatment for experiments with significant baseline offset and a brief description of the curve fitting routine frequently used in the interpretation and modelling of isotherm data are detailed below.

4.3.1 Peak Interpretation

In most experiments baseline resolution was excellent and tailing was minimal, so no treatment was required and the raw calculated mean was used as the true mean. However in cases where the baseline shifted significantly or when the second moment had to be known with accuracy (diffusion experiments)

some data treatment was required before the moments of the reponse peak could be calculated accurately. Since all integrations for calculation of the moments were executed on a spreadsheet, it was simple to determine to what degree the baseline shift affected the calculated mean. Usually the difference between the raw calculated mean and the mean of the treated data was negligible, but significant differences in the variance of the peak were noted.

The treatment method was simple. In the case of an offset which exceeded 15% of the peak height, or when accurate determination of the second moment was required, the raw data was modified before calculation of the first and second moments. A diagonal was drawn from the original baseline from where the response peak begins to the final baseline where the response peak ends. It is this area under the curve and over the diagonal, not the area under the curve and over the initial baseline level, which was used to calculate the moments of the peak. Thus it was assumed that the final level baseline is equal to the initial baseline. Various causes for the baseline drift encountered in this study are discussed in section 5. The 15% rule was used simply becuse the difference between the raw mean and the treated mean was negligible for cases with smaller baseline shifts. For determination of second moments, even a slight baseline shift largely affected the values, and all data used to this end was treated as described above.

4.3.2 Curve Fitting

In determining pure and mixed gas isotherms, and in some cases in modelling these isotherms, various nonlinear regressions were performed. All such regressions were done using very similar FORTRAN codes to call the IMSL subroutine RNLIN. This subroutine fits a nonlinear regression model using least squares and a modified Levenberg - Marquardt method for minimum point approximations. The subroutine operates with or without user supplied partial derivatives. The double precision form of this subroutine which allows user set arguments, DR2LIN, was used along with DR8LIN (which assigns initial argument values) for each nonlinear regression executed. A sample FORTRAN code for fitting the VST to pure isotherm data is listed in the appendix. Only the data, the nonlinear model, and some of the subroutine arguments change for the various applications of this simple program.

5. Results and Discussion

Presented below are the experimental results for all runs executed in the sorbent screening for various separation applications and for all diffusivity and isotherm determination experiments. Presented first are some simple vant Hoff plots for CO adsorption on 4A and 5A zeolites for comparison with literature. In each section following, Henry's Law constants are presented for the adsorption of various gases on a given zeolite. Separation factors for various systems of interest are then presented and discussed, leading to selection of a suitable system for diffusion and isotherm measurement. Measured values of micropore diffusion and the pure and binary component isotherms are then presented for this system. Modelling of the binary isotherms from the pure component data is then presented and analyzed.

5.1 Henry's Law Region Adsorption on Molecular Sieves

In preliminary studies of adsorption, it is common to study the sorption of sorbates at low concentration, thereby avoiding the effects of interactions with other sorbate molecules. This low concentration region, which is represented by the initial linear portion of a given adsorption isotherm, is the Henry's Law region. The Henry's Law constant, or slope of this linear portion of the isotherm is measured chromatographically by exposing only a small pulse of sorbate sample carried by a non adsorbing gas to the relatively large sorbent surface area. The following experiments were all conducted as such, and literature comparisons, heats of adsorption, and separation factors were determined through these measurements.

5.1.1 Henry's Law region adsorption - comparison to literature

Adsorption of CO, CH_4, and C_2H_4 on various molecular sieves has been well documented [Eagan & Anderson (1975), Harper et al. (1969), Tezel & Apolonatos (1993), Ruthven & Kumar (1979, 1980),

Ruthven (1976), Haq & Ruthven (1986 a), Yucel & Ruthven (1980 a, b), Brandt & Rudloff (1965)] and thus these systems were chosen to compare with literature to support the experimental method used. Henry's Law constants were determined at various temperatures and the resultant experimental vant Hoff plots and heats of adsorption were compared with those of other authors. Experimental vant Hoff plots from the present study for adsorption of CO on 4A and 5A zeolites are presented along with those of other authors in figure 5.1. The heats of adsorption calculated from equation 16 for various simple systems are compared to those in literature in table 5.1. Both the figure and the table show that the experimental results compare well with existing results. Experimental heats of adsorption are all within 20% (average of 10% difference) of existing reported values for the 16 comparsions made. Since the present study's results were supported by literature data, greater confidence could be taken in the results of the screening studies of other zeolites which were conducted in the same manner. The zeolites screened can then be compared with 4A and 5A zeolites for their capacity for various gas separations.

It should also be noted that in calculating equilibrium separation factors for any gas from N_2, the vant Hoff parameters for N_2 adsorption were required. Those for N_2 adsorption on the natural clinoptilolite and the activated carbon were determined experimentally and are presented under the appropriate headings below. Adsorption of N_2 on common zeolites 4A and 5A has been studied in depth by many authors [Tezel & Apolonatos (1993), Haq & Ruthven (1986 a, b), Miller et al. (1987), Yucel & Ruthven (1980 a, b)]. It was decided that instead of repeating these experiments, appropriate vant Hoff plots for N_2 adsorption on 4A and 5A zeolites and on H - Mordenite would be chosen from literature and used in the calculation of equilibrium separation factors. A vant Hoff plot for N_2 adsorption on H - Mordenite was taken from the work of Tezel & Apolonatos [Tezel & Apolonatos (1993)] as results of the present study compare well with those of Tezel & Apolonatos, and they also used an identical experimental method and the same H - Mordenite as used in the present study. Vant Hoff plots for N_2 adsorption on Linde 4A and 5A zeolites from various sources are presented in figure 5..2. The vant Hoff plots chosen for calculation of separation factors were those of Haq & Ruthven [Haq & Ruthven (1986 a, b)], as they best represent the

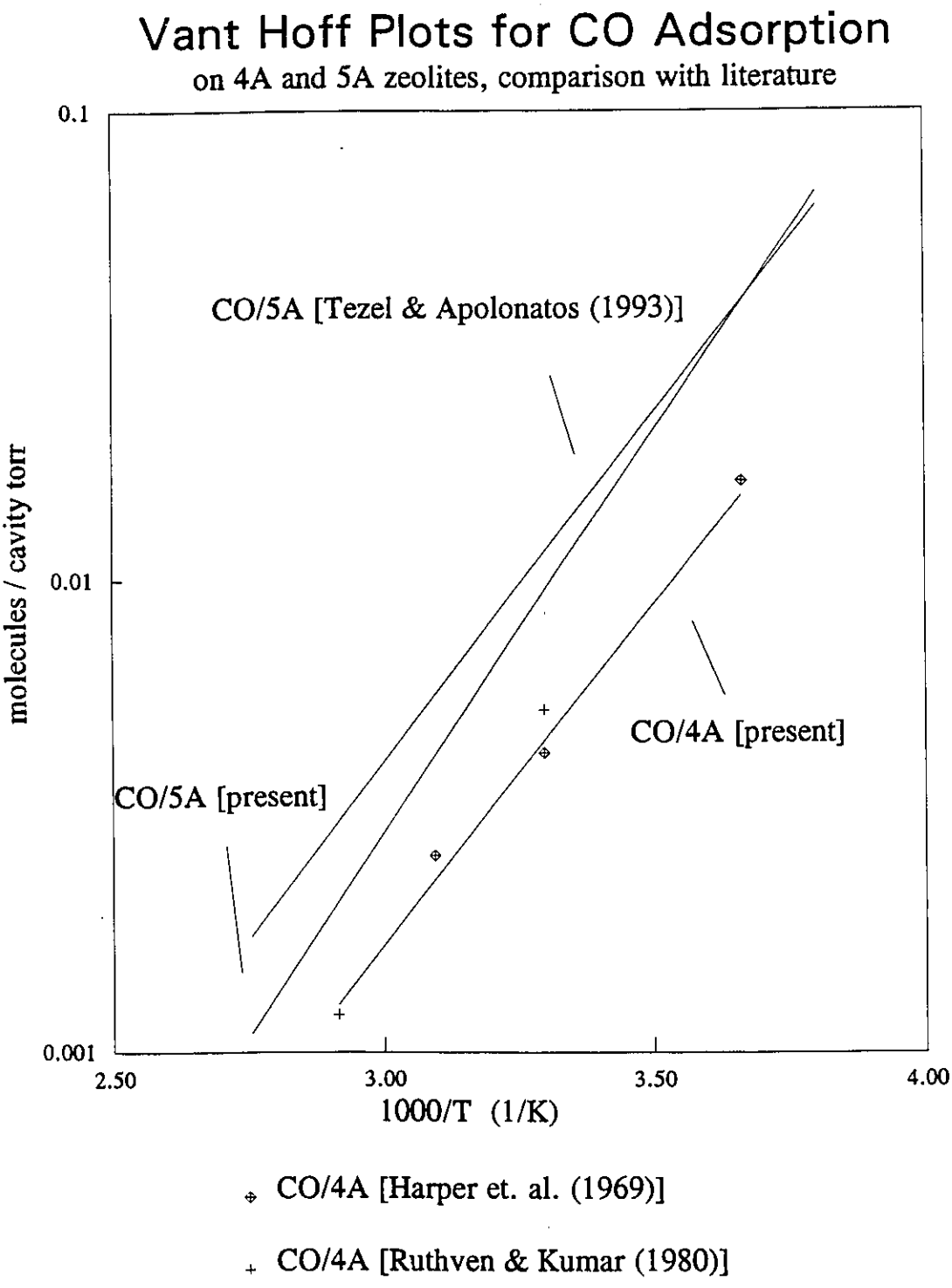

Figure 5.1 : Comparison of experimental van't Hoff plots with literature

Table 5.1 : Comparison of experimental heats of adsorption for CO, CH_4, and C_2H_6 with those in literature

Sorbate	Sorbent	Reference	Temperature Range (K)	$-\Delta H_0$ (kcal/mol)
CO	5A	Present	263 - 363	7.8
	5A	Tezel & Apolonatos (1993)	303 - 333	6.8
CO	4A	Present	243 - 363	6.6
	4A	Eagan & Anderson (1975)	193 - 213	5.3
	4A	Harper et al. (1969)	195 - 323	8.0
	4A	Ruthven & Kumar (1980)	305 - 366	6.1
CO	H - Mordenite	Present	303 - 373	5.6
	H - Mordenite	Tezel & Apolonatos (1993)	263 - 363	6.0
CH_4	5A	Present	243 - 448	4.5
	5A	Ruthven (1976)	190 - 273	5.1
	5A	Haq & Ruthven (1986 b)	290 - 448	4.5
	5A	Tezel & Apolonatos (1993)	273 - 333	4.5
CH_4	4A	Present	243 - 323	3.7
	4A	Yucel & Ruthven (1980 a)	273 - 323	4.3
	4A	Eagan & Anderson (1975)	253 - 273	4.6
	4A	Harper et al. (1969)	195 - 323	2.8 - 4.0
C_2H_6	5A	Present	233 - 358	6.7
	5A	Ruthven & Derrah (1972 a)	230 - 423	6.6
	5A	Brandt & Rudloff (1965)	296 - 372	6.8
C_2H_6	4A	Present	263 - 363	6.8
	4A	Brandt & Rudloff (1965)	296 - 373	6.4
	4A	Yucel & Ruthven (1980 a)	323 - 423	5.9
	4A	Eagan & Anderson (1975)	273 - 293	7.5

group of experimental data obtained over a similar temperature range to the one covered in the present study. Therefore it should be noted that the lines on vant Hoff plots presented below representing N_2 adsorption on H - Mordenite and on 4A and 5A zeolites have been taken from literature, not from the present study.

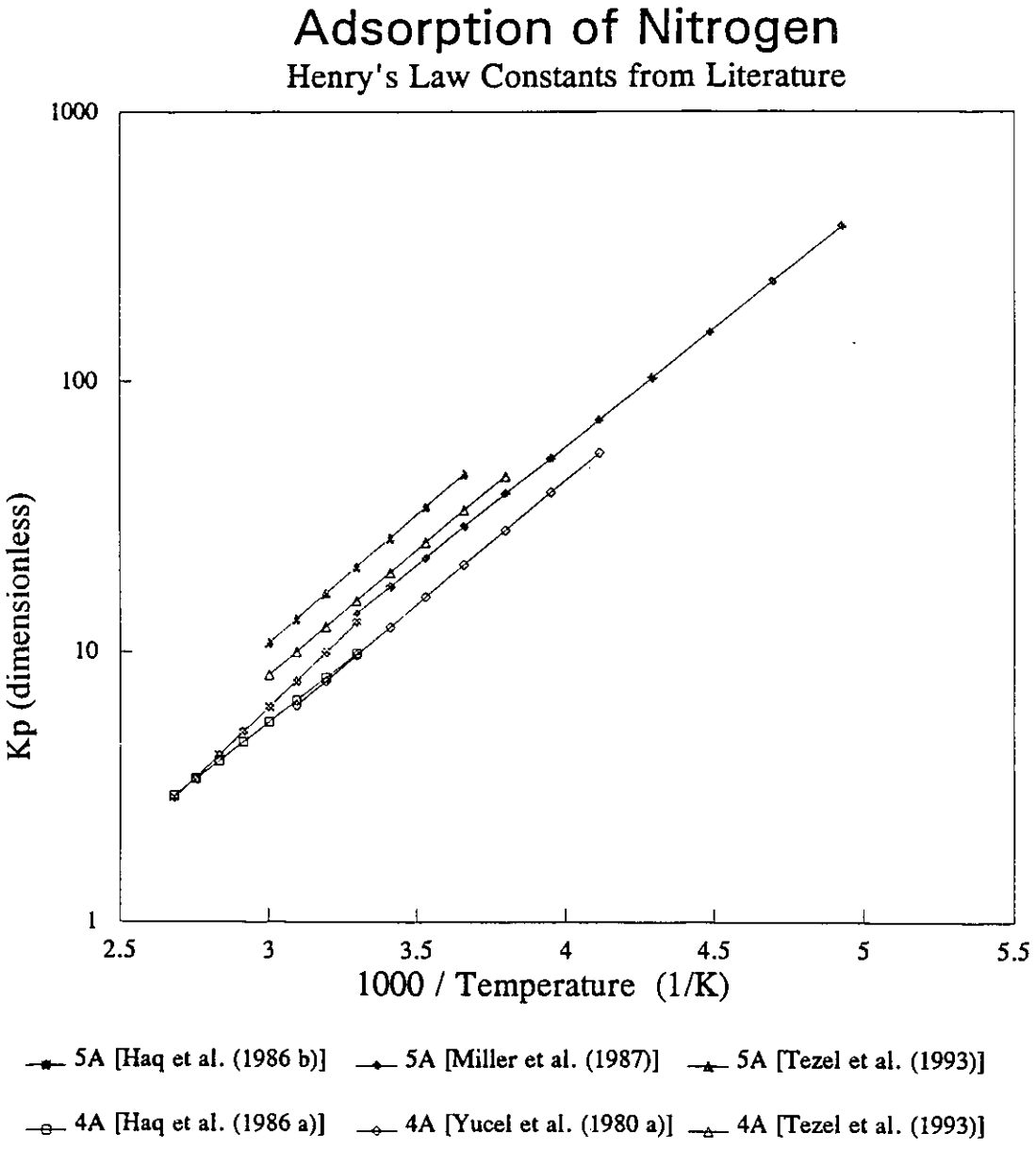

Figure 5.2 : Comparison of N_2 van't Hoff plots from literature

5.1.2 Henry's Law region adsorption on 4A Zeolite

Adsorption of the gases CO, CH_4, C_2H_4 and C_2H_6 was studied on 4A zeolite. Vant Hoff plots for these gases and N_2 [Haq & Ruthven (1986 a)] are presented in figure 5.3. Heats of adsorption and pre exponential factors are presented in table 5.2. The results show that the heats of adsorption decrease in the order C_2H_4 > C_2H_6 > CO > N_2 > CH_4. The C_2H_4 is most strongly adsorbed by the 4A zeolite, likely due to the interaction of the negatively charged p bond with the positive Na^+ cation sites. This is

Table 5.2 Vant Hoff parameters for adsorption on 4A zeolite

Sorbate	Temperature Range (K)	K_0 (dimensionless)	$-\Delta U_0$ (kcal/mol)	$-\Delta H_0$ (kcal/mol)
C_2H_4	313 - 373	.00054	9.96	10.64
C_2H_6	263 - 363	.0107	6.18	6.80
CO	243 - 363	.0022	6.0	6.6
CH_4	243 - 323	.0975	3.11	3.67
N_2	298 - 363	.0159	3.87	4.53

supported by previous work [Schoellner & Mueller (1986)] on adsorption of light hydrocarbons in modified 4A zeolites. The authors found that the π bonded hydrocarbons C_2H_4 and C_2H_6 were strongly retained in 4A zeolite compared to CH_4 and C_2H_6. The present study also shows that the π bonded C_2H_4 is adsorbed much stronger than other sorbates tested.

It is worth noting that the response curves obtained in the C_2H_6 adsorption experiments were not Gaussian distributions, but exhibited a significant degree of tailing. CH_4 adsorption showed tailing to a lesser degree. Sarma & Haynes [Sarma & Haynes (1974)] noted that as the kinetic diameter of the sorbate approaches the micropore diameter of the sorbent, tailing may be observed. C_2H_6 was the largest molecule tested in 4A sieve with a kinetic diameter of 4.0 A [Brandt & Rudloff (1964)], while CH_4 has a kinetic diameter of 3.8, both close to the rated pore diameter of 4A zeolite (3.8 A). Thus it is likely that most of the C_2H_6 passed through the column quickly, but that some was trapped and slowly diffused out of the

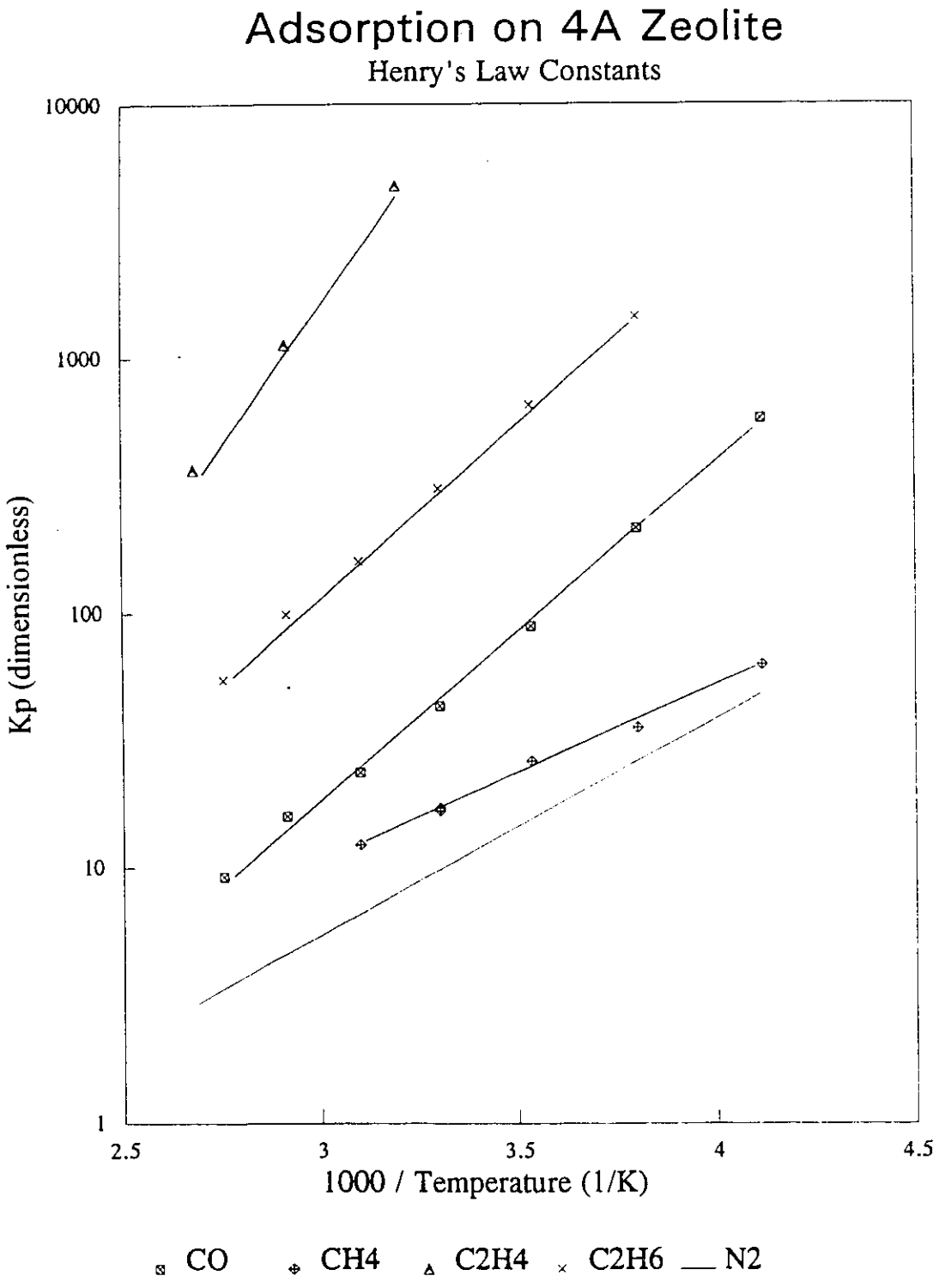

Figure 5.3 : Van't Hoff plots for adsorption on 4A zeolite

column, thereby causing the tailing of the response peak. This possibility is further supported in a letter by Habgood and MacDonald [Habgood & MacDonald (1970)] dealing with the effect of micropores on peak shape. They have concluded in analyzing results of C_2H_6 and CH_4 adsorption on 4A zeolite [Oberholtzer & Rogers (1969 a)] that the hydrocarbon diffusivities in the micropores are so low that the response peak shapes are attributed mostly to dead volume and macropore diffusion, with some tailing due to limited penetration into the micropores. Reasonable agreement with literature indicates that the heats of adsorption calculated in the present study are accurate, but measurement of micropore diffusivity in these hydrocarbon - 4A systems by chromatography under the present conditions would be difficult, as the response peak does not fully represent micropore diffusion. Methods of determining required column conditions for production of a response peak representing only micropore diffusion have been developed [Habgood & MacDonald (1970)], but require diffusivity data beyond the scope of this study.

Adsorption of the CO sample pulse produced response peaks with near Gaussian distributions and low means. The kinetic diameter of CO is also large relative to the pore diameter of 4A zeolite (3.76 A compared to 3.8 A), but no tailing was observed. As shown in table 5.1, the experimental heats of adsorption of CO on 4A zeolite obtained from literature range from 5.3 to 8 kcal/mol. The results of the present study show a heat of adsorption of 6.6 kcal/mol, in the middle of the literature range.

Adsorption parameters for N_2 adsorption on 4A zeolite were taken from Haq & Ruthven [Haq & Ruthven (1986 a)] and therefore will not be analyzed in depth. It is logical, however, that N_2 would be relatively weakly adsorbed in 4A zeolite due to its weak polarity (quadropole) and small size (3.64 A), as is shown in figure 5.3.

5.1.3 Henry's Law region adsorption on 5A Zeolite

Adsorption of the gases CO, NO, CH_4, C_2H_4 and C_2H_6 was studied on 5A zeolite. Vant Hoff plots for these gases and that for N_2 [Haq & Ruthven (1986 b)] are presented in figure 5.4. Heats of adsorption and pre exponential factors are presented in table 5.3. The results show that the heats of adsorption decrease in the order $C_2H_4 > CO > C_2H_6 > N_2 > NO > CH_4$. The C_2H_4 is most strongly adsorbed by the

Table 5.3 Vant Hoff parameters for adsorption on 5A zeolite

Sorbate	Temperature Range (K)	K_0 (dimensionless)	$-\Delta U_0$ (kcal/mol)	$-\Delta H_0$ (kcal/mol)
C_2H_4	343 - 473	.00091	10.51	11.32
C_2H_6	233 - 358	.0107	6.20	6.78
CO	263 - 363	.00062	7.2	7.8
N_2	273 - 373	.00455	4.78	5.44
NO	243 - 383	.016	4.4	5.0
CH_4	243 - 448	.0384	3.8	4.5

5A zeolite, and this is primarily due to the direct interaction between the π bonded C_2H_4 and the divalent Ca^{++} ions in the 5A zeolite, as discussed by Derrah, Loughlin & Ruthven [Derrah et al. (1972)] and Emesh & Gay [Emesh & Gay (1985)]. This phenomenon has attracted much attention, and Schoellner & Mueller [Schoellner & Mueller (1986)] have examined the effect of monovalent and bivalent cations on the adsorption of alkenes. They showed an increase in the strength of C_2H_4 adsorption and in the alkene / alkane separation factor with addition of divalent ions (up to 20% of original Na^+ ions exchanged). Ali & Gay [Ali & Gay (1980, 1981)] found through numerous NMR studies that olefins with the π bond readily accessible chemisorbed on ZnO forming a π complex bonding state. As the olefin grows in size this effect is diminished due to steric factors.

Adsorption of C_2H_6 on A zeolite has been studied in depth. It has been noted by Loughlin & Ruthven [Loughlin & Ruthven (1972)] that the low coverage heat of adsorption of C_2H_6 on A zeolites is relatively insensitive to the nature of the cation. The heat of adsorption arises principally from the dispersion, repulsion, and polarization potentials. The first two potentials do not vary significantly with cation nature as the major contribution is from the oxygen framework. The polarization potential, however, varies significantly with ion nature and is higher for divalent ions than for monovalent ions. This implies that if a cation change (monovalent to divalent) does not produce a large heat of adsorption change for a given gas in a given structure, then the polarizaton potential is not a major contribution to the

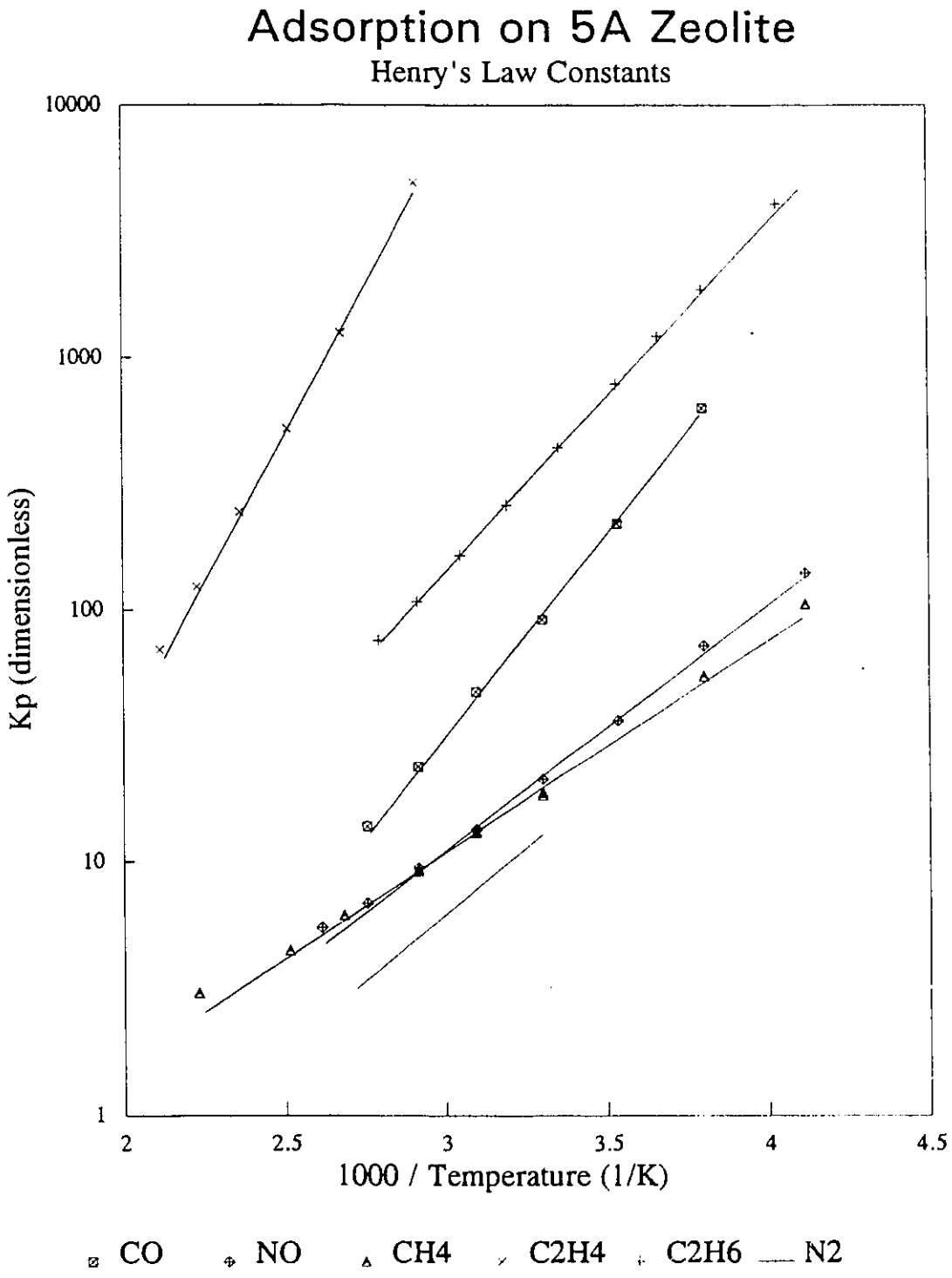

Figure 5.4 : Van't Hoff plots for adsorption on 5A zeolite

heat of adsorption. These observations are supported by the results of the present study, which show the heat of adsorption of C_2H_6 to be insignificantly different on 4A (Na^+) and 5A (Ca^{++} and Na^+) zeolites. Although the strongly quadropolar C_2H_4 shows an increase in heat of adsorption with introduction of divalent ions, the relatively non - polar C_2H_6 shows no such change. Adsorption of the small (kinetic diameter = 3.8 A), non - polar CH_4 on 5A zeolite resulted in a low heat of adsorption, as expected. The CH_4 heats of adsorption on A zeolites determined in this study agree well with literature results, as shown in table 5.1. It is evident that the addition of divalent cations can be useful for the alkene / alkane separation, as it will positively affect the heat of adsorption of the alkene and have only a small or negligible effect on the alkane adsorption. At high divalent ion levels this effect may be diminished due to probems with pore blocking and with bivalent cations occupying secondary, less accessible sites.

Adsorption of the polar compound CO (kinetic diameter = 3.76 A) shows similar trends to those observed with quadropolar C_2H_4. The heat of adsorption increases significantly with the inclusion of Ca^{++} ions in the zeolite A framework. Emesh & Gay [Emesh & Gay (1985)] have used NMR methods to determine that CO is specifically adsorbed on divalent cations in the A zeolite structure. Egerton & Stone [Egerton & Stone (1983)] have shown that CO adsorption may simply be interpreted as one CO molecule adsorbing on each divalent ion. Thus the higher heat of adsorption of CO in 5A (compared to 4A) zeolite is expected due to the presence of the stronger adsorption sites. Adsorption of NO (kinetic diameter = 3.17 A) in 5A zeolite yielded the lowest heat of adsorption of the polar molecules tested. This was still higher than that of non - polar CH_4 (kinetic diameter = 3.8 A). Kaneko & Inouye [Kaneko & Inouye (1988)] studied NO adsorption on a large variety of industrial and metal impregnated porous materials. Their experimental isotherms show that NO adsorption capacity up to 80 kPa is 4 to 5 times more on 5A zeolite than on 4A and 3A zeolites. These differences are too large to be attributed to change in pore capacity alone, and are likely due to the interaction of the NO dipole and the Ca^{++} ions in the 5A structure. The experiments on A zeolites revealed a significant increase in heat of adsorption of polar compounds with the introduction of divalent cations. It is important to recognize that the separations being considered in this study (alkene / alkane and CO, NO, and CO_2 / N_2) all involve separation of a relatively polar

compound from a non - polar one (N_2 is slightly quadropolar). It seems that any and all of these separations may be facilitated by the introduction of divalent cations into a given zeolite structure, provided that these ions are accessible and that they do not significantly block pores. The discussion of the effect of divalent cations on the adsorption of polar compounds continues as the remaining data is presented.

5.1.4 Henry's Law region adsorption on X - Zeolites

The use of the large pore X zeolites for hydrocarbon applications is quite common. As a result, an industrial 13X zeolite and an ion exchanged Ca X zeolite were tested for adsorption of C_2H_4 and CH_4. The vant Hoff parameters for these systems are presented in table 5.4, and plots of these relationships are given in figure 5.5.

Initially only 13X zeolite was examined. After reviewing the results on A zeolites and the existing literature, it was decided to examine the effect of adding a divalent cation to the X zeolite structure. The specific interaction between the divalent cations in zeolite A and the π bond of C_2H_4 resulted in strong adsorption of C_2H_4 and a high C_2H_4 / CH_4 separation factor on 5A zeolite. For this reason Ca^{++} was partially exchanged for existing Na^+ cations in the 13X zeolite (see section 4.2.1), replacing 61% of the Na^+ with Ca^{++}, yielding a cation content similar to that of industrial 10X zeolite. The exact compositions of the X zeolites used, as measured by direct current plasma spectroscopy methods are

Table 5.4 : Vant Hoff parameters for adsorption on X zeolites

System	Temperature Range (K)	K_0 (dimensionless)	$-\Delta U_0$ (kcal/mol)	$-\Delta H_0$ (kcal/mol)
C_2H_4 / 13X	323 - 473	.0038	8.37	9.17
CH_4 / 13X	323 - 473	.084	2.98	3.77
C_2H_4 / CaX	373 - 473	.00018	13.1	13.9
CH_4 / CaX	323 - 473	.09	3.11	3.89

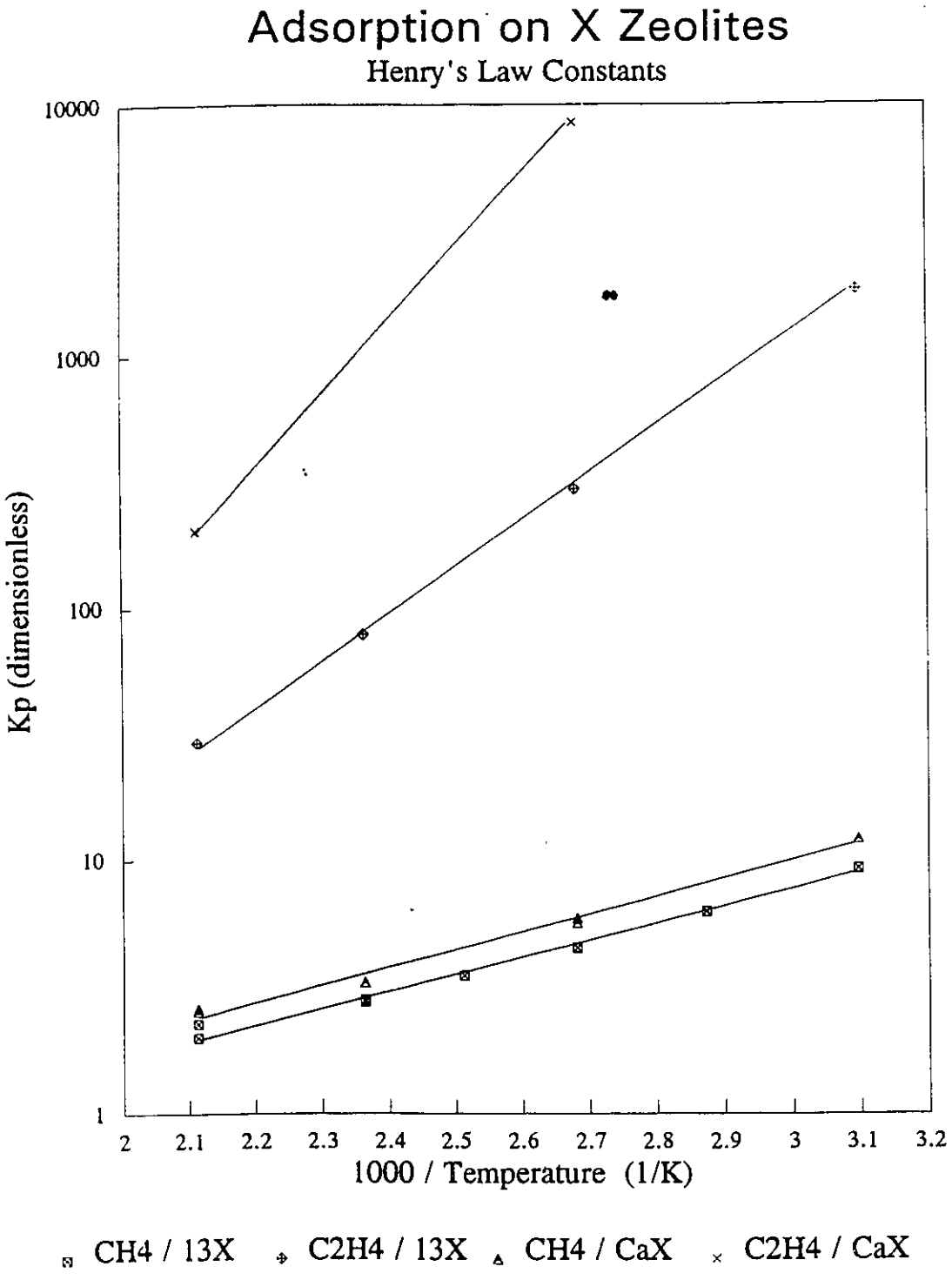

Figure 5.5 : Van't Hoff plots for adsorption on X zeolites

given in table 5.5. The remaining component (about 23%) in both X zeolites was H_2O. The CaX zeolite yielded a very high heat of sorption of C_2H_4, as expected. More information on the effect of divalent cations on this separation is provided in table 5.4. The heat of sorption of CH_4 changes negligibly(3%)

Table 5.5 : Composition of CaX zeolite

Zeolite	% SiO_2	% Al_2O_3	% MnO	% MgO	% CaO	% Na_2O	% K_2O	% Fe_2O_3
NaX	39.48	23.28	0.01	0.05	0.01	12.08	0.28	1.52
CaX	38.49	22.23	0.01	0.06	6.74	4.76	0.23	1.45

with the ion change in X zeolite. This is logical, as the non poiar CH_4 is relatively unaffected by the monovalent or divalent cation sites, and because the large pores of the 13X and the CaX (both > 7A) do not sterically hinder diffusion of CH_4 through the micropores. The heat of sorption of C_2H_4, however, increases 52% with partial exchange of the Na^+ cations. Thus it is clear that the nature of the adsorption of the non polar CH_4 is independent of the cation nature, while that of C_2H_4 is largely dependent on the nature of the cation. Carter has reported similar observations in the strong adsorption of C_2H_4 on AgX and CdX zeolites compared to that on NaX zeolite [Carter et al. (1966)]. Their reported calorimetric heat of adsorption of 8.6 kcal/mol for C_2H_4 on NaX agrees well with that determined here. However, the heat of adsorption of C_2H_4 on a CaX zeolite of undisclosed composition (probably near 100% Ca^{++}) was reported as being only slightly higher (9.1 kcal/mol) than that on NaX, contradictory to the results obtained here. Other results of C_2H_4 adsorption on X zeolites obtained by Habgood are more in agreement with those obtained in the present study [Habgood (1964)]. He chromatographically measured a heat of sorption of 8.4 kcal/mol for C_2H_4 on NaX zeolite, again in good agreement with Carter [Carter et al. (1966)] and with the experimental results obtained here. However, his experimental heat of sorption of C_2H_4 on a nearly 100% exchanged CaX zeolite (approximately 19 kcal/mol) showed notably stronger sorption than on NaX zeolite. With experimental heats of sorption of 9.1, 13.9 and 19 kcal/mol for various CaX / C_2H_4 systems, it seems that the heat of sorption of C_2H_4 is strongly dependent not only on cation type, but on specific amount and location of the cation. In any case the separation of C_2H_4 from CH_4 can be facilitated by the

inclusion of accessible divalent cations in the micropore structure. CaX zeolite has showed great promise for the separation of CO from N_2 and O_2 by the selective strong adsorption of the polar CO [Danner & Wenzel (1969)]. These literature results support the present ones in the use of divalent cations in the separation of components of greatly differing polarity.

Some problems were encountered in the repeatability of the measurement of C_2H_4 heats of sorption on the CaX zeolite. In running C_2H_4 adsorption experiments on three separate days in a 15 day period, the Henry's law constant at two temperatures decreased some 25% after the first and second sets of experiments. Treating these three data sets as separate vant Hoff plots yielded three virtually identical heats of adsorption. However, the value of K_o varied between the three data sets. There are a variety of possible reasons for this. It may be that the CaX zeolite was irreversibly adsorbing impurities in the carrier stream. This is unlikely given the purity of the carrier gas used (see table 3.1). Another possibilty is that some of the C_2H_4 was irreversibly adsorbed with each experiment, yielding lower capacities with each consecutive experiment under given conditions. Carter found it difficult to remove C_2H_4 from certain forms of X zeolite [Carter et al. (1966)]. This possibility is not supported by the experimental results, as good repeatability was found between identical condition experiments run consecutively (ie, both in one day), but not between identical condition experiments run ten days apart. The third possibility is that the cation distribution changed in some manner. Considering that the column was held at relatively high temperatures (373 to 473 K) for the entire time that the CaX zeolite was in the column, it is possible that the Ca^{++} and Na^{+} ions were gradually displaced in some manner.

The precise cause of this repeatability problem could be examined further by regenerating the sieve to conduct further experiments and by doing more experiments on a column of fresh CaX zeolite, but such studies were not within the scope of this project. To ensure reporting accurate parameters for adsorption on the freshly regenerated CaX zeolite, the vant Hoff plot was derived only from the first two runs taken on the same day at temperatures 100 K apart. Thus the adsorption parameters for C_2H_4 on CaX zeolite presented in table 5.4 were taken from a two point line.

A slight curvature of the vant Hoff plot for CH_4 adsorption on CaX zeolite was also noticed. This anomaly, however, is easily explained. It has been shown that for weakly adsorbed species at high temperatures, the temperature dependance of K_0 may become significant, leading to curvature of the vant Hoff plot [Ruthven & Kumar (1980)]. In the present case the CH_4 is weakly adsorbed (heat of sorption of 3.9 kcal/mol) at high temperatures (373 to 473 K). The curvature of the plot, then, is somewhat expected. Furthermore the chromatographic method is applicable to calculating Henry's Law constants only when K_p > 10. Since the K_p values for CH_4 on CaX zeolite range from 2.5 to 12 under these conditions, the chromatographic method used is suspect and a straight line vant Hoff relationship is not necessarily expected.

5.1.5 Henry's Law region adsorption on H - Mordenite

Adsorption of the gases CO, CH_4, and C_2H_4 was studied on H - Mordenite. The effectively uni - dimensional channel structure of H - Mordenite and the lack of bivalent cation sites did not make H - Mordenite a particularly promising sorbent for the separations under consideration, so it was not screened for adsorption of all gases. Vant Hoff plots for adsorption of these gases and N_2 [Tezel & Apolonatos (1993)] are presented in figure 5.6. The heats of adsorption and pre exponential factors are given in table 5.6. Heats of adsorption decrease in the order $C_2H_4 > CH_4 > CO > N_2$. The order seems to imply that steric factors rather than dipole - cation interactions are the main influence on adsorption capacity. Otherwise the heat of adsorption of CH_4 would be expected to be less than that of CO, as it was in 4A and 5A

Table 5.6 : Vant Hoff parameters for adsorption on H - Mordenite

Sorbate	Temperature Range (K)	K_0 (dimensionless)	$-\Delta U_0$ (kcal/mol)	$-\Delta H_0$ (kcal/mol)
C_2H_4	293 - 343	.0012	9.06	9.71
CH_4	233 - 323	.0041	5.37	5.92
CO	303 - 373	.005	5.0	5.6
N_2	243 - 448	.0384	3.42	3.67

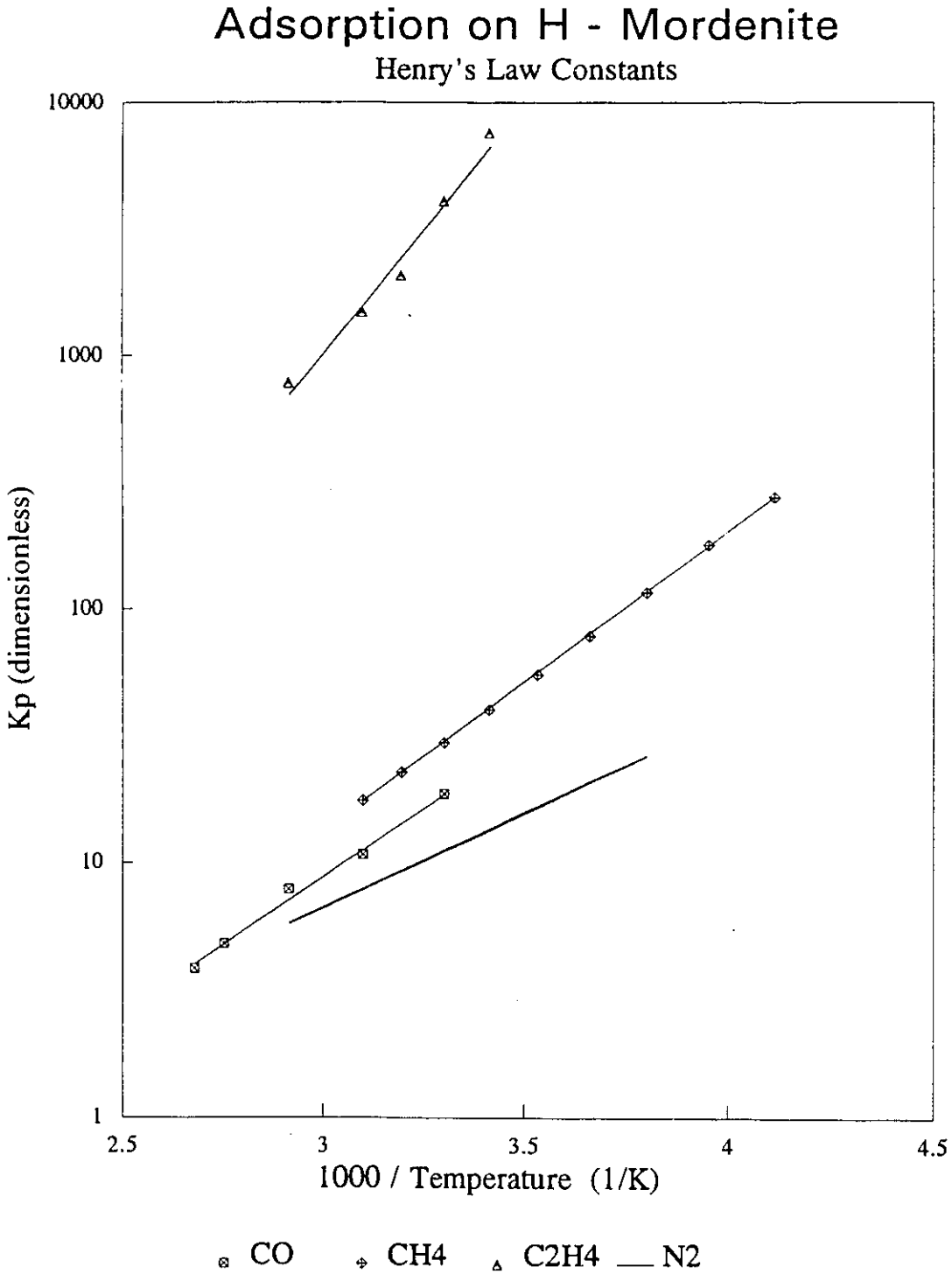

Figure 5.6 : Van't Hoff plots for adsorption on H - mordenite

zeolites. Hayhurst & Lee [Hayhurst & Lee (1983)] and Ma & Mancel [Ma & Mancel (1973)] have shown that adsorption of light hydrocarbons and weakly quadropolar gases is relatively independent of the electrostatic interaction between the mordenite monovalent cation(s) and the sorbate. They found the dispersion and repulsion forces to be dominant, and that heats of adsorption of these gases were more effected by steric factors than by electrostatic factors. These observations are supported by the present study, as the nonpolar CH_4 has a higher heat of adsorption than CO. Both molecules have similar kinetic diameters (3.8 and 3.76, respectively) so if the polarity of the sorbate significantly influenced the heat of adsorption, it would be expected that the heat of adsorption of polar CO would be greater than that of CH_4. Ruthven [Ruthven (1984 b)] has pointed out that although the rated pore diameter of H - Mordenite is approximately 7 A, the diffusion of hydrocarbons through these pores is impeded by extraneous matter. The listed order of heats of adsorption is logical if these factors are taken into consideration. The use of a monovalent cation in mordenite for the separations under consideration does not seem advantageous. The lack of strong adsorption sites and the slow diffusion for all species arising from the one dimensional pore structure of the mordenite crystal are significant drawbacks. A divalent form of mordenite may be found superior to monovalent forms for these polar / non polar separations assuming no significant pore blocking occurs. Evidence of divalent cations (Ca^{++}) strongly influencing the adsorption of slightly polar compounds on mordenite has been documented [Hayhurst & Lee (1983)].

5.1.6 Henry's Law region adsorption on Clinoptilolite

Adsorption of the gases CO, NO, CO_2, N_2, C_2H_6, CH_4, and C_2H_4 was studied on the natural clinoptilolite. Vant Hoff plots for adsorption of CO, NO, N_2, C_2H_6, and CH_4 are presented in figure 5.7. Major complications were encountered in the adsorption measurements of CO_2 and C_2H_4, and for this reason vant Hoff plots for these gases are not given in figure 5.7, nor are the heats of adsorption of these gases presented along with those of the other gases in table 5.7. The heats of adsorption decrease in the order CO > NO, N_2 > C_2H_6, CH_4. The nature of the clinoptilolite (a natural zeolite with various cations) makes analysis of adsorption results somewhat more complicated.

Table 5.7 Vant Hoff parameters for adsorption on Clinoptilolite

Sorbate	Temperature Range (K)	K_0 (dimensionless)	$-\Delta U_0$ (kcal/mol)	$-\Delta H_0$ (kcal/mol)
CO	323 - 473	.000073	10.8	11.6
NO	373 - 473	.00063	8.6	9.4
N_2	323 - 423	.00019	8.7	9.5
CH_4	373 - 523	.0099	6.2	7.1
C_2H_6	348 - 498	.0145	6.6	7.5

Heats of adsorption of CO, NO and N_2 were much higher on clinoptilolite than on any other zeolite tested. The clinoptilolite examined contained approximately 1.46 Ca^{++} ions, 1.02 Mg^{++} ions and 1.34 K^+ ions, with small quantities of Na^+ (.22 ions) in the average unit cell, as shown in table 5.8 [Sirkecioglu et al. (1992)]. Much work has been done on determinining ion location in clinoptilolite [Koyama & Takeuchi (1977)]. Figure 5.8 demonstrates the favored cation positions in channels A (10 member ring) and B (8 member ring) in the z direction and channel C (8 member ring) in the x direction

Table 5.8 : Unit cell composition of natural Turkish clinoptilolite (based on 72 O atoms)

Si	Al	Fe	Na	K	Ca	Mg	Si/Al
28.98	6.82	0.36	0.22	1.34	1.46	1.02	4.25

[Ackley & Yang (1991 b)]. It has been suggested that Ca^{++} and Na^+, in the M(1) and M(2) positions are the most efficient pore blockers in clinoptilolite as they are located at pore intersections. Given four combined M(1) and M(2) sites per unit cell, an average of 1.68 of these four sites are occupied by these intersection blocking ions. Some ten member rings would also be blocked by the Mg^{++} cations in the M(4) sites, an average of one in each cell. The M(3) sites would be partially filled by K^+ cations. It has been shown that excessive quantities of Ca^{++} or Na^+ in clinoptilolite can lead to molecular sieving of CO_2, CH_4 and N_2 due to excessive pore blocking [Sirkecioglu et al. (1992), Ackley & Yang (1991 b)]. In particular fully exchanged Ca^{++} clinoptilolites have shown almost complete exclusion of these gases. In the natural

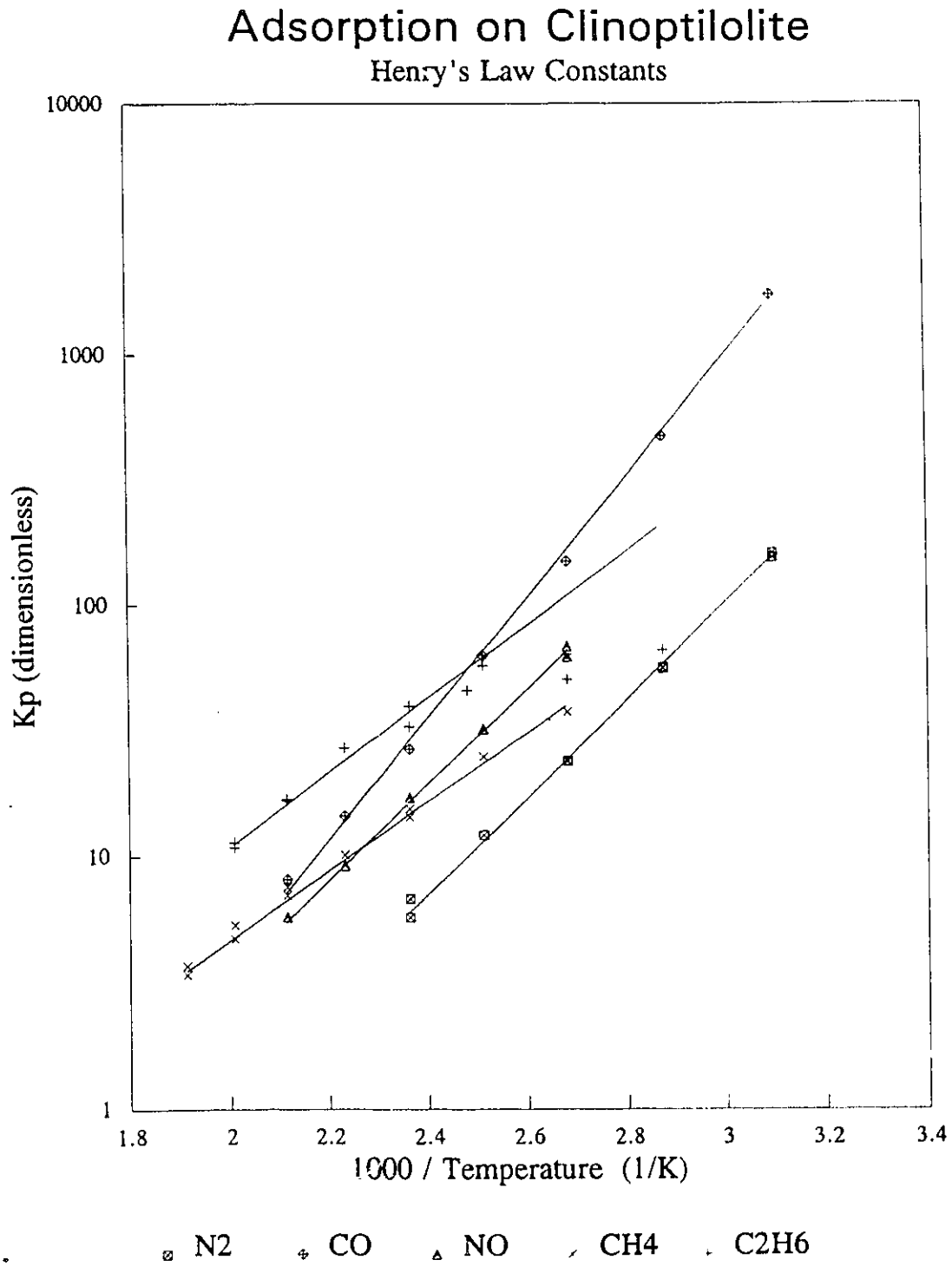

Figure 5.7 : Van't Hoff plots for adsorption on clinoptilolite

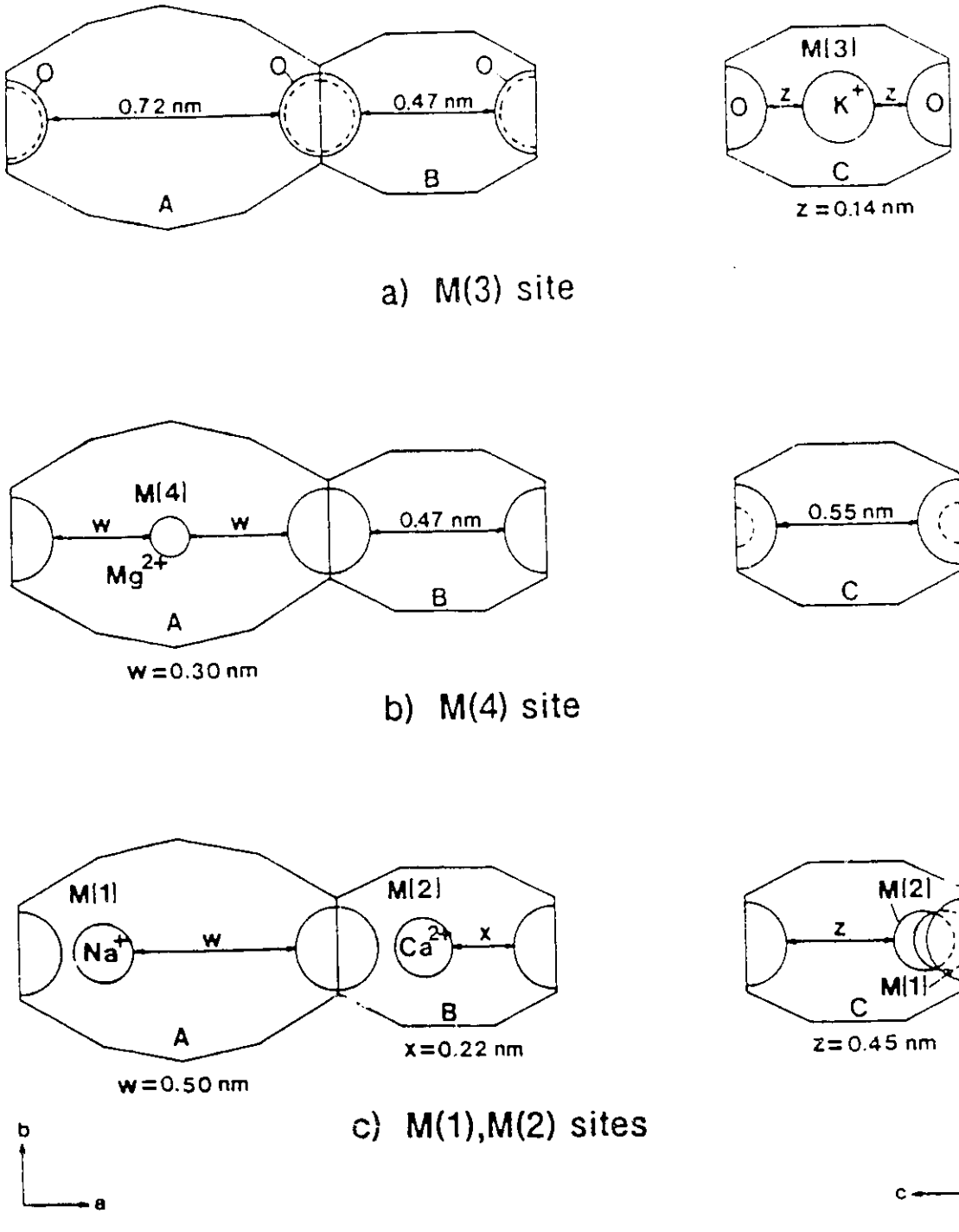

Figure 5.8 : Common cation locations in the clinoptilolite unit cell

zeolite examined these intersection blocking ions are not present in great quantities. The symmetrical nature of the experimental GC response curves and the high heats of adsorption seem to indicate that none of CO, NO or N_2 are severely subject to molecular sieving in the cationic form of clinoptilolite studied [Haynes (1975)]. The high heats of adsorption of these gases are probably attributed to the interaction of their dipole / quadropole with the accessible ions. CO has been found to form specific complexes with divalent ions in other zeolite structures [Emesh & Gay (1985)]. Strong interaction between the N_2 quadropole and the accessible divalent cations Ca^{++} or Mg^{++} in clinoptilolite has also been documented [Ackley & Yang (1991 a)]. Similarly the relatively high heat of adsorption of NO is likely due to polarization forces resulting from dipole interactions with the strong cationic sites. NO is significantly smaller than CO and N_2 (3.17 A compared to 3.76 and 3.64, respectively) and would not be strongly subject to the molecular sieving effects of the clinoptilolite. Since all three molecules (CO, NO, and N_2) appear to be small enough to diffuse into the clinoptilolite structure, it is reasonable to assume that the relatively high initial heats of sorption of these compounds is mainly a result of their dipolar or quadropolar interactions with the available divalent Ca^{++} and Mg^{++} ions.

Adsorption of CO_2 on the natural clinoptilolite was too strong to produce an interpretable response peak with the existing experimental set up. In recording the column response to a pulse injection of CO_2, no peak was discovered for 24 hours. Any peak emerging after this time would be so diffuse as to be undetectable. Even at tempertures in excess of 400 K no peak was detected. This indicates that the CO_2 injected was either irreversibly or at least very strongly adsorbed. Previous studies of CO_2 adsorption on clinoptilolite have shown strong adsorption and a high degree of irreversibility [Inui et al. (1988)]. It is possible that some ionic sites in the clinoptilolite undergo powerful interactions with the polar CO_2 holding it fast under the given conditions. CO_2 adsorption isotherms have been determined by other authors on the same clinoptilolite as used in this study, and the highly rectangular isotherms obtained also demonstrate strong adsorption of CO_2. Unfortunately the isotherms were not tested for reversibility [Sirkecioglu et al. (1992)]. The chromatographic method may be applied to CO_2 adsorption measurements,

but not with the given apparatus. A smaller column or even use of a zero length coulmn method may prove more useful for the measurement of such a strongly adsorbed species.

Adsorption of various hydrocarbons on the natural clinoptilolite was also studied, but various difficulties were encountered. In measuring the Henry's Law constants for CH_4 and C_2H_6, tailing was observed in the response peaks. Tailing of response curves in chromatographic measurement of adsorption properties has been found to be the result of limiting micropore or macropore diffusion. As diffusion into one of these systems is slow, some of the sorbate gas passes through the column never having penetrated the pores and some enters and very slowly diffuses through the porous structure [Habgood & MacDonald (1970), Haynes (1975)]. In the case of CH_4 and C_2H_6 adsorption on 4A zeolite, which has been studied here and by other authors [Oberholtzer & Rogers (1969 a)], skewed response curves were obtained in adsorption measurements over a wide temperature range. This was attributed to the slow diffusion of CH_4 and C_2H_6 (kinetic diameters of 3.8 and 4.0 A, respectively) through the 3.8 A pore openings in 4A zeolite. No such tailing was observed in the adsorption of these same hydrocarbons in 5A zeolite (pore diameter = 4.4 A). Given the rated pore diameters of clinoptilolite (see section 3.2.4), it seems that only the unblocked ten member rings would allow free passage for both of these light hydrocarbons. The eight member rings have pore dimensions comparable to 4A zeolite when partially blocked, and it has been shown that CH_4 is effectively blocked from the micropores in various ionic variations of clinoptilolite [Frankiewicz & Donnelly (1983), Ackley & Yang (1991 b)]. It is logical to assume that the tailing in the present study's CH_4 and C_2H_6 adsorption measurements are due to this limiting diffusion of the hydrocarbons into the micropore structure. The values obtained in this study for adsorption of CH_4 and C_2H_6 on clinoptilolite should therefore be taken cautiously, due to the fact that the response peaks analysed likely do not exclusively represent micropore diffusion, and due to the potential increase in calculational error resulting from analyzing tailing peaks.

Adsorption of C_2H_4 on the clinoptilolite was even more difficult to deal with. Initial experiments showed strong retention of C_2H_4, but subsequent experiments, even under identical conditions, revealed declining retention of C_2H_4. At 423 K the first response peak measured for C_2H_4 adsorption yielded an

extremely high dimensionless K_p' of approximately 15000. Following two weeks of C_2H_4 adsorption experiments on the same column, an identical run at 423 K yielded a highly skewed peak and a dimensionless K_p' of approximately 2500. It seemed that with each exposure of the clinoptilolite column to a C_2H_4 pulse, the capacity of the zeolite was affected. This was supported by CH_4 adsorption experiments done before and after some C_2H_4 experiments. On a fresh column the dimensionless Kp of CH_4 at 423 K was measured to be about 20. After two weeks of C_2H_4 experiments the CH_4 experiment was repeated, yielding a dimensionless Kp of about 5 and showing a profound change in the response curve. Repeating both the C_2H_4 and CH_4 experiments on a fresh clinoptilolite column yielded results matching those obtained on the original column. Given the varying nature of the clinoptilolite cations and cation sites, it is likely that some cations (probably divalent ones) have a great affinity for the C_2H_4 π bond and as a result they irreversibly adsorb the C_2H_4, leaving fewer adsorption sites and contributing to pore blocking. Evidence for strong interaction between the C_2H_4 π bond and divalent cations in A and X zeolites has been well documented [Derrah et al. (1972), Loughlin & Ruthven (1972), Emesh & Gay (1985), Schoellner & Mueller (1986), Carter et al. (1966)]. The assumption that the partial irreversible adsorption of C_2H_4 is the cause of the clinoptilolite's decreasing capacity with each C_2H_4 adsorption experiment seems reasonable. As a result, no exact value for the initial heat of adsorption of C_2H_4 was obtained. An estimate derived from only two points (the first two experiments executed on the fresh column) yielded a heat of adsorption of approximately 14 kcal / mol, the highest heat of sorption measured for C_2H_4 on the molecular sieves tested.

5.1.7 Henry's Law region adsorption on Activated Carbon

Adsorption of CO, NO, CO_2, and N_2 were studied on a Supelco activated carbon. Figure 5.9 shows the vant Hoff plots and table 5.9 gives the Arrhenius equation parameters for these gases on the activated carbon. The heats of adsorption were found to decrease in the order $CO_2 > CO > N_2 > NO$. It should be noted that the heats of sorption seem to decrease with molecular size, with the exception of CO_2.

The kinetic radii of the compounds CO_2, CO, N_2, and NO are 3.3, 3.76, 3.64, and 3.17 A, respectively. The molecular mass of a compound is inversely proportional to its macropore diffusion (Knudsen and molecular) characteristics, and the molecular mass of CO_2 is some 30% greater than that of the other compunds. If wall effects are negligible due to the relatively large micorpore size distribution, then diffusion through the micropores would be controlled by species size, shape and mass. In this case one may expect the CO_2 to be slower in moving through the pores than the other larger, lighter species. The lack of cations and the rated pore diameter of 3 to 40 A are the reasons that the measured heats of sorption and K_p values for the activated carbon are lower than those on all other zeolites tested.

Table 5.9 : Vant Hoff parameters for adsorption on Activated Carbon

Sorbate	Temperature Range (K)	K_0 (dimensionless)	$-\Delta U_0$ (kcal/mol)	$-\Delta H_0$ (kcal/mol)
CO_2	303 - 423	.0063	5.9	6.7
CO	303 - 423	.044	3.5	4.2
N_2	303 - 403	.042	3.2	3.9
NO	303 - 403	.084	3.0	3.7

The vant Hoff plots for adsorption on the activated carbon, particularily that of N_2, seem to show some curvature. Just as with the adsorption of CH_4 on CaX zeolite, these species are weakly adsorbed (in general K_p less than 10) at relatively high temperatures. The curvature of the vant Hoff plot arises from the fact that the species is relatively weakly adsorbed, as discussed at the end of section 5.1.4.

Although an activated carbon more suitable to the specific separations being studied here could have been selected, it would likely not have provided the high separation factors of the zeolites. The zeolites take advantage more of the sorbates' differences in charge distribution (ie, polarity) than the size and mass of the sorbent. Activated carbons offer various industrial advantages but were not considered any further in this study due to the low measured separation factors. They do, however, provide some interesting insight to the different separation mechanisms of zeolites and molecular sieve carbons. For the zeolites with strong, accessible cationic sites, the heats of sorption were large and generally decreased

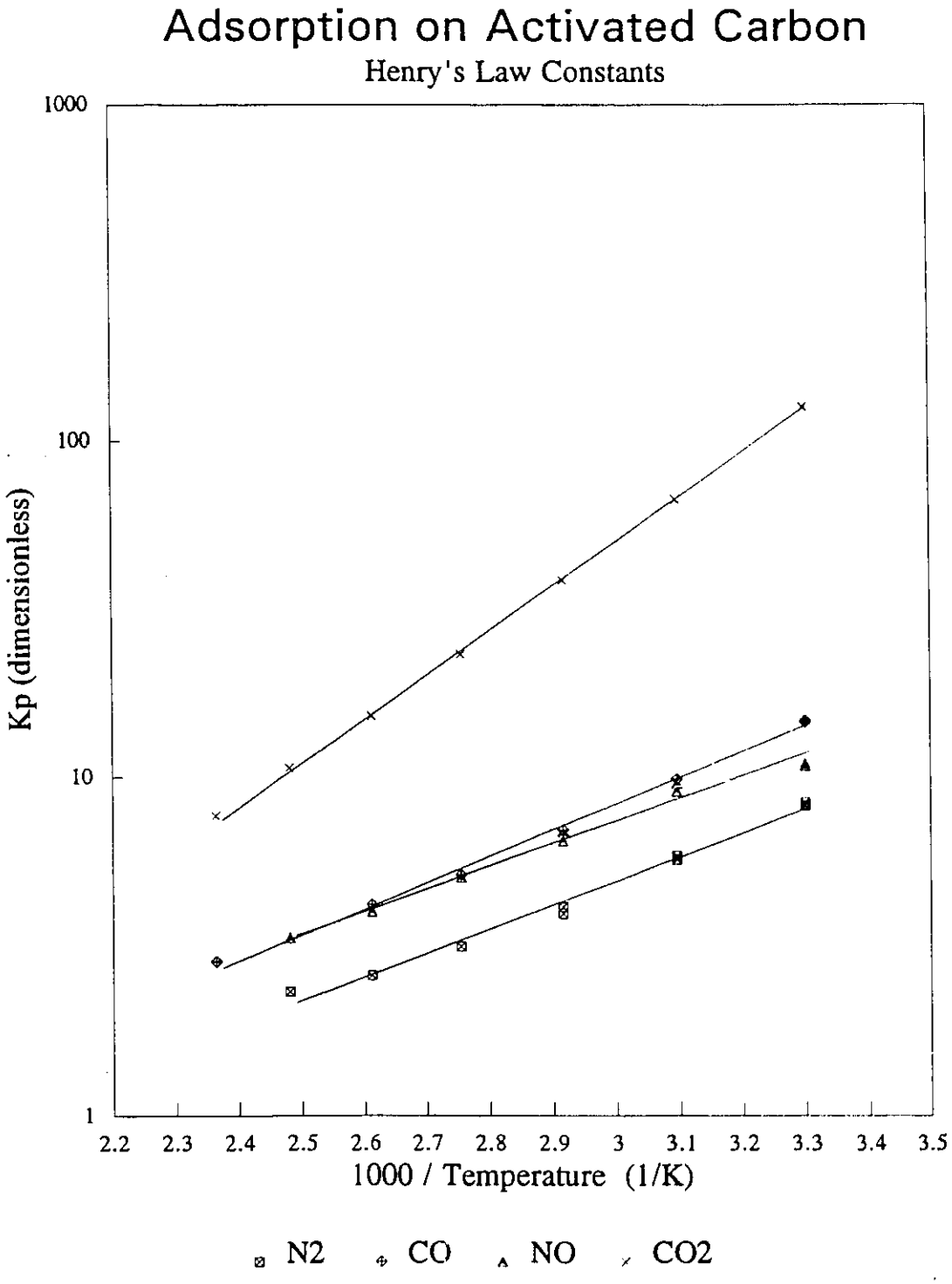

Figure 5.9 : Van't Hoff plots for adsorption on activated carbon

with the polarity of the sorbates. For the activated carbon the heats of sorption were small and decreased with molecular size and mass. This observation is consistent with hydrocarbon adsorption results in literature.

Adsorption of light hydrocarbons on activated carbon has been studied extensively in literature [Myers & Ou (1983), Costa et al. (1985, 1981), Huang & Fair (1988), Lewis et al. (1950), Hart & Thomas (1991), Kaul (1987), Reich et al. (1980)] and as a result Henry's law constants for CH_4, C_2H_6, and C_2H_4 were not measured in this study. The results of previous studies show the trends expected. C_2H_6 was adsorbed more strongly than C_2H_4 in various activated carbons tested due to its larger kinetic diameter. However in the zeolites examined in this study, C_2H_4 yielded a higher heat of sorption than C_2H_6 in every case. Again, steric effects dominate adsorption on the cation free carbon molecular sieves, but polarization effects seem to dominate adsorption on zeolites. For all separations considered in this study, molecular size of the species to be separated is not drastically different, except perhaps for NO which is significantly smaller than the rest. Therefore application of zeolites for these separations provides better separation factors than carbon molecular sieves, mostly due to the effect of cationic sites on the adsorption of polar species in the micropore structure.

5.1.8 Henry's Law region Separation Factors

Separations of various combinations of the gases studied are of interest to industry. Apart from the main separations under consideration, those being removal of CO, NO and CO_2 from N_2 and alkene removal from light alkanes, separation factors for other separations are also presented. These are the CO / CH_4 and the CH_4 / N_2 separations. Each potential application is discussed along with presentation of appropriate initial separation factors (ratios of Henry's law constants). From these a promising separation was chosen for further, high concentration studies. It should be noted that since no proper CO_2 adsorption measurements could be conducted on the clinoptilolite (see section 5.1.6), separation of CO_2 / N_2 was not considered further, as the other materials studied have been examind in detail for this application. It should also be noted that only separation factors for the C_2H_4 / CH_4 system are presented as an alkane /

alkene separation. This is because the adsorption of C_2H_6 was not studied on all zeolites, and because adsorption of C_2H_6 on some of the zeolites caused tailing problems and the accuracy of such results could not be ensured.

Figure 5.10 shows the separation factors for the CO / N_2 system on all materials which were tested for these two gases. The figure clearly shows that the natural clinoptilolite provided the highest separation factors for the entire temperature range. CO and N_2 are similar in size (3.76 and 3.64 A, respectively), but CO has a significant dipole whereas N_2 has a weak quadropole. It is not surprising, then, that the two zeolites with accessible bivalent cations provided the highest separation factors. Both clinoptilolite and 5A zeolite yielded better separation factors than the two zeolites with monovalent cations. The two zeolites with monovalent cations provided higher separation factors than the activated carbon except at higher temperatures. At these temperatures the cation - dipole interaction is weakened and the separation is attributed more to steric factors, so the separation factor on activated carbon can exceed that of H - Mordenite. This decrease in cation - CO dipole interaction with increasing temperature was likely the reason for the decreasing separation factors on all zeolites as the temperature increases. At one extreme, a high temperature would prohibit the specific CO dipole - cation interaction and the separation would be affected only by steric factors, decreasing the separation factor. For the CO / N_2 separation at approximately ambient temperatures, clinoptilolite was found to be the favored sorbent according to the separation factors derived from the initial heats of adsorption.

The separation factors for the NO / N_2 separation are shown in figure 5.11. Since the size difference between NO and N_2 is more significant (3.17 and 3.62 A, respectively), steric factors may play a larger role in the separation of these gases. Again, the clinoptilolite offered the highest separation factor over the entire experimental temperature range, but the reason is likely a combination of steric and polarization contributions. It is interesting to note that as the temperature increased the separation factor provided by 5A zeolite also increased. This indicated that the NO / N_2 separation on 5A zeolite is more efficient when polarization factors are reduced, and that the size difference of the two species is primarily responsible for the difference in their micropore diffusion behaviour. The separation factors offered by the

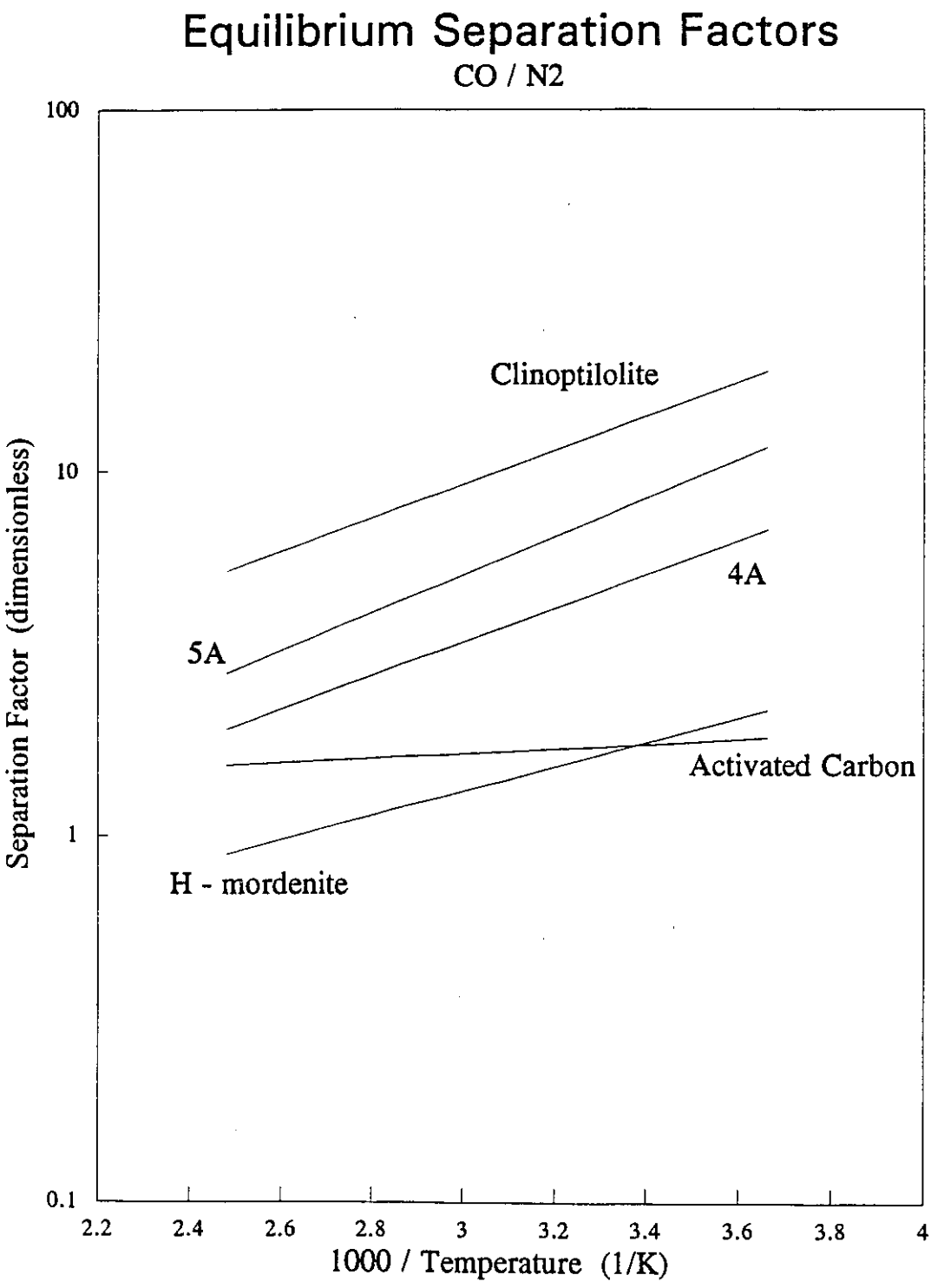

Figure 5.10 : Adsorption equilibrium sepraration factors for the CO / N_2 separation

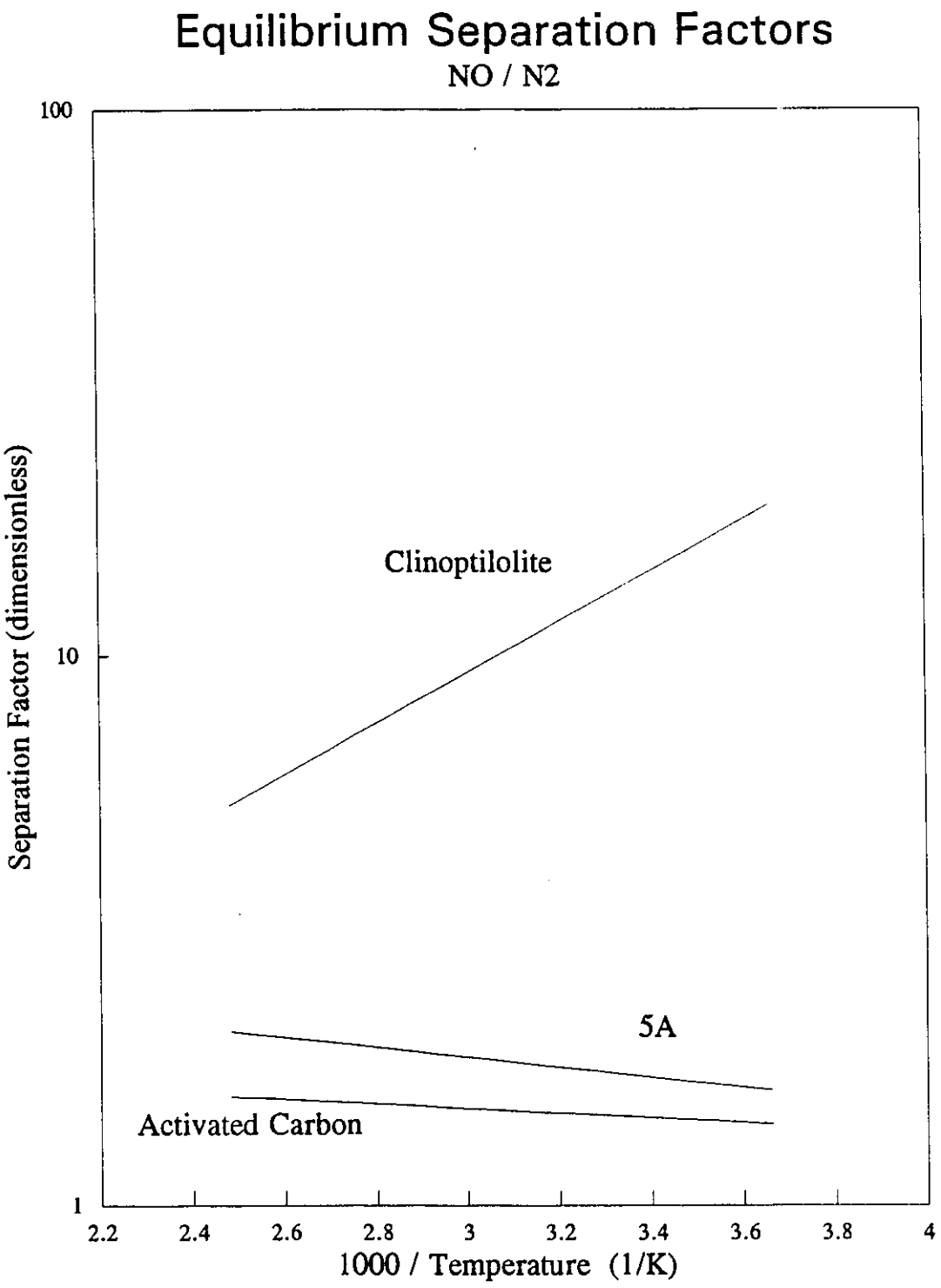

Figure 5.11 : Adsorption equilibrium sepraration factors for the NO / N_2 separation

activated carbon are low. This is because of the lack of cations in the activated carbon and because the sizes of the sorbate molecules lie around the minimum of the carbon pore size distribution of 3 to 40 A. Thus only minimal molecular sieving effects could be expected. It is interesting to note that in the two separations considered so far, the separation factors provided by the activated carbon, although low, demonstrated the least temperature dependance. This is again likely due to the fact that there are no cation - sorbate interactions being drastically affected by the temperature. Rather, increasing the temperature more equally and ideally effects the diffusion of both gases in the activated carbon pores, only slightly affecting the separation factors. For the NO / N_2 separation at approximately ambient temperatures, clinoptilolite was found to be the favored sorbent according to the separation factors derived from the initial heats of adsorption.

Separation of C_2H_4 from CH_4 was examined on 4A, 5A , 13X, and 10X zeolites, H - Mordenite, and on the natural clinoptilolite. As discussed in section 5.1.6, C_2H_4 was anomalously adsorbed on clinoptilolite yielding only a crude estimate of the initial heat of sorption and therefore separation factors are not presented for this zeolite. Separation factors on the other synthetic zeolites are presented in figure 5.12. This figure clearly shows the effect of divalent cations on the separation of C_2H_4 from CH_4. The zeolites with exclusively monovalent cations yielded the lowest heats of adsorption of C_2H_4, and consequently yielded the lowest separation factors, all with curves lying in the same area of figure 5.12. A large jump in the heat of sorption of C_2H_4 on A and X zeolites was noticed with the addition of Ca^{++} ions, whereas the heat of sorption of CH_4 on A and X zeolites was relatively unchanged with the addition of divalent cations. This is the reason for the excellent separation factors offered by the Ca^{++} - exchanged versions of A and X zeolites. It is worth noting that in every case the separation factor decreased with increasing temperature. Since the separation is believed to be largely based on differences in the polarity of the species, increasing the temperature reduces the polar interactions between the sorbate and cation sites of the sorbent, thereby reducing the difference in micropore diffusion behaviour between C_2H_4 and CH_4. For the C_2H_4 / CH_4 separation at approximately ambient temperatures, CaX was found to be the favored sorbent according to the separation factors derived from the initial heats of adsorption.

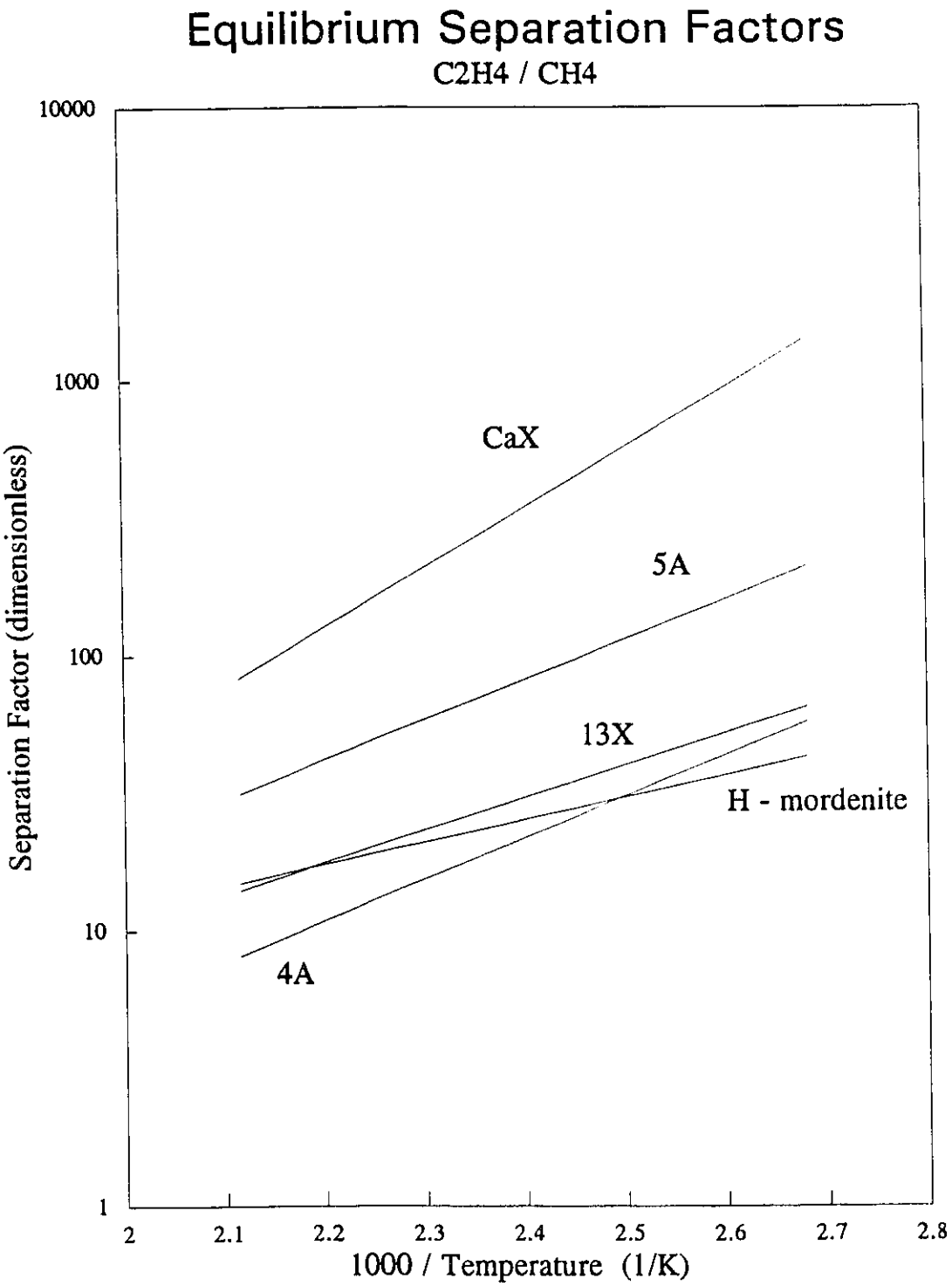

Figure 5.12 : Adsorption equilibrium separation factors for the C_2H_4/CH_4 separation

With the data collected to this point, a variety of other gas separations of interest could be examined. Figure 5.13 shows the separation factors for the CO / CH_4 system on all materials which were tested for these two gases. Again, the natural clinoptilolite provided the highest separation factors for the entire temperature range. CO and CH_4 are similar in size (3.76 and 3.8 A, respectively), but CO has a significant dipole whereas CH_4 is non - polar. Again, for the separation of a polar and non - polar species, the two zeolites with divalent cations provided the highest separation factors. This has also held true for the separation of both NO and CO from N_2, strongly supporting the use of divalent cations for enhanced separation of polar / non - polar gas mixtures. The trend of the separation factor decreasing with increasing temperature is also the same. As temperature increases, the difference in the polar interaction of the two species decreases and molecular sieving becomes dominant. Since the molecules to be separated are very similar in size, molecular sieving does not provide a strong separation. Thus we find low separation factors (approximately =1) for this separation at high temperatures for all zeolites tested. Clinoptilolite has shown the most promise for the CO / CH_4 separation over the entire temperature range considered based on initial separation factors.

Another potential separation that has been examined is that of N_2 / CH_4. Separation factors derived from initial heats of sorption on 4A zeolite, 5A zeolite, H - mordenite and clinoptilolite are plotted against reciprocal temperature in figure 5.14. The results show relatively low separation factors for all zeolites tested over the entire temperature range. All zeolites but clinoptilolite show higher Henry's law constants for CH_4 than for N_2, and thus most separation factors shown in figure 5.14 are smaller than1. This separation of the two least polar compounds (one weakly quadropolar and the other non - polar) demonstrates some expected difficulties. The previous separations of polar from non - polar compounds have been shown to be most promising when divalent cations are included in the micropores to take advantage of the significant polarity differences. In this case these polarity differences are not so pronounced, as neither species has high interaction with the monovalent or divalent cationic sites. Since N_2 and CH_4 are very similar in size (3.64 and 3.8 A, respectively) and not drastically different in polarity, the separation is not as simple to conduct or analyze as were those previously examined. It has been found

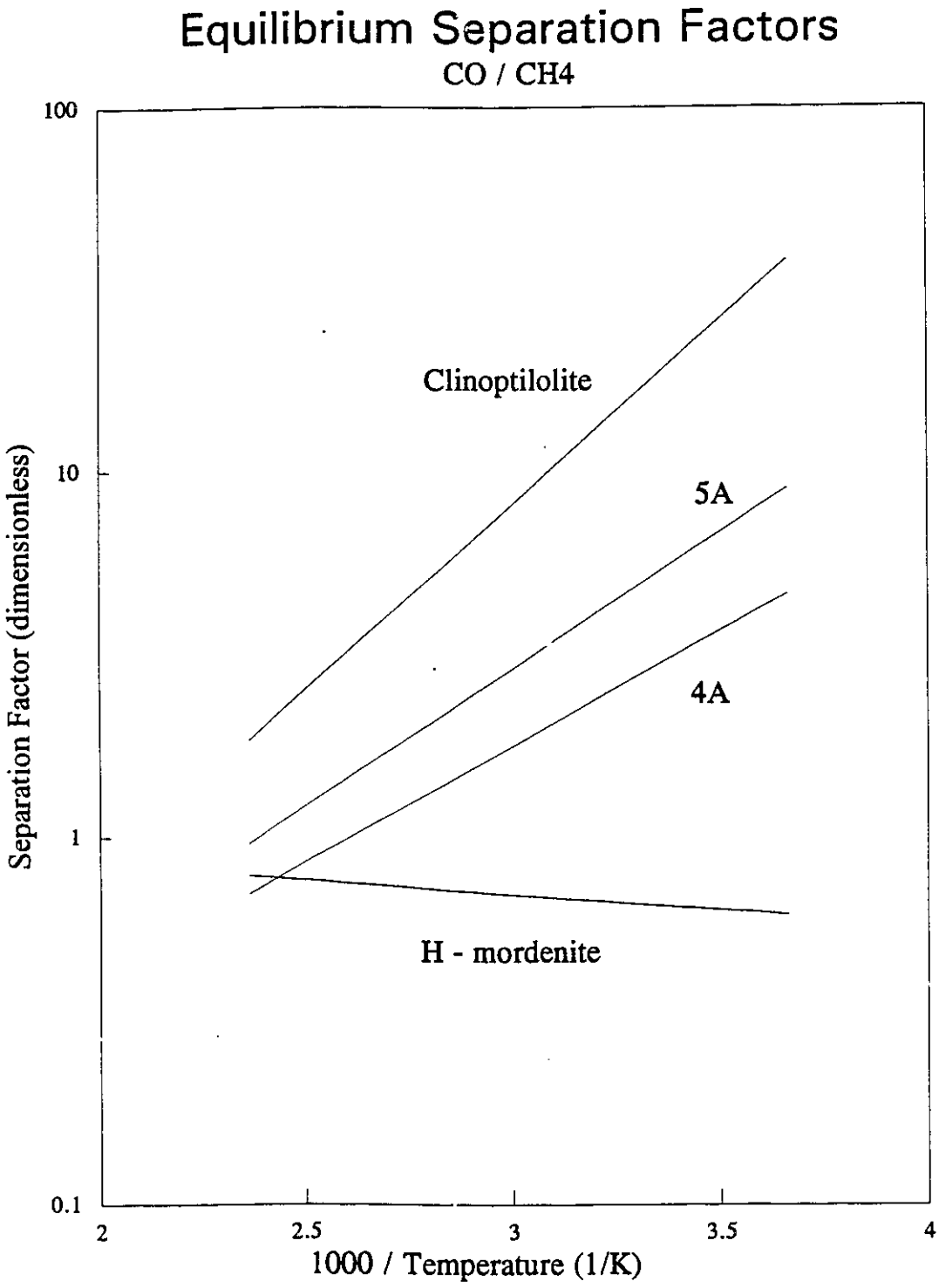

Figure 5.13 : Adsorption equilibrium sepraration factors for the CO / CH_4 separation

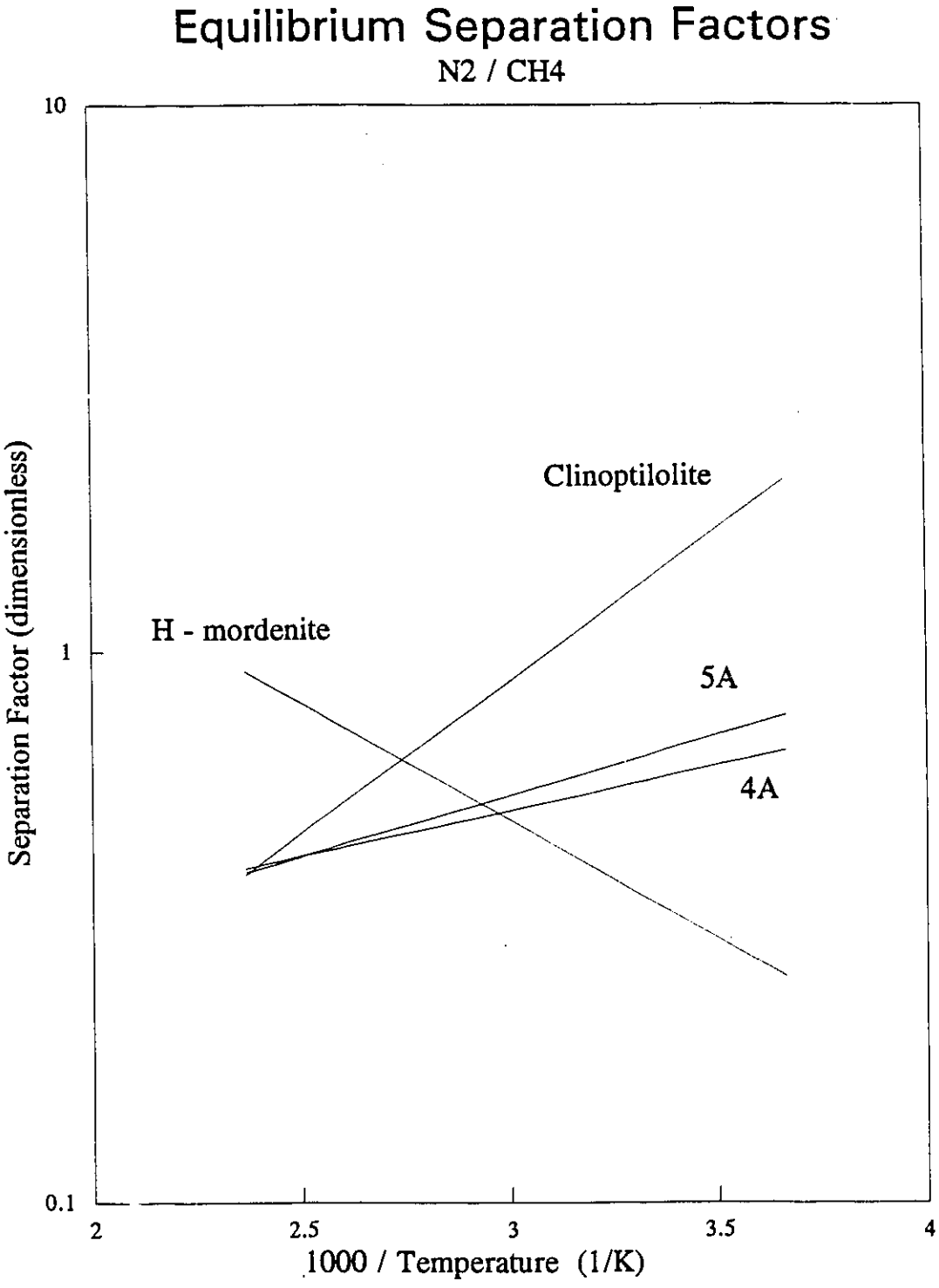

Figure 5.14 : Adsorption equilibrium sepraration factors for the N_2 / CH_4 separation

that the selectivity of clinoptilolite for the N_2 / CH_4 separation can be completely reversed with ion exchange due to the effect of pore blocking cations [Ackley & Yang (1991 a, b)]. The results of the present study demonstrate a reversal in the selectivity of clinoptilolite for this separation. At low temperatures the N_2 weak quadropole may have limited interaction with the clinoptilolite cation sites, leading to a N_2 / CH_4 separation factor > 1. At higher temperatures this effect is reduced and molecular sieving takes over, resulting in a N_2 / CH_4 separation factor <1. 4A and 5A zeolites demonstrate increasing separation factors with increasing temperature (since the entire vant Hoff plots for 4A and 5A zeolites in figure 5.14 are below 1, a decreasing value of the N_2 / CH_4 separation factor is an increasing CH_4 / N_2 separation factor). This may be because when the N_2 is adsorbed at low temperatures, its quadropolar interaction with the zeolite cations allows it to compete with the adsorption of CH_4 (for the divalent 5A more than for the monovalent 4A) yielding separation factors close to 1. It is possible then that as temperature increases, the polar interactions diminish and the CH_4 / N_2 separation factors increase due to increased molecular sieving. The trend shown by H - mordenite is difficult to explain, as with weak cation sites and limited one dimensional diffusion the contributing factors to the separation are less apparent. It is clear, however, that the mordenite offers the highest initial CH_4 / N_2 separation factor at low temperatures (up to approximately 330 K), whereas the other zeolites offer higher CH_4 / N_2 separation factors at higher temperatures.

In any case, the separation factors for this separation, which did not provide us with a large polar difference between the two species to be separated, yielded the lowest separation factors of all the separations tested for. Valuable insight can be gained from this information. This poor potential separation is not only due to the species small difference in size, as many other separations were considered with components of more similar sizes. It is also largely due to the lack of difference in the electrical properties of the species, as in all other cases separation of a strongly polar species from a weakly or non - polar species yielded high separation factors, particularly for zeolites containing divalent cations.

After considering these separations, one system was chosen for further examination. Some promising separations were not considered further for reasons of experimental difficulty and / or

availability of data on these systems in literature. One system, that of CO / N_2 / clinoptilolite, yielded promising separation factors at practical conditions. All experiments conducted with these gases on clinoptilolite also showed excellent repeatability. Since the potential of natural clinoptilolites has not been presented to a great degree in literature, and since the separation of CO from ambient streams is of industrial and environmental interest, this system was chosen for determination of diffusion characteristics and for measurement and modelling of pure and binary isotherms.

5.2 Micropore Diffusivity of CO and N_2 in Clinoptilolite

It was desired to study the diffusion characteristics of CO and N_2 in the natural Turkish clinoptilolite. The gas chromatographic method is limited in the measurement of micropore diffusivity. The experimental parameter determined from diffusion experiments (dispersion) represents a combination of various mass transfer resistances. Only if micropore diffusion is the dominant mass transfer mechanism can it be accurately measured by chromatography. Thus preliminary experiments were done to determine if micropore diffusivity could be measured with the chosen experimental system, apparatus and conditions. Then experiments for the determination of micropore diffusivity could be conducted at various temperatures. Results of these experiments and of the theoretical calculations of other mass transfer contributions are presented below.

Response peaks from adsorption of CO and N_2 on clinoptilolite at various temperatures were used to produce plots of total dispersion ($\sigma^2 L/2\mu^2 \upsilon$, see equation 43) vs. temperature in figure 5.15. The figure clearly demonstrates that the dispersion of both species is strongly dependent on the temperature. Since all terms other than the micropore diffusion on the right hand side of equation 43 are weak functions of temperature, this result suggests that the micropore diffusion is a significant if not dominant resistance over this temperature range and that it may be measured by gas chromatographic methods [Tezel & Apolonatos (1993)].

Diffusivity experiments were then conducted for both gases at four temperatures, varying gas velocity at each temperature. The results, plotted as total dispersion vs $1/\upsilon^2$, are shown in figures 5.16 and

5.17 for CO and N_2, respectively (each figure is presented separately to avoid clutter, as the data points for the individual gases at all 4 temperatures lie in the same area). The slope of these plots represents the axial dispersion, and the intercept represents the other combined mass transfer resistances, as is clear from equation 43. The contributions of external film mass transfer and macropore diffusion on the right hand side of equation 43 must be determined theoretically so that the micropere diffusivity may be calculated by difference.

In estimating the macropore diffusivity, values of the average macropore diameter, the void fraction of the pellet (Θ), and the tortuosity factor (τ) had to be determined. The macropore diameter was required in the calculation of Knudsen diffusivity. The macropore size distribution of the natural Turkish clinoptilolite has been determined to be bidisperse with a small, almost normal distribution around 300 A (21% of pores) and a much larger, skewed, distribution between 1000 and 100000 A (46% of pores) with a mean of approximately 11000 A [Sirkecioglu et al. (1992)]. For calculation of the Knudsen diffusivity a weighted mean macropore size of 7460 A was used. The pellet void fraction for the clinoptilolite was also determined experimentally. A value of .38 was determined for the sample used in this study, and this value was used for further diffusivity calculations. Since it was desirable to determine if the macropore resistance was large enough to be significant when compared to the micropore diffusion, and since an exact tortuosity factor was not available, it was decided to estimate a high tortuosity factor, thereby overestimating the macropore diffusional resistance. If the macropore resistance calculated this way was small or negligible compared to the micropore resistance, then the true macropore mass transfer resistance would be smaller still. Thus by taking a conservative estimate of the representative mean pore size from the experimental pore size distribution, the experimentally determined void fraction, and a high estimate of the tortuosity factor, the maximum possible contribution of macropore diffusion to the total mass transfer resistances may be calculated. Experimental values of macropore tortuosities in zeolites range from 1.7 to 6 [Yang (1987), Ruthven (1984 b)]. Thus a tortuosity of 6 was chosen for the calculation. The resulting worst case macropore diffusion resistances are presented along with experimentally measured values of the total mass transfer resistance and axial dispersion (from figures 5.16 and 5.17), along with

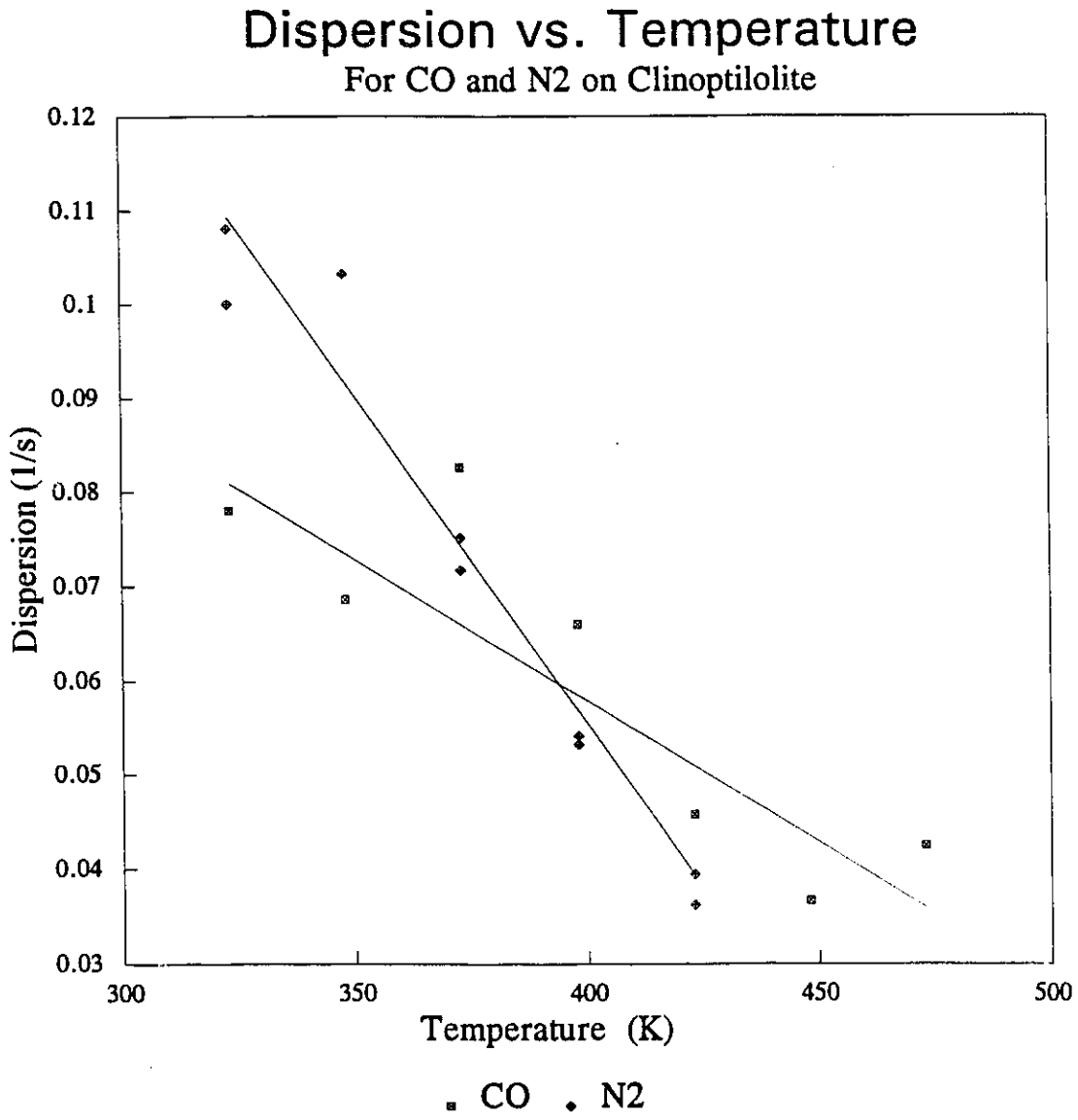

Figure 5.15 : Dispersion vs. T for CO and N_2 on clinoptilolite

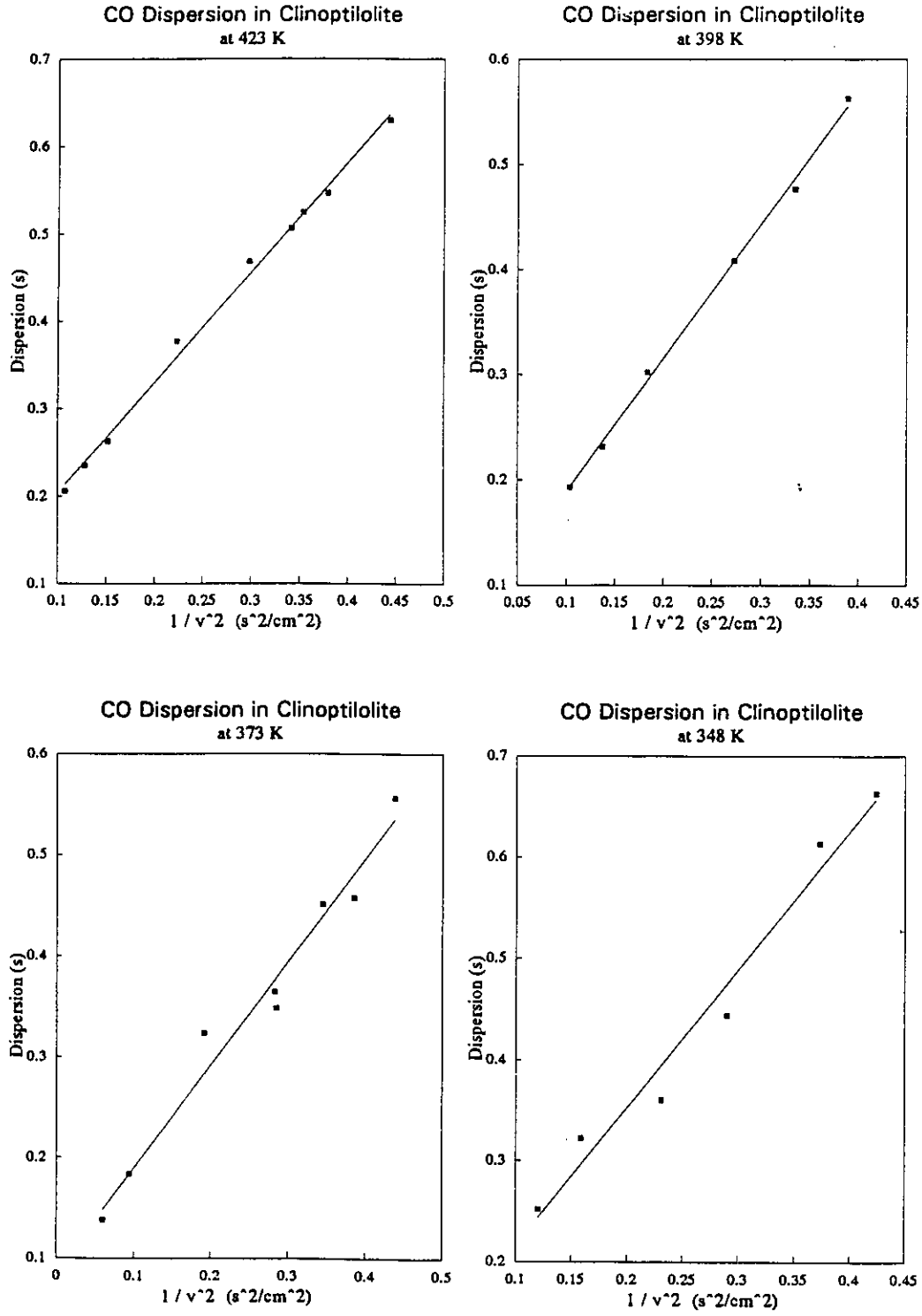

Figure 5.16 : Dispersion vs. $1/v^2$ for CO on clinoptilolite

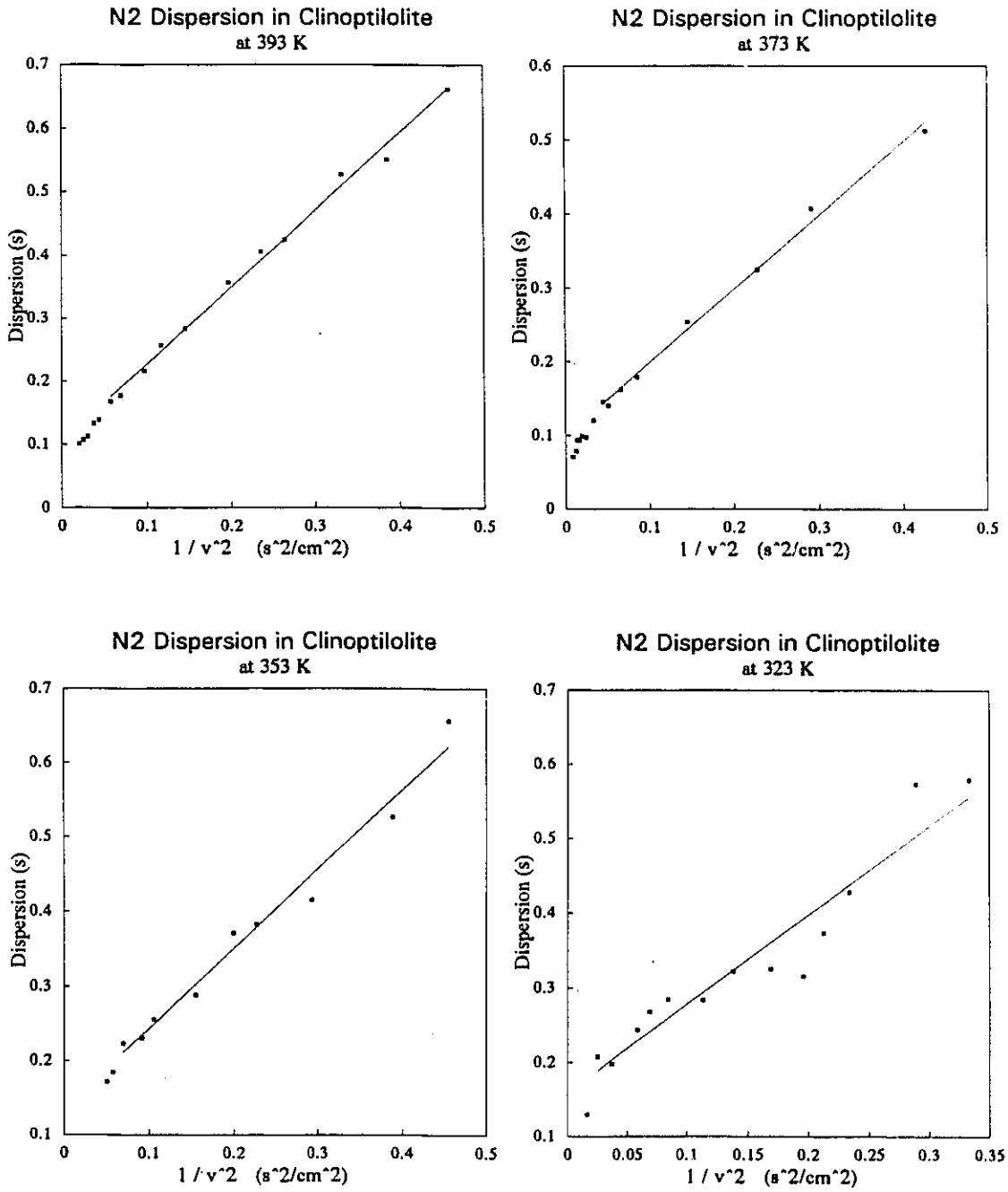

Figure 5.17 : Dispersion vs. $1/v^2$ for N_2 on clinoptilolite

empirically determined values of molecular diffusion in table 5.10. Since the estimated maximum contribution of external film mass transfer and macropore diffusion resistance consisted of only 2 to 5% of the total resistance, the micropore diffusion was clearly found to be the dominant mass transfer

Table 5.10 : Mass Transfer Resistances for CO and N_2 in Clinoptilolite

Temperature (K)	D_L/υ^2 (s)	$R_p^2/3D_M$ (s) [1]	$R_p^2/15\theta D_p$ (s x 10^{-3}) [2]	$\sigma^2L(1-\varepsilon)/2\mu^2\upsilon\varepsilon$ (s)	% contribution of [1] and [2]
CO at 348	1.36	11.8×10^{-4}	5.05×10^{-3}	0.14	4.51
CO at 373	1.02	10.5×10^{-4}	4.6×10^{-3}	0.15	3.79
CO at 398	1.27	9.42×10^{-4}	4.22×10^{-3}	0.1	4.93
CO at 423	1.26	8.51×10^{-4}	3.89×10^{-3}	0.13	3.57
N_2 at 323	1.21	13.5×10^{-4}	5.65×10^{-3}	0.27	2.58
N_2 at 353	1.06	11.7×10^{-4}	5×10^{-3}	0.23	2.63
N_2 at 373	.998	10.6×10^{-4}	4.64×10^{-3}	0.17	3.41
N_2 at 393	1.22	9.76×10^{-4}	4.33×10^{-3}	0.18	2.97

mechanism. The slight inaccuracies in calculating the contributions other than micropore diffusion to mass transfer resistance proved inconsequential, as these terms are virtually negligible compared to the total dispersion term. The values of the micropore diffusivity (as D_c/r_c^2) could then be calculated from the slopes and intercepts of the dispersion vs $1/v^2$ plots, and the results are plotted against reciprocal temperature in figure 5.18. The temperature dependance of the micropore diffusivity may be expressed by an Arrhenius type equation:

$$\frac{D_c}{r_c^2} = \frac{D_0}{r_c^2} \exp\left(\frac{-E_a}{R_g T}\right) \tag{48}$$

The values of the parameters D_0/r_c^2 and E_a resulting from a linear regression of the data are presented in table 5.11. Both of the lines have similar slopes, with diffusivities increasing with temperature as expected. The diffusivity of N_2 is 2 to 3 times higher than that of CO over the entire temperature range, yielding a kinetic separation factors (ratio of micropore diffusivities) approximately half the magnitude of

the previously determined initial equilibrium separation factors. These diffusion results were not easily compared to similar results in literature. Since this was a natural clinoptilolite, its ion distribution and

Table 5.11 : Diffusion Parameters for N_2 and CO adsorption on Clinoptilolite

Sorbate	Temperature Range (K)	D_o/r_c^2 (1/s)	E_a (kcal/mol)
CO	348 - 423	4,602.6	10.0
N_2	323 - 393	20,091	10.4

thus diffusion characteristics were unique. A reasonable comparison of the N_2 micropore diffusion in clinoptilolite with that in H - mordenite and 4A zeolite is possible, as these experiments were conducted by other researchers on the same apparatus under similar conditions [Tezel & Apolonatos (1993)]. This comparison is shown in figure 5.19. The line for CO is given only for reference. The comparison shows that the diffusion of N_2 is over 100 times greater in H - mordenite than in 4A zeolite or clinoptilolite, likely due to the lack of polar interactions between N_2 and the cations in H - mordenite, and due to mordenite's large pore size (rated at 8 to 9 A). 4A and clinoptilolite show similar pore sizes and similar measured values of D_c/r_c^2. The activation energy of diffusion for N_2 on clinoptilolite was, however, found to be much higher than that on 4A zeolite or H - mordenite (10.4 kcal/mol compared to 6.7 and 5.2 kcal/mol, respectively). This high activation energy results from a combination of pore blocking in the clinoptilolite structure from the various cations (effectively reducing the open pore diameter), and from the interaction of some of these cations with the quadropole of N_2.

Kinetic separation factors ($[D_c/r_c^2\ N_2] / [D_c/r_c^2 CO]$) were compared with initial equilibrium separation factors (K_p CO / K_p N_2) in figure 5.20. Selectivities are reversed for the two types of separations (ie, N_2 diffuses into the clinoptilolite pores faster than CO, but CO is retained more at equilibrium). The equilibrium separation seems the most promising, yielding a separation factor greater than 10 at ambient temperature. It is clear that this natural form of clinoptilolite is promising for the CO / N_2 separation at ambient conditions, as both initial equilibrium and diffusion experiments yield reasonable separation

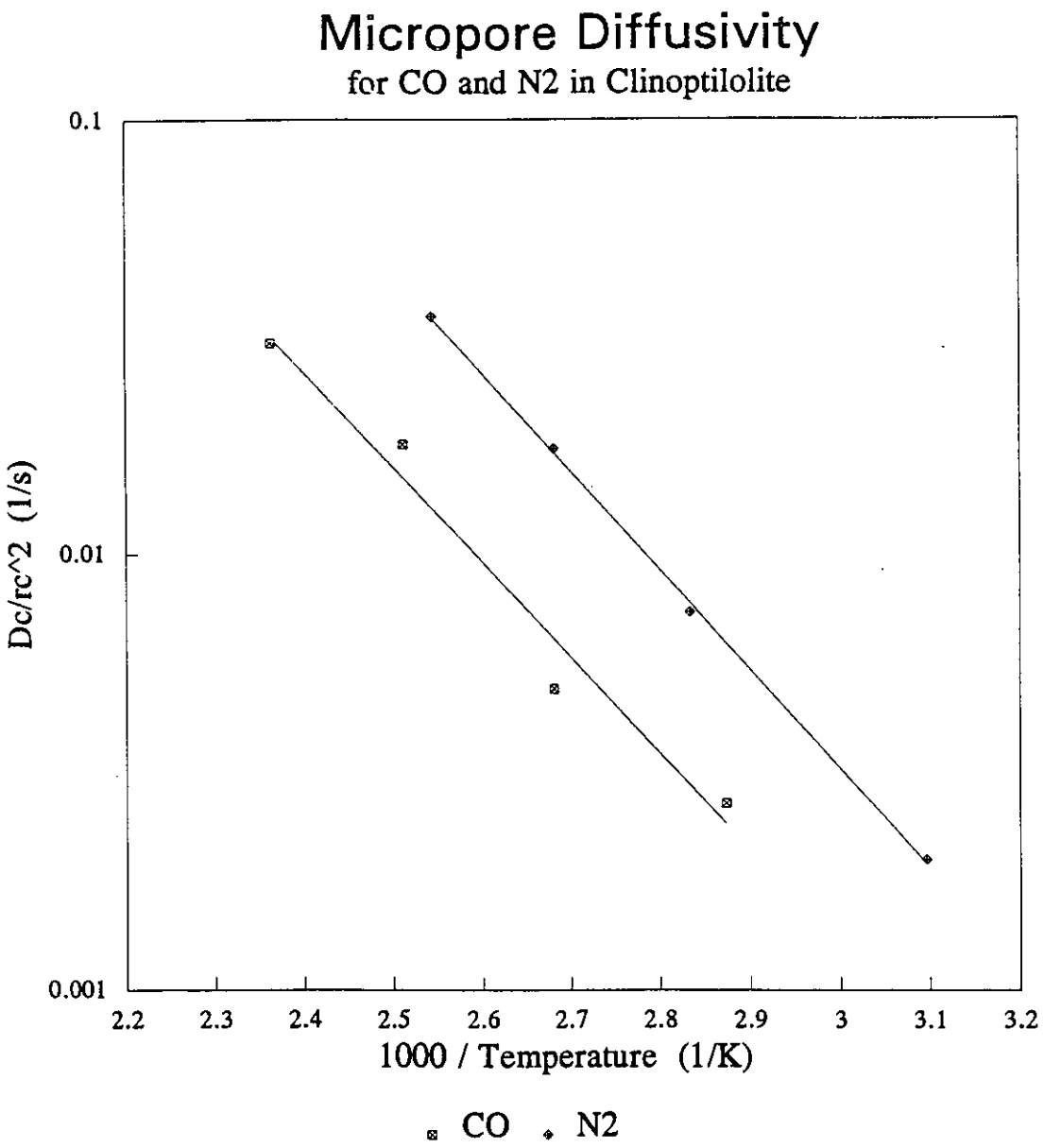

Figure 5.18 : Micropore diffusivity vs. 1/T for CO and N_2 on clinoptilolite

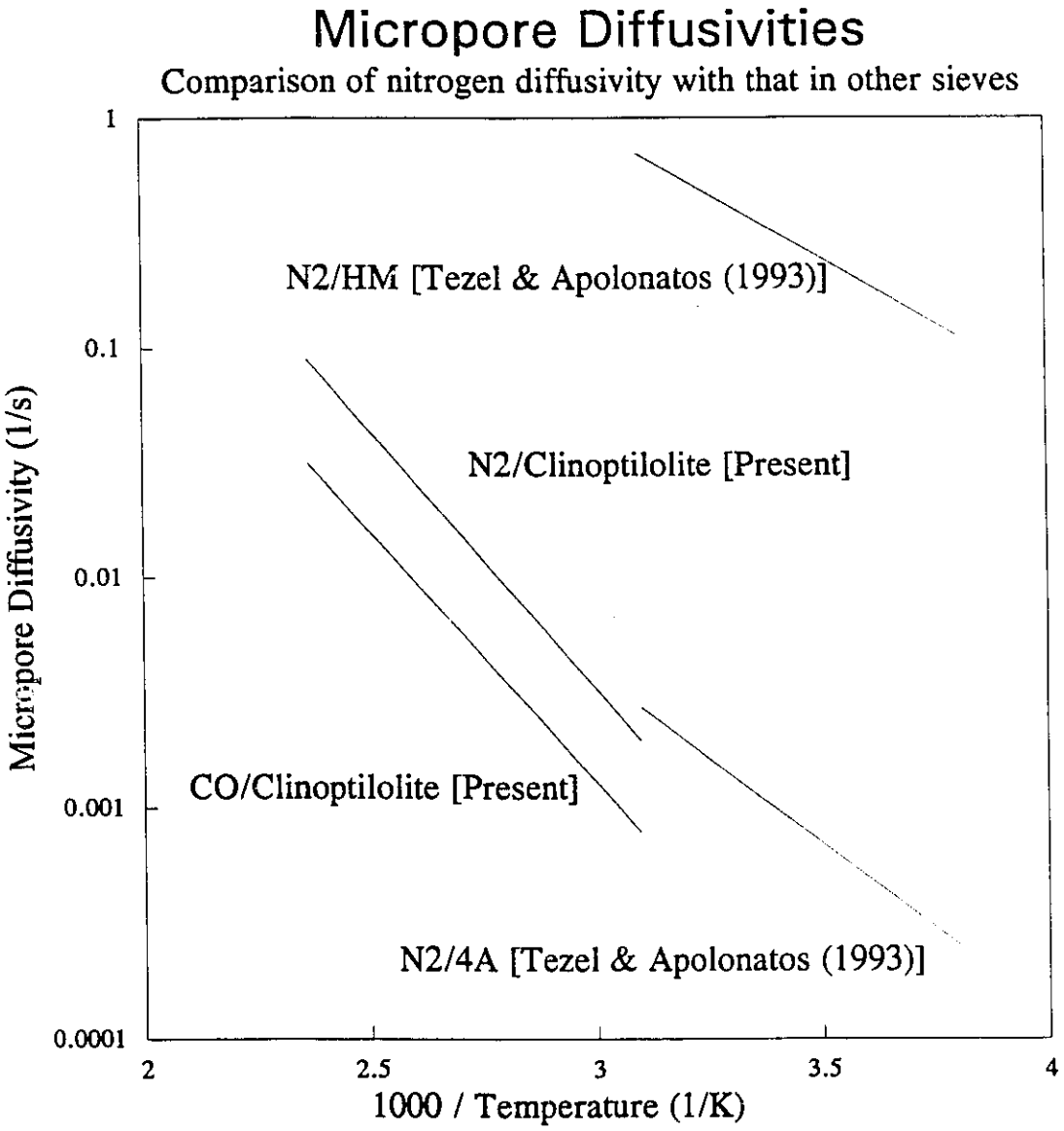

Figure 5.19 : Comparison of experimental N_2 / clinoptilolite micropore diffusivity with literature

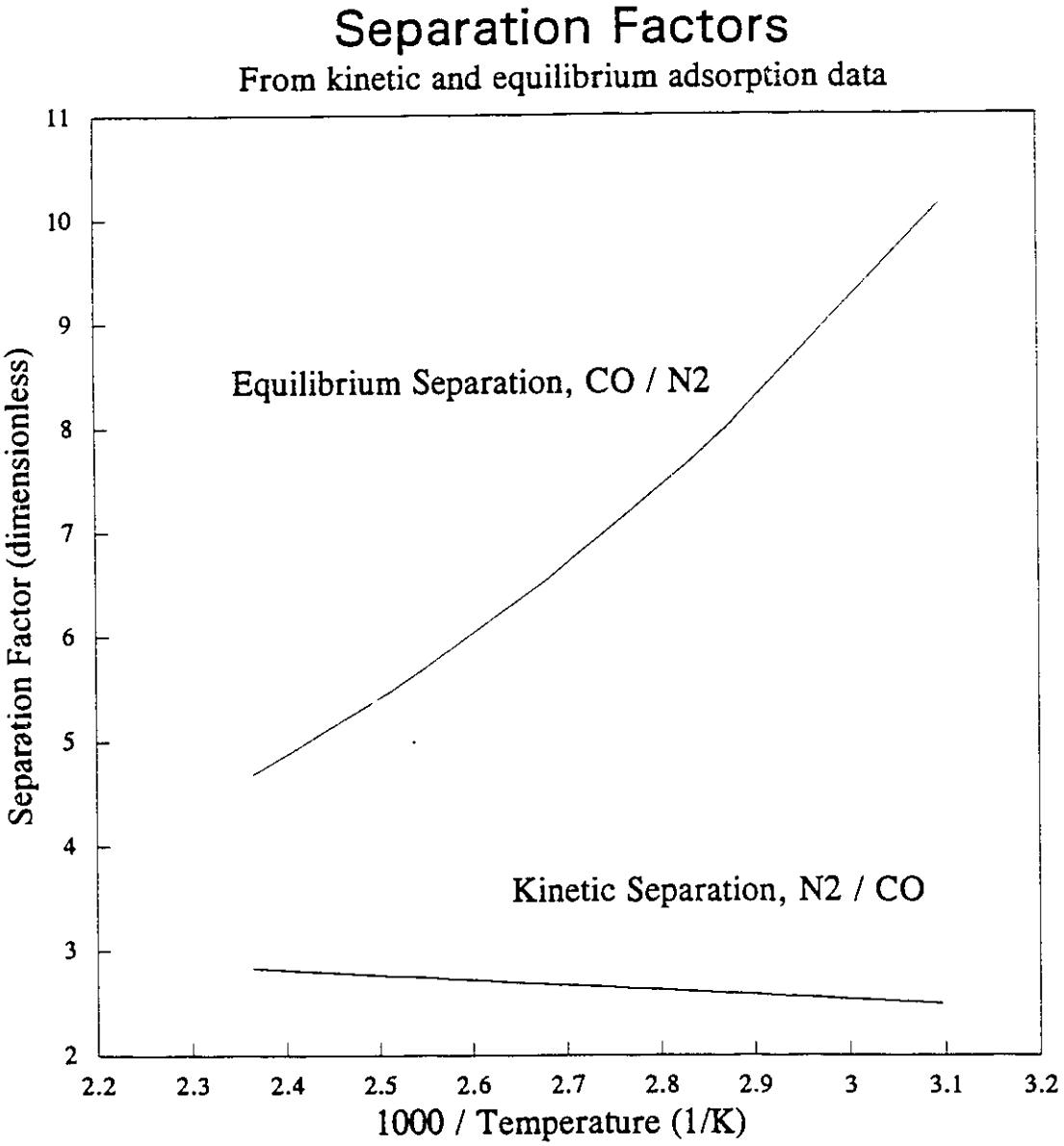

Figure 5.20 : Comparison of experimental kinetic and equilibrium CO / N_2 separation factors

factors, with equilibrium separation apparently being favorable. The next step was to determine equilibrium adsorption behaviour of the pure and mixed gases at non - dilute concentrations, with individual component pressures ranging up to .9 atmospheres. This will provide valuable information on the use of this clinoptilolite for the CO / N_2 separation.

5.3 Adsorption Isotherms on Clinoptilolite

Adsorption of N_2 and CO was studied chromatographically using a binary carrier gas consisting of the sorbate gas and He. The carrier gas sorbate concentration was varied from 0 to approximately 90% in order to determine adsorption characteristics at higher sorbate pressures. By sending a pulse sorbate sample through the column at equilibrium with the mixed carrier, values for the slope of the mixed gas isotherm, K_p', can be determined from equations 17 and 18 at different sorbate partial pressures. This was done with He as a non - adsorbing carrier makeup to determine pure gas adsorption isotherms of CO and N_2, and was done with mixed CO / N_2 carrier to determine binary component isotherms in which both species are adsorbed.

5.3.1 Pure component adsorption of N_2 on Clinoptilolite

The adsorption of pure N_2 on clinoptilolite at 303 K and 1 atmosphere total pressure was examined first. Carrier composition was adjusted up to 90% and then back down to 0% N_2 to test for repeatability and reversibility. The value of K_p' was determined experimentally at each point. The plot of K_p' vs. % N_2 yields the constant value of dp_2/dq_2 from the intercept as the N_2 fraction approaches 1. This allows rearrangement of equation 18 to solve for q_1 by integrating with respect to p_1. The integral yields the isotherm as the quantity of N_2 adsorbed, q_1, vs. %N_2. The experimental integrand is shown in figure 5.21.

On examining this function it is clear that a numerical integration is subject to error due to the gaps in the data, particularly the gap between data at 0% N_2 and 2% N_2, ie, between the first two

concentrations. Error in interpolating between these two points will directly contribute to an erroneous zeolite capacity. A straight line drawn between the two points would surely overestimate the capacity, as the area under the integrand would be inaccurately large. To attempt to minimize this error the integrand data was fitted with a mathematical model. A functional form identical to the Flory - Huggins VST was chosen because it was known that such a function could accurately fit a rectangular - isotherm shaped curve. An excellent fit was obtained using combined functions of the same form, one for the more vertical part of the curve and one for the horizontal. The resultant fit of the integrand is shown in figure 5.22, and the result of the integration, ie, the isotherm, is shown in figure 5.23. The fit in figure 5.22 is shown only for the data at 2% N_2 and greater to better demonstrate the goodness of fit. The integration was done by Simpson's one - third rule on a spreadsheet. The sensitivity of the isotherm to the curve fitting is not unreasonably high. Only a small fraction of the area is subject to significant variation from the interpolated line, that being the area between 0 and 2%. One extreme, a straight line fit between the first two points, increases the total area under the integrand and thus the total capacity by 37%, whereas the other extreme, a vertical line coincident with the Y axis down to the data at 2% N_2, decreases the total area by 8%. The rest of the curve is rather flat and modelling introduces negligible error in the interpretation of the results at these higher N_2 concentrations. The precise amount of error introduced in the N_2 isotherm by the interpolation between the first two data points cannot be determined, but given the potential error caused by this interpolation and the sensitivity revealed above, the ultimate capacity determined here may be considered to have up to 25% error, the actual capacity being more likely higher than lower than that determined through the interpolation. Acquiring more data points at these low N_2 concentrations (ie, between 0 and 2%) is the simple solution, but equipment limitations prevented this in the present study.

The inital slope of the isotherm yields a dimensionless Henry's law constant of 186. That calculated from the Arrhenius equation describing the temperature dependence of the Henry's law constant for N_2 on clinoptilolite is calculated to be 370. This agreement is reasonable, since drawing Henry's law constants from isotherms is always subject to error. This seems to indicate that the true

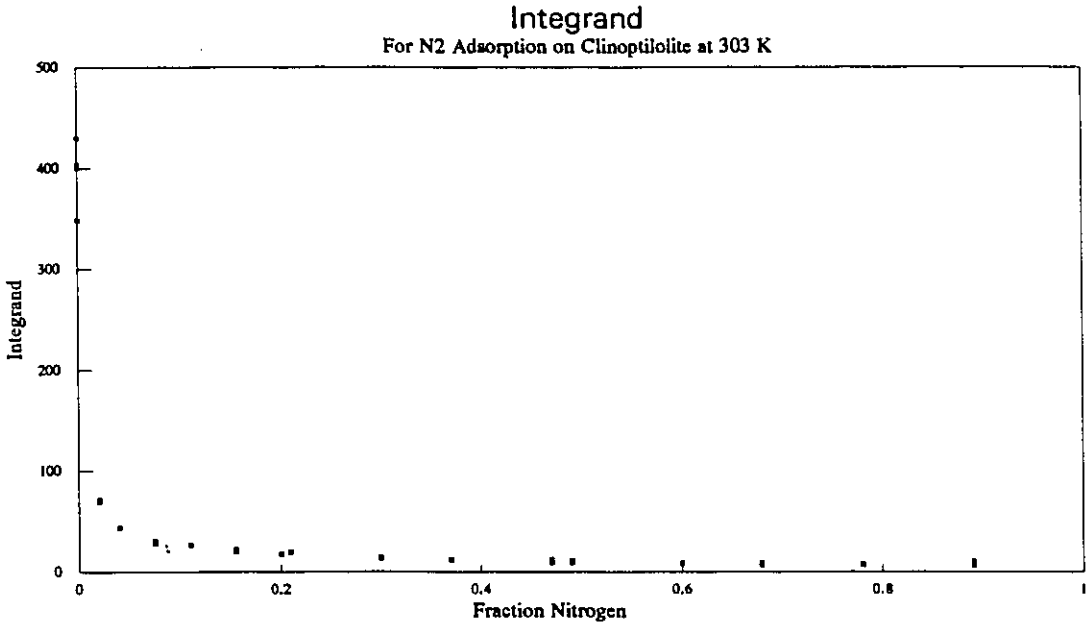

Figure 5.21 : Integrand for determination of N_2 / clinoptilolite adsorption isotherm

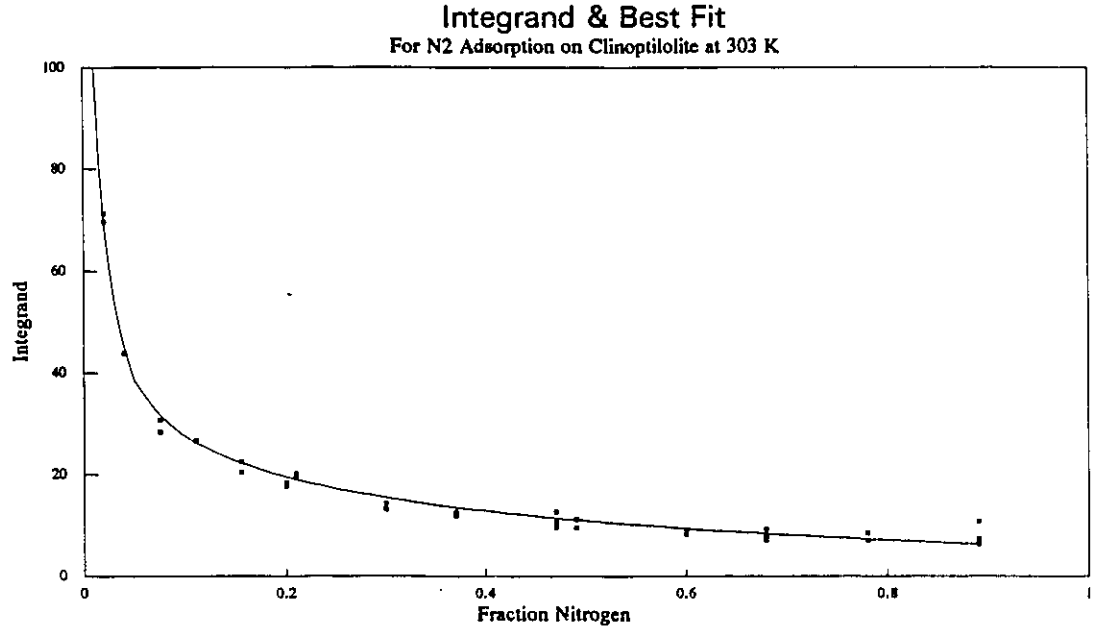

Figure 5.22 : Integrand and best fit for determination of N_2 / clinoptilolite adsorption isotherm

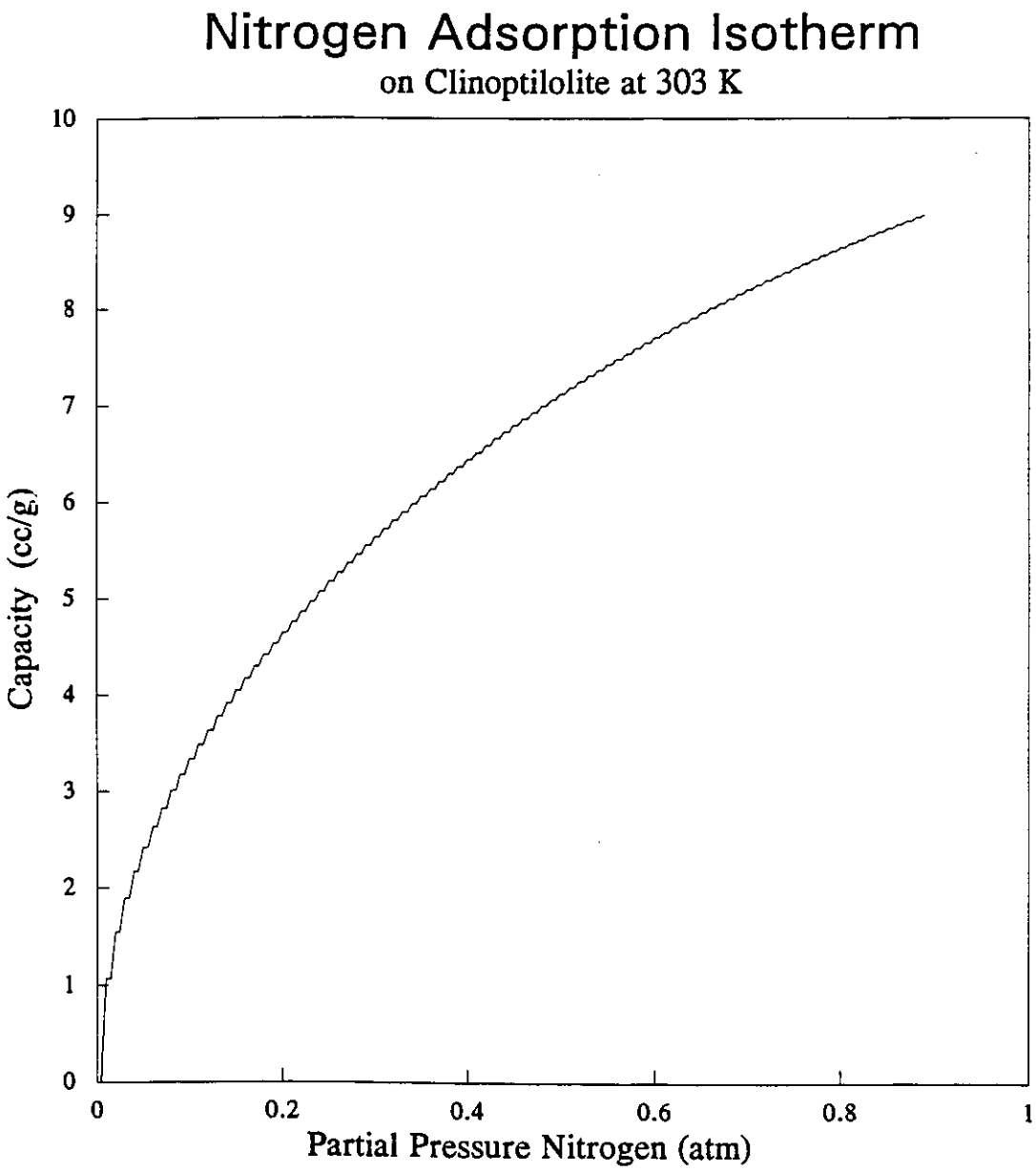

Figure 5.23 : Experimental N_2 / clinoptilolite adsorption isotherm at 303 K up to .9 atm

Henry's law constant for adsorption of N_2 on clinoptilolite is closer to the high 370 value, and that the initial slope of the experimental isotherm may therefore be slightly low.

Translating these results from dimensionless adsorption capacities to units of mmol / gram and comparing them to N_2 adsorption isotherms at 300 K on other natural and modified clinoptilolites yields some interesting observations, as shown in figure 5.24. The clinoptilolite used in the two studies have slightly different Si:Al ratios (4.25 for the Turkish clinoptilolite compared to approximately 5 for that used by Ackley & Yang [Ackley & Yang, (1991 b)]) and were determined at slightly different temperatures (303 K for the Turkish clinoptilolite and 300 K for the ion exchanged clinoptilolites). The pure clinoptilolite used by Ackley & Yang has an average of 3.1 Na^+ cations, 1.1 K^+ cations, and .73 Ca^{++} cations per unit cell, with some Mg^{++} and Fe^{+++} present, compared to that used in the present study which has Ca^{++}, K^+, and Mg^{++}, in that order, as the major cations (see table 5.8 for detailed cation content). The isotherms from literature given for N_2 adsorption on the exchanged forms of clinoptilolite are for fully or almost fully exchanged clinoptilolites [Ackley & Yang (1991 a)]. Figure 5.24 shows that the experimental isotherm determined in the present study lies amongst the literature isotherms for exchanged Na^+, K^+, and Mg^{++} clinoptilolites. As discussed earlier, Ca^{++} cations are significant pore blockers in the clinoptilolite channels. Ackley & Yang's results show that the Ca^{++} form of clinoptilolite has low capacity for N_2 and completely rejects CH_4, supporting the fact that Ca^{++} blocks pores. It seems logical that the high Ca^{++} content in the natural Turkish clinoptilolite may be responsible for the capacity of the Turkish clinoptilolite being lower than that of the pure and Mg^{++}, Na^+, and K^+ exchanged clinoptilolites due to this pore blockage. Since the experimental error in the isotherm from the present study may be high, these conclusions cannot be strongly supported. Furthermore the complexities introduced when dealing with multi - cation zeolites and the 3 degree difference in experimental temperatures make any quantitative analysis of the results difficult, and therefore the comparisons made here give only possible explanations for the phenomena observed, and the actual reasons for the isotherms lying where they do may be much more complicated. However it would be reasonable to assume that a reduction in the Ca^{++} cation content may lead to a higher N_2 adsorption capacity on the natural Turkish clinoptilolite. Regardless of the large

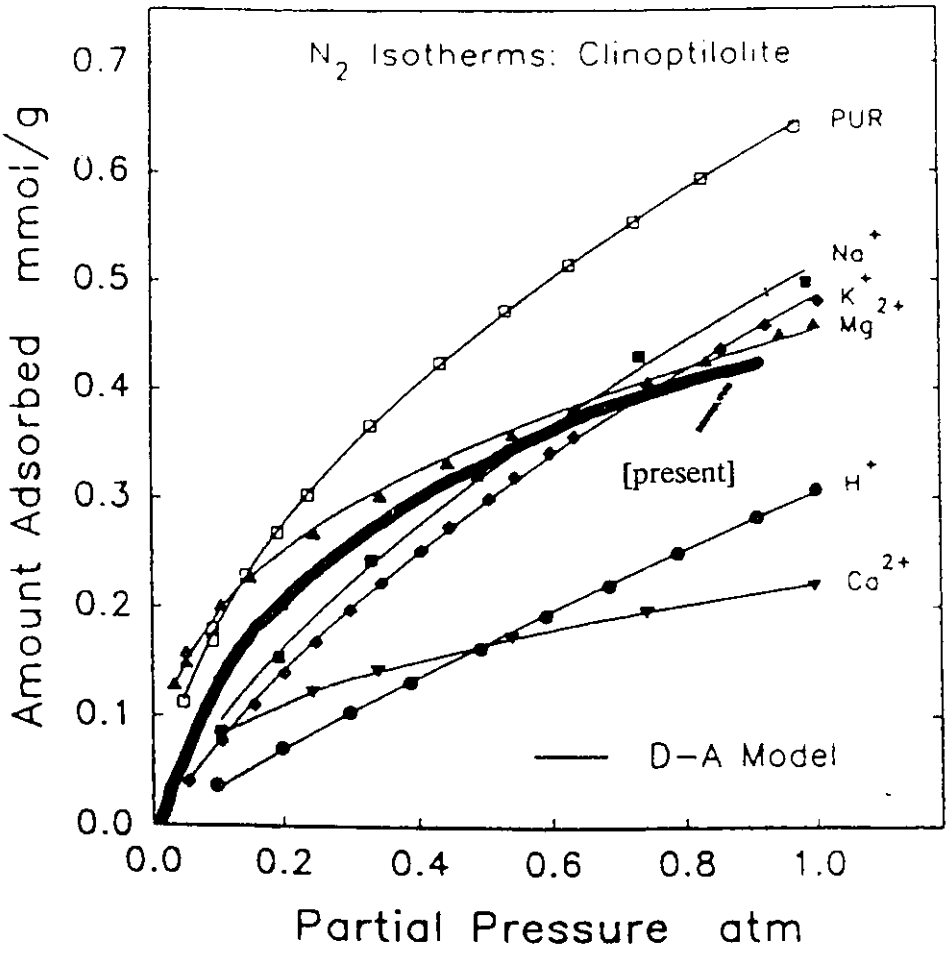

Figure 5.24 : Experimental N_2 / clinoptilolite adsorption isotherm at 303 K up to .9 atm compared with various other N_2 adsorption isotherms on ion exchanged clinoptilolites

degree of potential error in the isotherm, it is clear that the true isotherm will lie amongst those with similar ionic composition as shown in figure 5.24. Qualitatively the isotherm lies in the area it should relative to the other ionic forms of clinoptilolite.

5.3.2 Pure component adsorption of CO on Clinoptilolite

The adsorption of pure CO on clinoptilolite at 303 K and 1 atmosphere total pressure was also examined. Carrier composition was adjusted up to 90% and then back down to 0% CO (balance being He) to test for repeatability and reversibility. The value of K_p' was determined experimentally at each point. The plot of K_p' vs. %CO yields the value of dp_2/dq_2 from the intercept as the CO fraction approaches 1. This allows rearrangement of equation 18 to solve for q_1 by integrating with respect to p_1. The integral yields the isotherm as the quantity of CO adsorbed, q_1, vs. %CO. The integrand is shown in figure 5.25.

The problem encountered in interpretation of the N_2 adsorption experiments is amplified with the CO - clinoptilolite system, as expected. The CO is adsorbed much stronger than the N_2, and therefore it was expected that when the column was allowed to come to equilibrium with a carrier containing 1% CO that the CO pulse introduced to this system would be virtually non adsorbed, as the zeolite was already saturated from the 1% CO in the carrier. This was clearly the case, as shown in figure 5.25. The mean of the response peak produced when a CO pulse was introduced in a pure He carrier was some 20000 seconds, and that produced in a 1% CO carrier was approximately 1000 seconds. Thus the interpolation error discussed in the N_2 adsorption is even more severe with CO. Again, to attempt to minimize this error the integrand data was fitted with the same mathematical model used for the N_2 results. An excellent fit was obtained and is shown in figure 5.26, and the result of the integration of figure 5.26, (ie, the isotherm) is shown in figure 5.27. The fit in figure 5.26 is shown only for the data at 1% CO and greater to better demonstrate the goodness of fit.

It is the interpolation between 0% and 1% CO carrier that is critical. The curve provided by the model was used to produce figure 5.27, but the error resulting from this could be very large. The area under the curve represents the capacity, and the area under the curve is strongly dependant on the

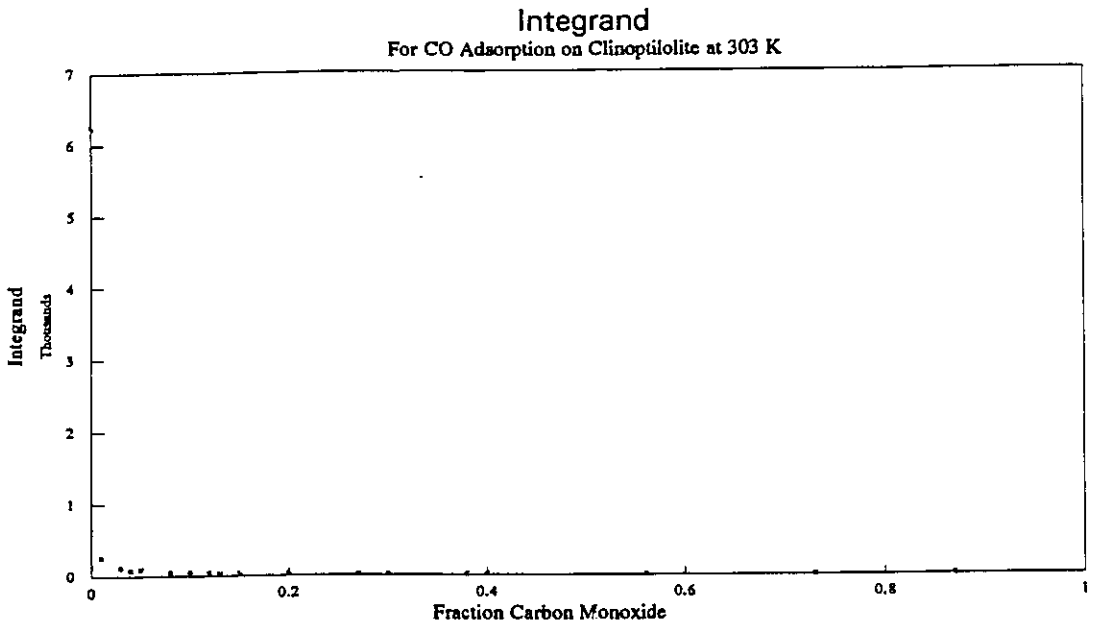

Figure 5.25 : Integrand for determination of CO / clinoptilolite adsorption isotherm

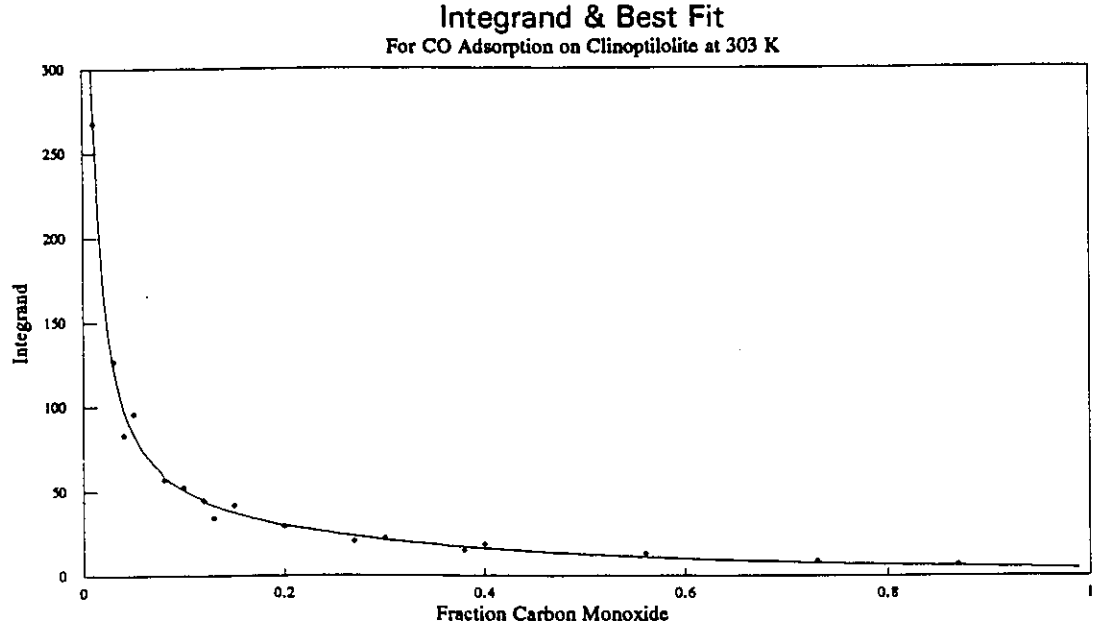

Figure 5.26 : Integrand and best fit for determination of CO / clinoptilolite adsorption isotherm

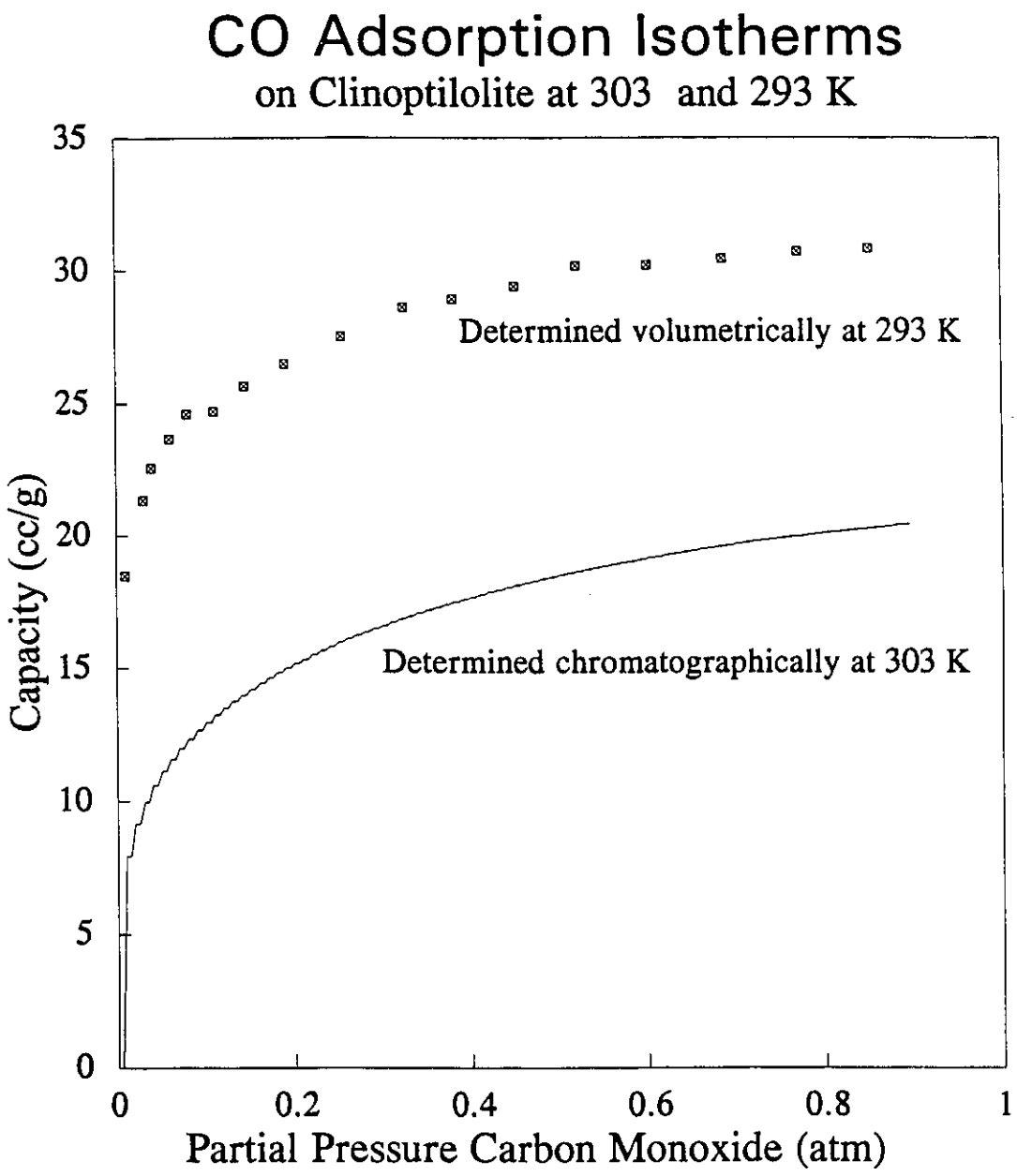

Figure 5.27 : Experimental CO / clinoptilolite adsorption isotherm at 303 K up to .9 atm compared with one at 298 K obtained voulmetrically [Sirkecioglu et al. (1992)]

interpolation between 0 and 1% CO carrier. Checking this area as before shows that the ultimate CO capacity of the clinoptilolite would be 50% greater than that shown for the present study in figure 5.27 on one extreme (if the 0% and 1% lines were connected with a straight line interpolation) and 30% smaller on the other (if the integrand were coincident with the y axis down to the first data point). Although this potential error is large, the interpolation cannot be significantly improved. The exact area under the integrand from 0 to 1% CO carrier could only be determined accurately if more data points were taken between these first two points, which was not possible with the present experimental system.

An adsorption isotherm for the CO / Turkish clinoptilolite system at 293 K has been determined independantly with a volumetric apparatus by other researchers [Sirkecioglu et al. (1992)] . This isotherm is also shown for comparison with that from the present study in figure 5.27. This figure shows that the shapes of the isotherms determined by both authors are quite similar. The ultimate capacity (at 1 atmosphere) at 303 K is some 30% lower than that obtained from the isotherm at 293 K. It was expected that the capacity decrease with increasing temperature, but it should be noted that this difference may not be solely due to the temperature difference. Much of the difference may arise from the error caused by the interpolation involved in obtaining the chromatographic isotherm. As mentioned above, if the line connecting these two points were closer to a straight line, the area under this initial part of the curve could increase up to 50% and the isotherm at 303 K would shift up towards that at 293 K. The initial slope of the isotherm at 293 K also seems to be greater than that at 303 K, as expected, but lack of data for the chromatographic isotherm at low partial pressures makes this comparison qualitative at best. The shape of the chromatographic isotherm would not change appreciably due to the interpolation error that may have so drastically affected the measurement of capacity. It is safe to conclude that the true CO isotherm at 303 K lies below that at 293 K, but by how much is difficult to determine due to the errors discussed. Furthermore slight differences in regeneration methods may have contributed to the difficulties in comparing the two isotherms.

The error due to interpolation in the calculation of the chromatographic isotherm brings about an important observation concerning the use of the chromatographic method for measurement of adsorption isotherms. If the initial slope of any given isotherm under specified conditions is large (ie, large Henry's

law constant), use of the chromatographic method for accurate measurement of the complete isotherm under these conditions is only viable if carrier gas compositions can be controlled to the fraction of a per cent level. Systems with large Henry's law constants will generally yield large retention times for pure carriers and small retention times when a minimal amount of sorbate is included in the carrier. This is because a strongly adsorbed species will reach saturation or near saturation in the zeolite at very low partial pressures. If this rapid change in retention time with increasing partial pressure cannot be accurately followed, the required interpolation between these low partial pressure data points may lead to severe error. Therefore given a system for chromatographic determination of a pure gas isotherm, the Henry's law constant should be examined. If it is relatively large, accurate gas mixing will be required to determine retention times at extremely low partial pressures. If this accurate blending is not available, a system with smaller initial slope should be chosen if an accurate isotherm is required. Gravimetric and volumetric methods do not suffer from this disadvantage. Thus the measurement of strongly rectangular pure isotherms with the chromatographic method is limited by the sensitivity of the carrier gas mixing system.

5.3.3 Binary adsorption of CO and N_2 on Clinoptilolite

Experiments were conducted with mixed CO / N_2 carriers to determine isotherms for the CO / N_2 / clinoptilolite system at 303 K. K_p' was measured experimentally as for pure gas isotherms, but both derivatives in equation 18 were not constant. A polynomial fit (equation 24) of the K'_p vs Y data (as described in section 2.4) was attempted, yielding values of 205.9, -1265, 2331, and -1280 for the coefficients A_0, A_1, A_2, and A_3, respectively. The fit was found to be poor due to oscillations. The functional form suggested by Tezel [Tezel (1991)] was then attempted and yielded a far superior fit than the polynomial, as shown in figure 5.28. The A coefficients in equation 25 were determined through a non - linear regression and the resulting values of A_{-1}, A_0, A_1, and A_2 were -31.7, 45.5, -9.48, and 1.91, respectively. From these values, the values of B_0, B_1, B_2, C_0, C_1, and C_2 were determined by simultaneously solving the system of equations 28 to 35. The resulting mixed gas isotherms for CO and N_2 on

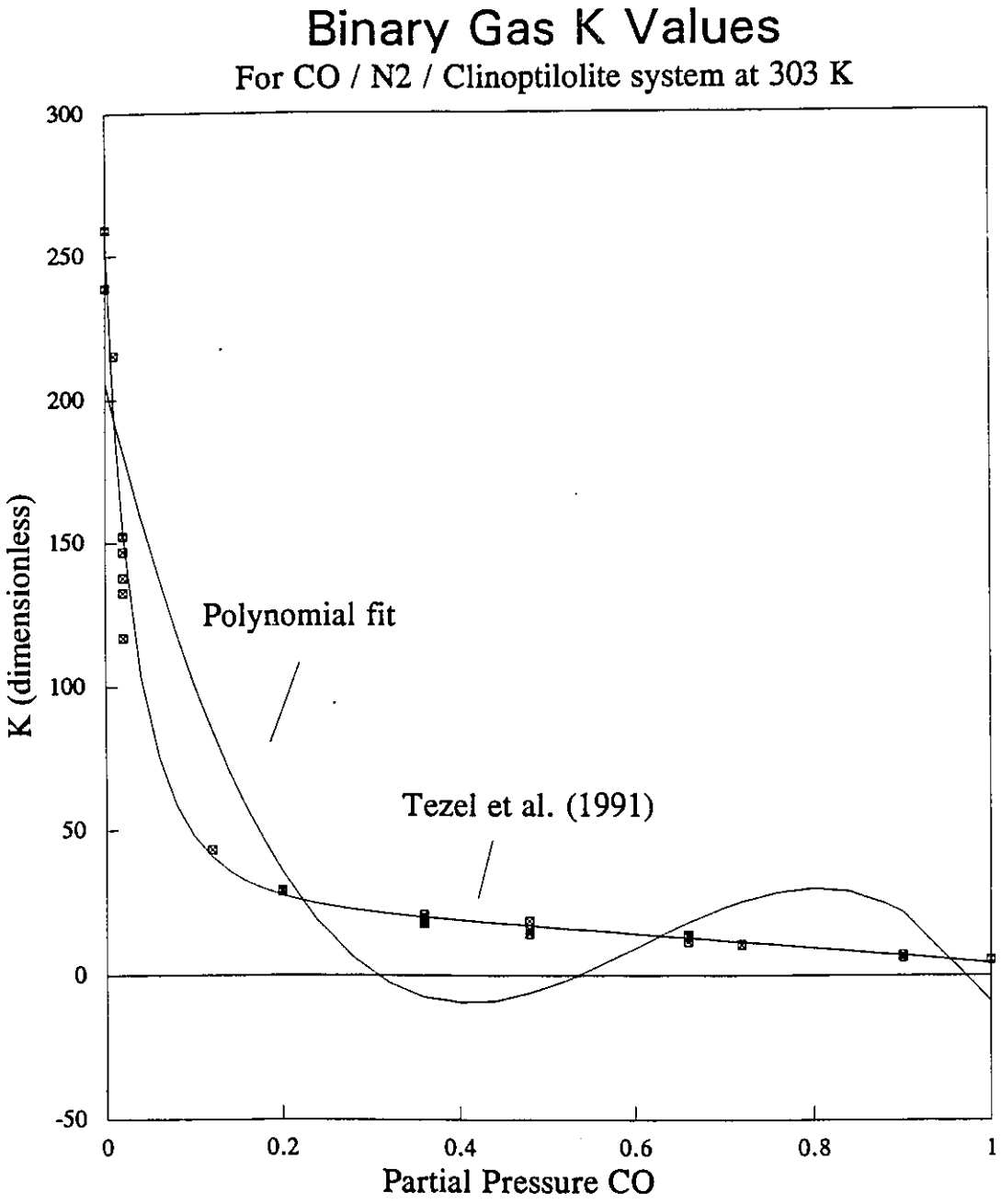

Figure 5.28 : Fit of experimental N_2 / CO / clinoptilolite adsorption isotherm raw data

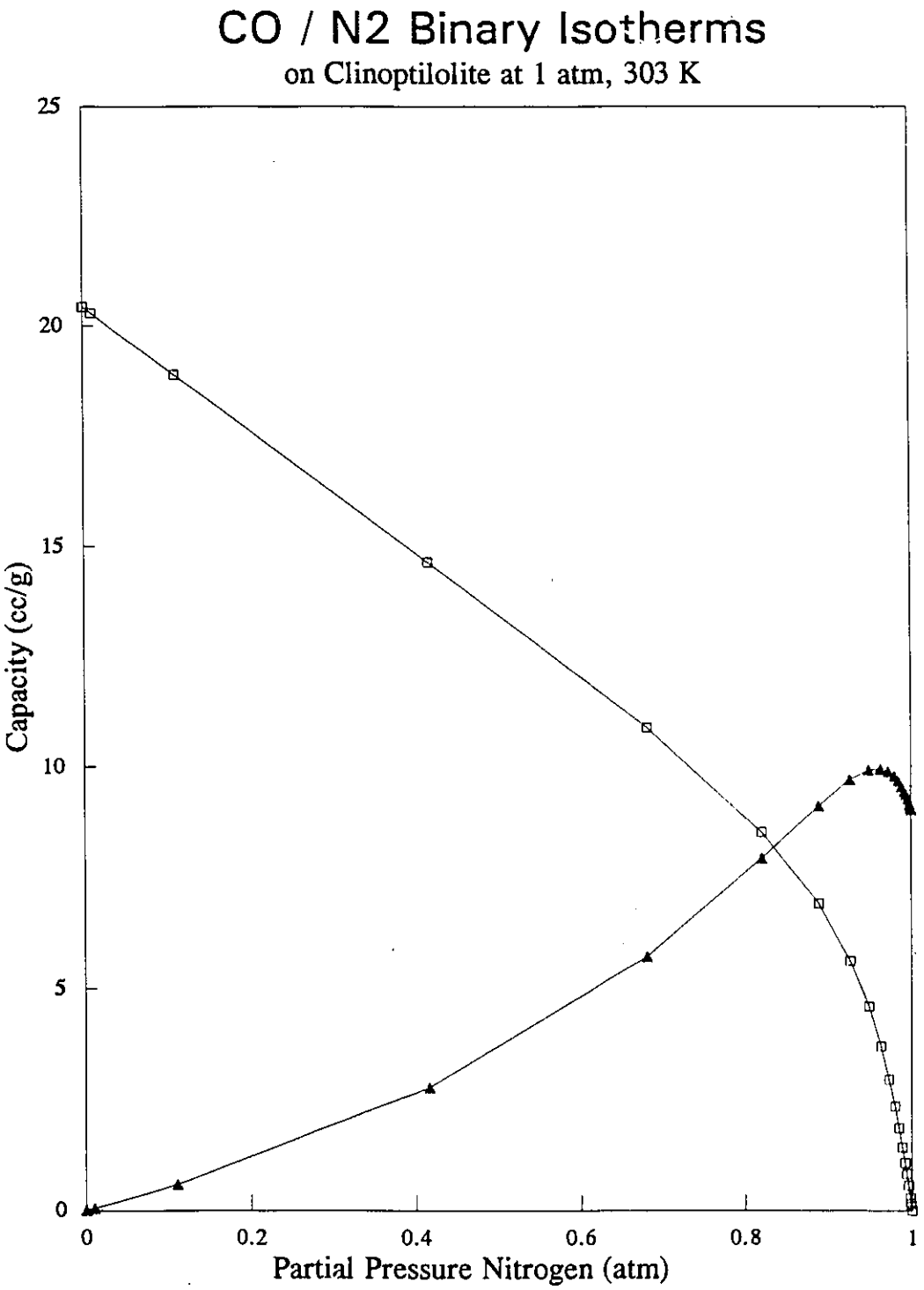

Figure 5.29 : Experimental N_2 / CO / clinoptilolite adsorption isotherm at 303 K

clinoptilolite at 303 K in the forms of equations 32 and 33 are described by equations 49 and 50 (where Y is the mol fraction of CO in the gas phase) and are shown in figure 5.29.

$$q_{CO} = 0.5738P\left[27.23Y_{CO} - 4.54\ln\left(\frac{Y_{CO}+.075}{.075}\right) + \frac{1.65Y_{CO}}{.075(Y_{CO}+.075)}\right] \text{ (cc/g)} \quad (49)$$

$$q_{N_2} = 0.5738P\left[-4.47(1-Y_{CO}) - 15.85\ln\left(\frac{Y_{CO}+.075}{1.075}\right) - \frac{1.77(1-Y_{CO})}{(1.075)(Y_{CO}+.075)}\right] \text{(cc/g)} \quad (50)$$

Some difficulties were encountered during the mixed CO / N_2 carrier experiments. Firstly, high purity CO is very expensive and the purity of CO obtained was limited to 99.99%, not a carrier grade purity. The TCD filaments in the GC detector are meant for use with filtered carrier grade He (99.999%), and thus the potential O_2 content in the CO may be 10 to 100 times greater than that in normal carrier. This was shown in the experimental results, as with the increase in the CO fraction in the carrier came an increase in the rate detector offset change. As the CO content increased, the amount of detector offset per unit time of running the detector increased drastically, producing high baseline shifts in those experiments. This is a result of the O_2 content in the carrier and of the plumbing of the GC. If the carrier were split and passed through both sides of the detector, no such offset would be expected as both filaments would oxidize at relatively similar rates. However the plumbing for these experiments ran a single carrier stream first through the reference side, then through the cloumn, and then through the detector side, as illustrated in figure 4.3. Thus the first filament would be exposed to higher O_2 levels and oxidize to a greater extent, leaving a lower O_2 level in the carrier which passes over the second filament. This is fully consistent with the experimental results. To compensate for this offset it was assumed that the rate of baseline shift was relatively constant for the duration of the experiment. This assumption was supported by blank runs which showed constant baseline shift rates at various CO levels when no sample gas was introduced. For this reason the experimental response peak obtained from the introduction of a pulse of either sample gas to the column at equilibrium was modified by subtracting the straight line offset, bringing the peak down to the baseline. Examples of a raw and corrected peak for adsorption of CO and N_2 on clinoptilolite is shown in figure 5.30. A linear regression was run on the latter part of the

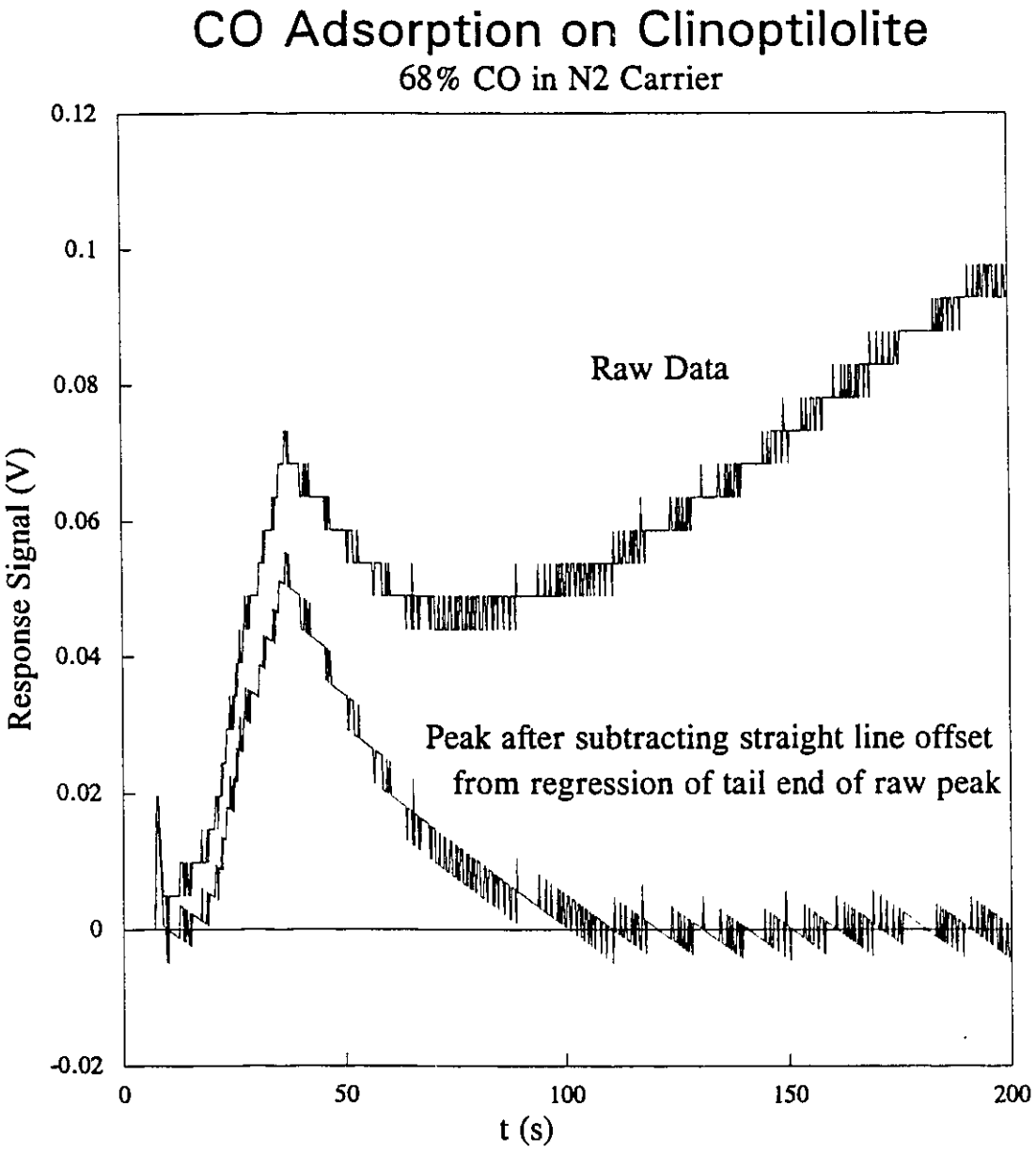

Figure 5.30 : Mathematical treatment of drifting peaks obtained in experiments with CO carrier

response (ie, where the sample pulse is assumedly out of the system) and this line was subtracted from the raw response yielding the modified response. The modified response was used to calculate the mean of the response curve. The same problem was encountered with the pure CO isotherm measurements, but not to the same degree. The relative size of the offset was much smaller for response peaks produced with CO / He carrier than for those with a CO / N_2 carrier due to the weak response signals resulting from the similarity in the conductivities of CO and N_2. Thus the correction of baseline offset caused by the dirty CO carrier is not nearly as critical when the CO sample produces a strong peak.

Another slight problem was encountered with the use of the TCD. The molecular masses and conductivities of CO and N_2 are virtually identical (only 3% difference in conductivities at 373 K), and as the mixture approaches 50% CO the difference in conductivity between either sample gas and the carrier diminishes. At some compositions it was very difficult to accurately determine the means of response peaks due to this limited difference in conductivity combined with the effect of the shifting baseline. This is the reason for some of the gaps in the experimental points presented in figure 5.28, including the significant gap between 2 and 12%. Nonetheless the shape of the K'_p vs Y curve was relatively well defined by the experimental points.

5.4 Modelling of Pure & Binary Adsorption Isotherms

The modelling of isotherms was attempted with the Langmuir, Ideal Adsorbed Solution Theory and Vacancy Solution Theory models. All calculations were done either on a spreadsheet or in FORTRAN programs executed on the CMS mainframe at the University of Ottawa. It should be noted that in all three cases the model prediction of the binary isotherm is to some degree based on the two experimental pure gas isotherms. Therefore the error in the experimental isotherms discussed in section 5.3 will affect the accuracy of the binary isotherm predictions. Furthermore, in determining the accuracy of these models, no sum of squared errors (SSE) was calculated. The reason for this is that the experimental isotherms are not represented by discrete points but rather by an integrated curve. Thus arbitrarily selecting the points with

which to calculate the SSE would influence the value of the SSE. This is true of the pure and binary isotherms. Therefore the fits of the models were evaluated qualitatively.

5.4.1 Langmuir & Extended Langmuir Models

The Langmuir equation coefficients (q_m, q_s and b) yielding the best fits of the experimental isotherms are given below for CO and N_2, and plots of the resultant fits are compared to the experimental isotherms for N_2 and CO in figures 5.31 and 5.32, respectively. It is clear from these figures that the Langmuir equation does not accurately fit the experimental curve for either pure gas

$$\frac{1}{q_{N_2}} = \frac{.00878}{P} + .1594 \tag{51}$$

$$\frac{1}{q_{CO}} = \frac{.00084}{P} + .0593 \tag{52}$$

system, overestimating the initial slope of the isotherm and underestimating the ultimate capacity of the zeolite. Using equation 30 to calculate the predicted binary isotherm from the Langmuir pure gas adsorption isotherms yields the curves shown in figure 5.33, presented along with the experimental curves. The results show what is expected; the shortcomings in the pure gas models are carried into the binary model. The predicted pure capacity of the clinoptilolite for both gases in the binary model is low as a direct result of the Langmuir pure gas isotherm model yielding low pure gas capacities at 1 atmosphere. Otherwise the Extended Langmuir equation fits the CO curve quite well, drifting away from the experimental values at low N_2 concentration. The shape of the Extended Langmuir prediction of the N_2 curve is similar to the experimental curve, but the predicted N_2 capacity rapidly grows distant from the experimental curve, again likely to the low predicted value of the pure gas adsorption capacity at high N_2. The predictions of the Extended Langmuir equation are therefore quite good considering the relatively poor fits of the Langmuir equation to the pure gas isotherms, but they do not well represent the experimental data.

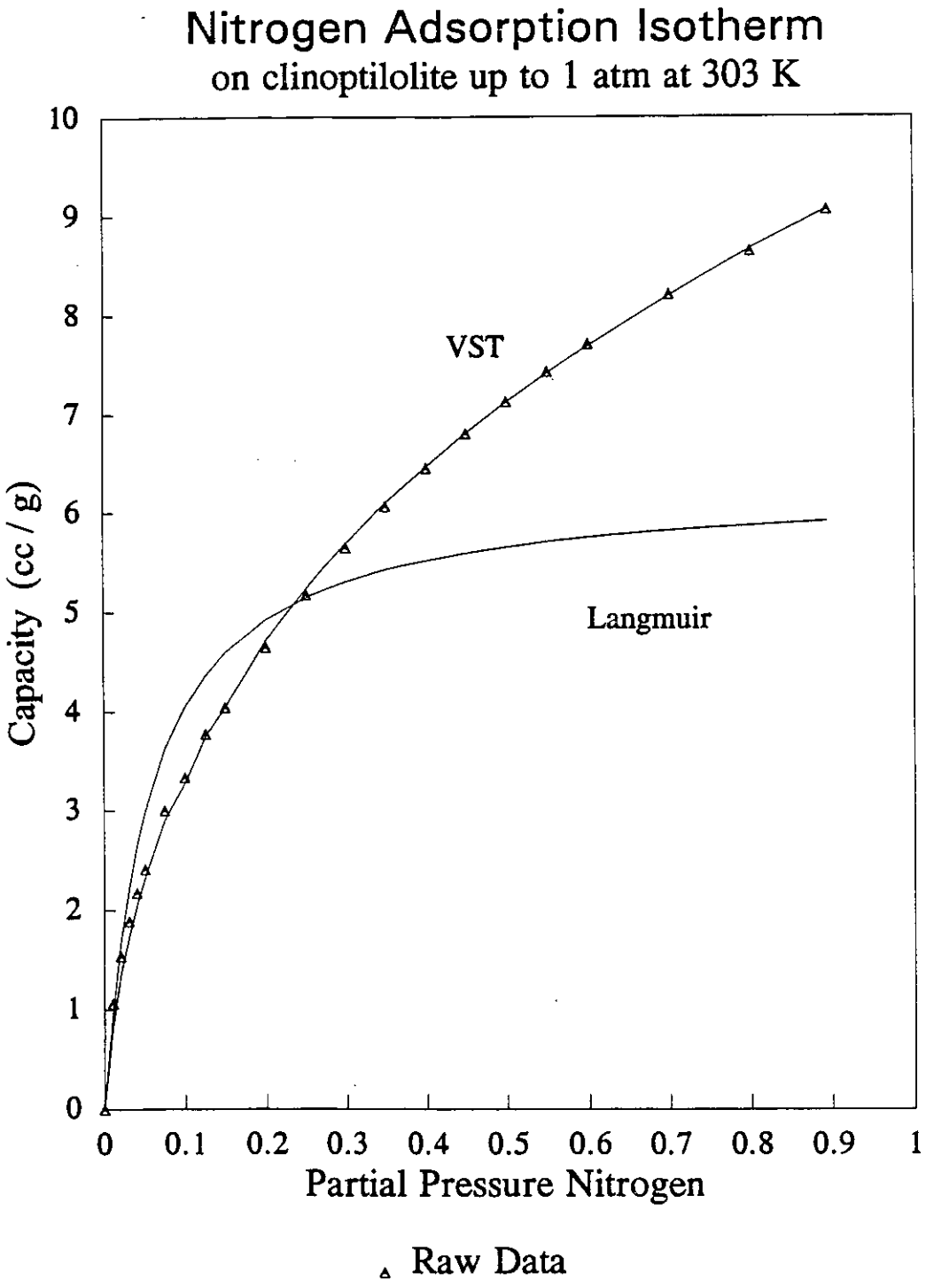

Figure 5.31 : Langmuir and VST model fits of experimental pure N_2 / clinoptilolite adsorption isotherm at 303 K

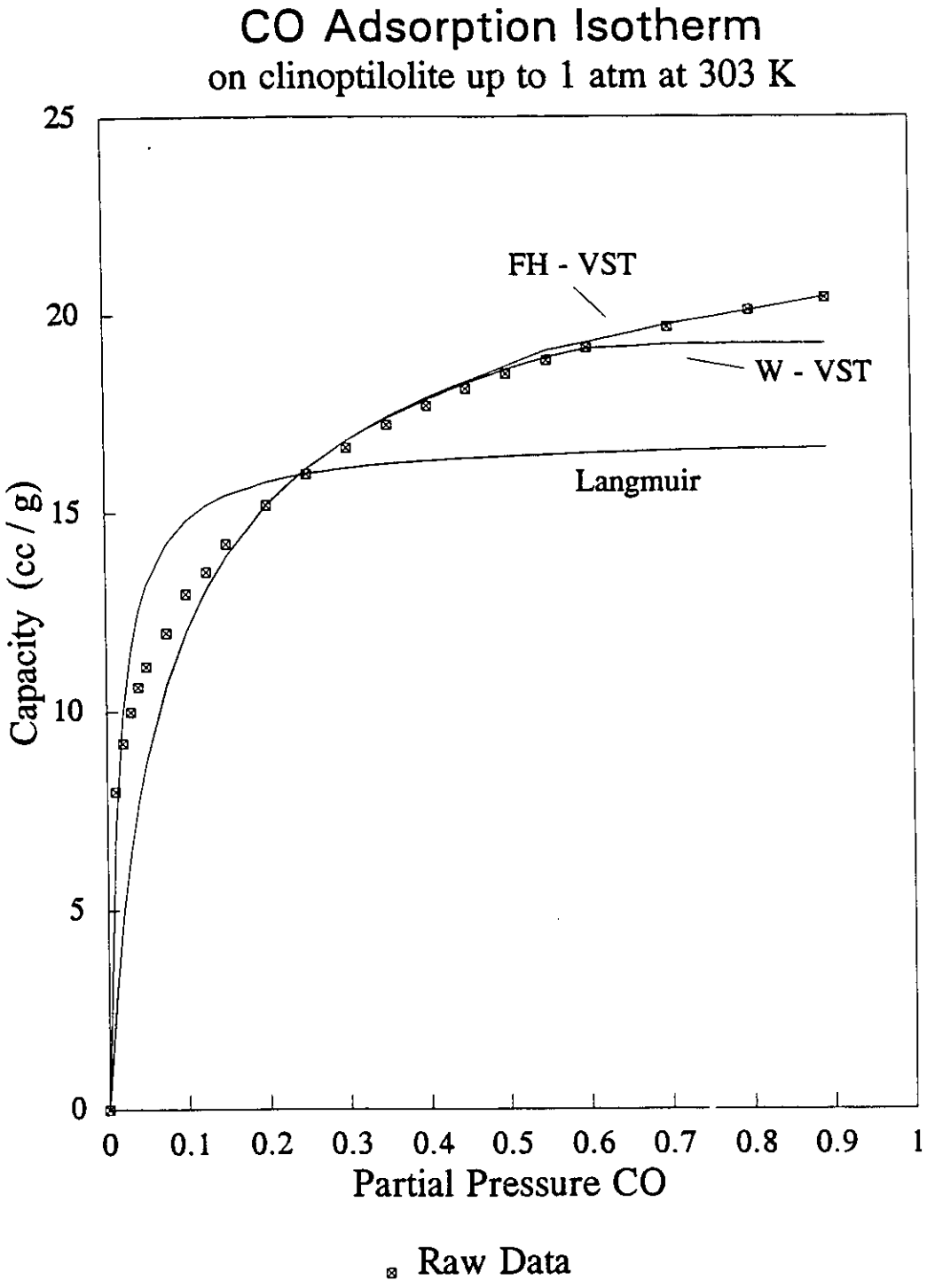

Figure 5.32 : Langmuir and VST model fits of experimental pure CO / clinoptilolite adsorption isotherm at 303 K

5.4.2 Ideal Adsorbed Solution Theory

The ideal adsorbed solution theory predicts binary adsorption isotherms from experimental pure isotherms. The integrations of the individual isotherms were done by Simpson's rule on a spreadsheet. The result of solving equations 37, 38, and 39 are shown in figure 5.33, along with the Extended Langmuir equation prediction and the experimental curves.

The results show a relatively poor fit of the experimental curves, poorer even than that provided by the Extended Langmuir model. The end points are correct, but this is mathematically inherent in the IAST model. In the region above N_2 fraction of .2 the difference between the experimental and IAST predicted curves grows until an N_2 fraction of .9. It is clear that this model is lacking, and this may be due to the fact that the IAST does not take into account strong surface - sorbate interactions [Yang (1987)]. Since the heats of adsorption of both these gases are very high (see table 5.7), it is reasonable to assume that there are strong surface - sorbate interactions, and this may well be the cause of the poor prediction yielded by the IAST.

Another source of error when dealing with the IAST is that integration under the experimental isotherm is often required beyond the experimental pressure range. In this study it was required that the N_2 isotherm be extrapolated up to a maximum pressure of over 5 atmospheres in order to meet the equality condition of equation 37. This extrapolation was done by using the VST pure N_2 isotherm fit to predict capacities beyond 1 atmosphere. Since the VST model N_2 isotherm is still increasing at 1 atmosphere, this extrapolation can lead to large errors in assuming a continuing rise instead of the more likely levelling of the isotherm. The VST predicted an ultimate N_2 capacity of 24 cc/g, which is likely well above the true ultimate capacity. Thus with two strongly adsorbed species and without fully defined isotherms (ie, a well defined final capacity) the model errors and extrapolation errors contribute to a poor fit of the experimental binary adsorption data.

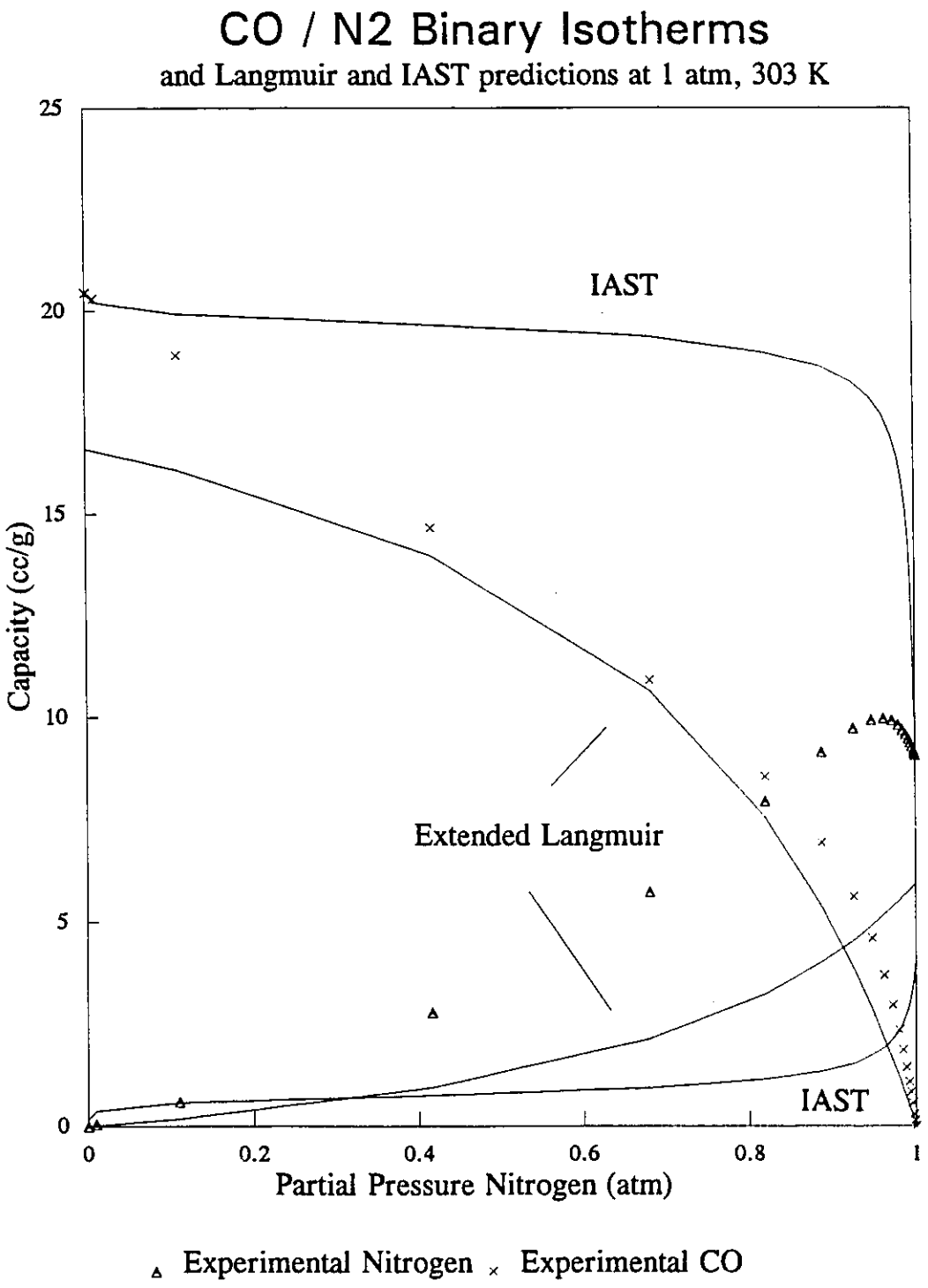

Figure 5.33 : Langmuir and IAST predictions of binary CO / N_2 / clinoptilolite adsorption isotherms at 303 K

5.4.3 Vacancy Solution Theory

The vacancy solution theory (VST) also predicts binary adsorption equilibria from pure gas adsorption isotherms. This model takes into account specific interactions between the adsorbed species and the sorbate by incorporating another coefficient into the isotherm equation (see section 2.4.1). The Flory Huggins and Wilson forms of the VST were both applied in the fitting of the pure isotherms. The best fits of the experimental isotherms for CO and N_2 were plotted and compared to the experimental isotherms in figures 5.31 and 5.32, respectively.

The results show that for N_2 the fits provided by the two VST forms are virtually identical, to the point of having the same values of the coefficients b and n^{inf}, as shown in table 5.12. Both fits match the experimental data very well. A numerical calculation of the sum of squared errors would be misleading, as the points are arbitrarily selected from the experimental isotherm curve. The two VST fits of the CO isotherm again show strong similarities. However, the coefficients show some important differences, as displayed in table 5.12. The two models yield largely different values of n^{inf}. This indicates that the three parameter Flory Huggins form predicts an ultimate capacity of 32 cc/g, while the four parameter Wilson form predicts an ultimate capacity of approximately 19 cc/g. Furthermore, the interaction parameter for the FH-VST was found to be negative, which is not explicitly forbidden, but it was not found to be negative in any of the articles examined, and a negative value of the interaction parameter leads to problems in modelling the binary isotherms. The best fit of the experimental data was actually achieved by the FH-VST when the value of the interaction parameter was largely negative (-46.9) and the value of the predicted ultimate capacity was over 11,000 cc/g. Clearly this was a purely mathematical fit, and the implications of the coefficients are lost (ie, the clinoptilolite cannot, under any conditions, adsorb 11,000 cc/g of CO). Furthermore the large negative value of α_{iv} when used in the binary modelling yields a logarithm of a negative number, which makes the binary modelling with these coefficients impossible. Alternate fits were attempted with the FH-VST to yield an interaction parameter that would allow prediction of the binary system behaviour. The resultant coefficients are those given in table 5.12.

Table 5.12 : VST coefficients for fits of pure component adsorption data

	FH - VST			W - VST			
Sorbate	b (cc/g atm)	$n^{inf.}$ (cc/g)	α_{iv}	b (cc/g atm)	$n^{inf.}$ (cc/g)	Λ_{iv}	Λ_{vi}
N_2	131.3	24.1	3.62	131.3	24.1	0.22	4.62
CO	347.8	32.0	-0.99	349	19.3	2.5	.0016

Convergence was never achieved with the FH-VST when $\alpha_{iv}>0$, and as a result the binary equilibrium predictions from the FH-VST would likely be poor. The values of the coefficients of the W-VST equations were found to be within a logical range, and it was expected that the binary predictions yielded by the four parameter W-VST would therefore be superior to that of the three parameter FH-VST.

The binary equilibrium predictions from the VST models are presented with the experimental binary isotherms in figure 5.34. The results show what was expected; the W-VST yields a better prediciton of the binary adsorption equilibrium than the FH-VST due to the reasonable values of the W-VST coefficients. The W-VST is, in fact, clearly the best model of all those tested for the prediction of the binary gas adsorption isotherms, and the only model which accurately predicted the experimental binary data.

The high heats of adsorption of both N_2 and CO on clinoptilolite indicate a strong specific interaction between both sorbates and the sorbent. It is expected then, that the models not taking these specific interactions into account would predict the binary isotherm poorly. Thus the poor predictions of the IAST and extended Langmuir models. The two forms of the VST take into account these interactions, the FH-VST with one coefficient and the W-VST with two. It is apparent from the binary equilibrium predictons and from the FH-VST fit of the pure CO isotherm that one interaction parameter is not enough, and that the two interaction parameters of the W-VST are required to accurately represent the expermintal adsorption data. In conclusion, despite the poor binary predicitons of most models tested, the models behaved as expected for the given binary system.

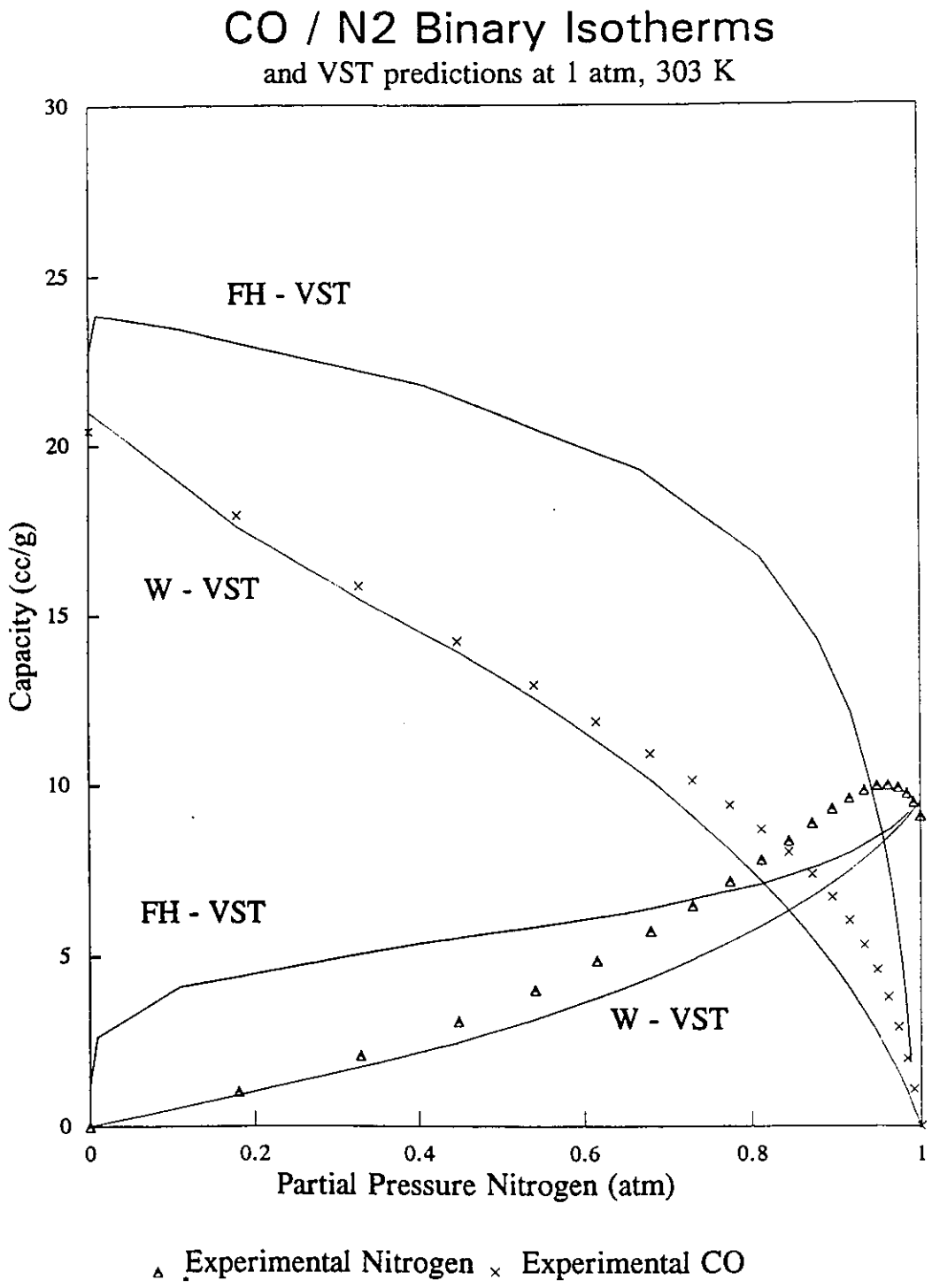

Figure 5.34 : VST predictions of binary CO / N_2 / clinoptilolite adsorption isotherm at 303 K

6. Conclusions

1. Equilibrium separation factors for separation of C_2H_4 from CH_4 and C_2H_6 are promising, particularily in molecular sieves with accessible divalent cations.

2. Equilibrium separation factors for separation of CO and NO from N_2 are promising, particularily in molecular sieves with accessible divalent cations.

3. Compounds with relatively strong dipoles or quadropoles are easily separated from weakly polar species in zeolites with divalent cations due to the strong specific interactions between the molecule and the accessible divalent ion.

4. Of all molecular sieves tested, the clinoptilolite yielded the strongest adsorption of CO, NO and N_2 between 323 and 473 K.

5. CO_2 was strongly and possibly irreversibly adsorbed on the clinoptilolite.

6. C_2H_4 was strongly and possibly irreversibly adsorbed on the clinoptilolite and the CaX zeolite.

7. Experimental heats of sorption for CO on A zeolites and H - mordenite, and experimental vant Hoff plots for CO adsorption on A zeolites agree well with those in literature.

8. Micropore diffusion is the dominant mass transfer mechanism for both CO and N_2 in clinoptilolite.

9. Diffusion of N_2 in the clinoptilolite micropores is three time greater than that of CO under the

conditions examined.

10. Equilibrium selectivity of clinoptilolite favors CO over N_2 whereas kinetic selectivity favors N_2 over CO over the temperature range considered.

11. The gas chromatographic method is limited by the accuracy of its gas blending system in the experimental measurement of rectangular isotherms.

12. Both N_2 and CO have sharply rectangular adsorption isotherms on clinoptilolite at 303 K.

13. At .9 atmosphere the capacities of clinoptilolite for CO and N_2 are approximately 20 and 9 cc/g, respectively.

14. The Langmuir model fails in fitting the pure component isotherms.

15. The Langmuir, IAST and FH - VST models fail in their prediction of the binary CO / N_2 / clinoptilolite adsorption isotherm due to their misrepresentation of the pure gas isotherms.

16. The Wilson form of the VST accurately predicts the binary adsorption behaviour of the CO / N_2 / clinoptilolite system at 303 K from the pure adsorption isotherms of these components.

17. Clinoptilolite has been shown to be a promising and versatile sorbent for various gas separation and purification applications.

7. Recommendations

1. The chromatographic method should continue to be used to screen zeolites for potentially promising separations.

2. The chromatographic method should not be used for determination of pure gas isotherms with large (greater than 1000) K_p. For measurement of isotherms with K_p values larger than 100, accuracy of gas blending will limit the accuracy of the final results.

3. More research on the effects of bivalent ions on the separation of polar and non - polar compounds should be conducted.

4. Clinoptilolite is a promising sorbent, but consistency of natural zeolites is an issue. Properties of ion exchanged Turkish clinoptilolite should be compared with those of Ackley & Yang (1991 a, b) to determine consistency of the adsorption properties of ionically identical clinoptilolite from different sources.

5. Measurement of highly rectangular isotherms (K_p> 1000) should be conducted volumetrically or gravimetrically.

6. Measurement of strongly adsorbed species (CO_2 and C_2H_4) could be attempted with smaller zeolite sample size to increase the strength of the response peak (ZLC methods).

7. Prediction of binary isotherms using any of the models presented here should not be attempted if the model does not involve an accurate representation of the pure gas adsorption isotherms.

8. The FH - VST should not be considered a simple replacement for the W - VST. In some cases the more complex W - VST will yield far better results than the FH - VST.

9. The clinoptilolite should be checked for attrition resistance to determine ite potential for application in industry.

8. References

Ackley, M. W., Giese, R. F., and Yang, R. T., Clinoptilolite: Untapped Potential for Kinetic Gas Separations, *Zeolites*, **12**, pp 780 - 788, 1992.

Ackley, M. W., and Yang, R. T., Adsorption Characteristics of High - Exchange Clinoptilolites, *Ind. Eng. Chem. Res.*, **30**, pp 2523 - 2530, 1991 a.

Ackley, M. W., and Yang, R. T., Diffusion in Ion - Exchanged Clinoptilolites, *AIChE J.*, **37**, No. 11, pp 1645 - 1656, 1991 b.

Ackley, M. W., and Yang, R. T., Kinetic Separation by Pressure Swing Adsorption: Method of Characteristics Model, *AIChE J.*,**36**, No. 8, pp 1229 - 1238, 1990.

Ali, I. T., and Gay, I. D., Adsorption of Olefins on Zinc Oxide. Observations by Carbon 13 Nuclear Magnetic Resonance, *J. Phys. Chem.*, **85**, pp 1251 - 1254, 1981.

Ali, I. T., and Gay, I. D., Adsorption and Hydrogenation of Ethylene on Pure and Doped Zinc Oxide: Studies by Proton Magnetic Resonance, *J. Catal.*, **62**, pp 341 - 348, 1980.

Ames, Jr., L. L., Cation Sieve Properties of the Open Zeolites Chabazite, Mordenite, Erionite and Clinoptilolite, *Am. Mineral.*, **46**, pp 1120 - 1131, 1961 a.

Ames, Jr., L. L., Cation Sieve Properties of Clinoptilolite, *Am. Mineral.*, **45**, pp 689 - 701, 1961 b.

Apolonatos, G., *Gas Adsorption With Molecular Sieve Zeolites*, M. A. Sc. Thesis Diss., Department of Chemical Engineering, University of Ottawa, 1990.

Barrer, R. M., and Makki, M.B., Molecular Sieve Sorbents from Clinoptilolite, *Can. J. Chem.*, **42**, pp 1481 - 1487, 1964.

Barrer, R. M., and Townsend, R. P., Transition Metal Ion Exchange in Zeolites, *J. Chem. Soc., Faraday Trans. 1.*, **72**, pp 2650 - 2660, 1976.

Bird, R. B., Stewart, W. E., and Lightfoot, E. N., *Transport Phenomena*, John Wiley & Sons Inc., New York, 1960.

Brandt, W. W., and Rudloff, W., Diffusion of Ethane in Modified Synthetic Zeolites, *J. Phys. Chem. Solids*, **26**, pp 741 - 745, 1965.

Brandt, W. W., and Rudloff, W., Rapid Sorption Processes on Granular Zeolite, *J. Phys. Chem. Solids*, **25**, pp 167 - 176, 1964.

Breck, D. W., *Zeolite Molecular Sieves: Structure, Chemistry and Use*, John Wiley & Sons Inc., New York, 1973.

Brunauer, S., Emmett, P. H., and Teller, E., Adsorption of Gases in Multimolecular Layers, *J. Amer. Chem. Soc.*, **60**, pp 309 - 319, 1938.

Carter, J. L., Yates, D. J. C., Lucchesi, P. J., Elliott, J. J., and Kevorkian, V., The Adsorption of Ethylene on a Series of Near - Faujasite Zeolites Studied by Infrared Spectroscopy and Calorimetry, *J. Phys. Chem.*, **70**, No. 4, pp 1126 - 1136, 1966.

Carter, J. L., Lucas, P. J., and Nightingale, E. R. Jr., Olefin Separation with Strontium and Cadmium Molecular Sieves, U. S. Patent 3355509, 1967.

Cochran, T. W., Kabel, R. L., and Danner, R. P., Vacancy Solution Theory of Adsorption Using Flory - Huggins Activity Coefficient Equations, *AIChE. J.*, **31**, No. 2, pp 268 - 277, 1985 a.

Cochran, T. W., Kabel, R. L., and Danner, R. P., The Vacancy Solution Model of Adsorption - Improvements and Recommendations, *AIChE J.*, **31**, No. 12, pp 2075 - 2082, 1985 b.

Costa, E., Calleja, G., and Domingo, F., Adsorption of Gaseous Hydrocarbons on Activated Carbon: Characteristic Kinetic Curve, *AIChE J.*, **31**, No. 6, pp 982 - 991, 1985.

Costa, E., Sotelo, J. L., Calleja, G., and Marron, C., Adsorption on Binary and Ternary Hydrocarbon Gas Mixtures on Activated Carbon: Experimental Determination and Theoretical Prediction of the Ternary Equilibrium Data, *AIChE J*, **27**, No. 1, pp 5 - 12, 1981.

Coughlan, B., Kilmartin, S., McEntee, J., and Shaw, R. G., The Interpretation of Zeolitic CO_2 Equilibria Using a Theoretical Isotherm Equation, *J. Colloid Interface Sci.*, **52**, No. 2, pp 386 - 390, 1975.

Danner, R. P., Application of Vacancy Solution Theory to Gas Adsorption, prepared for presentation at the Fundamentals of Adsorption Conference, Upper Bavaria, Germany, May 6 - 11, 1983.

Danner, R. P., and Choi, E. C. F., Mixture Adsorption Equilibria of Ethane and Ethylene on 13X Molecular Sieves, *Ind. Eng. Chem. Fundam.*, **17**, No. 4, pp 248 - 253, 1978.

Danner, R. P. and Wenzel, L. A., Adsorption of Carbon Monoxide - Nitrogen, Carbon Monoxide - Oxygen, and Oxygen - Nitrogen Mixtures on Synthetic Zeolites, *AIChE J.*, **15**, No. 4, 1969.

Davis, M. E., Zeolites and Molecular Sieves: Not Just Ordinary Catalysts, *Ind. Eng. Chem. Res.*, **30**, No. 8, pp 1675 - 1683, 1991.

Derrah, R. I., Loughlin, K. F., and Ruthven, D. M., Sorption of Ethylene, Propylene and Cyclopropane in 5A Zeolite, *J. Chem. Soc. Faraday Trans. 1.*, **68**, pp 1947 - 1955, 1972.

Dexin, Z., and Youfan, G., Prediction of breakthrough curves in the system of CH_4, C_2H_6 and CO_2 coadsorption on 4A molecular sieve, *Gas Sep. Purif.*, **2**, pp 28 - 33, 1988.

Dorfman, L. R., and Danner, R. P., Equilibrium Adsorption of Nitrogen - Oxygen - Carbon Monoxide Mixtures on Molecular Sieve Type 10X, *AIChE Symp. Ser.*, **71**, No. 152, pp 30 - 39, 1975.

Eagan, J. D., and R. B. Anderson, Kinetics and Equilibrium of Adsorption on 4A Zeolite, *J Colloid Interface Sci.*, **50**, No. 3, pp 419 - 433, 1975.

Eberly, Jr., P. E., Diffusion Studies in Zeolites and Related Solids by Gas Chromatographic Techniques, *Ind. Eng. Chem. Fundam.*, **8**, No. 1, pp 25 - 30, 1969.

Egerton, T. A., and Stone, F. F., *Trans. Faraday Soc.*, **69**, 1983.

Emesh, I. T. A., and Gay, I. D., Adsorption and ^{13}C N. m. r. Studies of Ethene, Ethane, and Carbon Monoxide on Zn- and Cd- exchanged A Zeolites, *J. Chem. Tech. Biotechnol.*, **35A**, pp 115 - 120, 1985.

Federova, M. F., and Aliev, A. N., Low Temperature Adsorption of Gases on Zeolites at Low Pressure, *Russian J. Phys. Chem.*, **40**, 1966.

Frankiewicz, T. C., and Donnelly, R. G., Methane / Nitrogen Gas Separation over the Zeolite Clinoptilolite by the Selective Adsorption of Nitrogen, in *Industrial Gas Separations*; Whyte, T. E. et al., Eds., American Chemical Society, Washington D. C., pp 213 - 233, 1983.

Giacobbe, F. W., Adsorption of very low level carbon dioxide impurities in oxygen on a 13X molecular sieve, *Gas Sep. Purif.*, **5**, pp 16 - 19, 1991.

Giacobbe, F. W., Use of physical adsorption to facilitate the production of high purity oxygen, *Gas Sep. Purif.*, **3**, pp 133 - 138, 1989.

Gottardi, G., and Galli, E., *Natural Zeolites*, Springer - Verlag, Berlin, 1985.

Habgood, H. W., Adsorptive and Gas Chromatographic Properties of Various Cationic Forms of Zeolite X, *Can. J. Chem.*, **42**, pp 2340 - 2349, 1964.

Habgood, H. W., The Kinetics of Molecular Sieve Action. Sorption of Nitrogen - Methane Mixtures by Linde Molecular Sieve 4A, *Can. J. Chem.*, **36**, pp 1384 - 1397, 1958.

Habgood, H. W. and MacDonald, W. R., Effects of Micropores on Peak Shape and Retention Volume in Gas - Solid Chromatography, *Analytical Chem.*, **42**, No. 4, pp 543 - 546, 1970.

Hampson, J. A., and Rees, L. V. C., Sorption of Ethene and Propene and their Binary Mixtures in Zeolites, *Proc. 4th. Int. Conf. Fund. Ads.*, M. Suzuki, ed., pp 259 - 266, 1992.

Haq, N., and Ruthven, D. M., Chromatographic Study of Sorption and Diffusion in 4A Zeolite, *J. Colloid Interface Sci.*, **112**, No. 1, pp 154 - 163, 1986 a.

Haq, N., and Ruthven, D. M., A Chromatographic Study of Sorption and Diffusion in 5A Zeolite, *J. Colloid Interface Sci.*, **112**, No. 1, pp 164 - 169, 1986 b.

Harper, R. J., Stifel, G. R., and Anderson, R. B., Adsorption of Gases on 4A Zeolite, *Can. J. Chem.*, **47**, pp 4661 - 4670, 1969.

Hart, J., and Thomas, W. J., Gas separation by pulsed pressure swing adsorption, *Gas Sep. Purif.*, **5**, pp 125 - 133, 1991.

Hashimoto, N., and Smith, J. M., Macropore Diffusion in Molecular Sieve Pellets by Chromatography, *Ind. Eng. Chem. Fundam.*, **12**, No. 3, pp 353 - 359, 1973.

Hayhurst, D. T., and Lee, J., C., High Pressure Oxygen, Nitrogen and Argon Adsorption in Mordenites, *AIChE Symp. Ser.*, **79**, No. 230, pp 67 - 77, 1983.

Haynes, Jr., H. W., The Determination of Effective Diffusivity by Gas Chromatography. Time Domain Solutions, *Chem. Eng. Sci.*, **30**, pp 955 - 961, 1975.

Haynes, Jr., H. W., and Sarma, P. N., A Model for the Application of Gas Chromatography to Measurements of Diffusion in Bidisperse Structured Catalysts, *AIChE J.*, **19**, No. 5, pp 1043 - 1046, 1973.

Hsu, L. K. P., and Haynes, Jr., H. W., Effective Diffusivity by the Gas Chromatographic Technique: Analysis and Application to Measurements of Diffusion of Various Hydrocarbons in Zeolite NaY, *AIChE J.*, **27**, No. 1, pp 81 - 91, 1981.

Huang, C. C., and Fair, J. R., Study of the Adsorption and Desorption of Multiple Adsorbates in a Fixed Bed, *AIChE J.*, **34**, No. 11, pp 1861 - 1877, 1988.

Hyun, S. H., and Danner, R. P., Determination of Gas Adsorption Equilibria by the Concentration - Pulse Technique, *AIChE Symp. Ser.*, **78**, No. 219, pp 19 - 28, 1982 a.

Hyun, S. H., and Danner, R. P., Equilibrium Adsorption of Ethane, Ethylene, Isobutane, Carbon Dioxide and their Binary Mixtures on 13X Molecular Sieves, *J. Chem. Eng. Data*, **27**, No. 2, pp 196 - 200, 1982 b.

Hyun, S. H., and Danner, R. P., Gas Adsorption Isotherms by use of Perturbation Chromatography, *Ind. Eng. Chem. Fundam.*, **24**, pp 95 - 101, 1985.

Iijima, A., Composition and Origin of Clinoptilolite in the Nakanosawa Tuff of Rumoi, Hokkaido, *Molecular Sieve Zeolites - I*, Am. Chem. Soc., pp. 334 - 341, 1971.

Inui, T., Okugawa, Y., and Yasuda, M., Relationship between Properties of Various Zeolites and Their CO_2 Adsorption Behaviours in Pressure Swing Adsorption Operation, *Ind. Eng. Chem. Res.*, **27**, pp 1103 - 1109, 1988.

Joithe, W., Bell, T. B., and Lynn, S., Removal and Recovery of NO_x from Nitric Acid Plant Tail Gas by Adsorption on Molecular Sieves, *Ind. Eng. Process Des. Develop.*, **11**, No. 3, pp 434 - 439, 1972.

Kallo, D., Papp, J., and Valyon, J., Adsorption and catalytic properties of sedimentary clinoptilolite and mordenite from the Tokaj Hills, Hungary, *Zeolites*, **2**, pp 13 - 16, 1982.

Kaneko, K., and Inouye, K., Adsorption Activity of NO on Iron Oxide Dispersed Porous Materials, *Adsorption Sci. Tech.*, **5**, pp 239 - 250, 1988.

Kasuya, F., and Tsuji, T., High purity CO gas separation by pressure swing adsorption, *Gas Sep. Purif.*, **5**, pp 242 - 246, 1991.

Kaul, B. K., Modern Version of Volumetric Apparatus for Measuring Gas - Solid Equilibrium Data, *Ind. Eng. Chem. Res.*, **26**, pp 928 - 933, 1987.

Khulbe, K. C., Mann, R. S., and Ajaka, C. D., Characterization of MoO_3 - zeolite prepared from ammonium molybdate, *Zeolites*, **13**, pp 572 - 580, 1993.

Kimberlin, C. N. Jr., and Judson, M. W., Olefin Separation and Recovery, U. S. Patent 2866835, 1958.

Komorowska-Czepirska, E., Adsorption of Carbon Dioxide on Dealuminated Y Type Zeolites, *Polish J. Chem.*, **65**, pp 405 - 411, 1991.

Kondis, E. F., and Dranoff, J. S., Kinetics of Isothermal Sorption of Ethane on 4A Molecular Sieve Pellets, *Ind. Eng. Chem. Process Des. Develop.*, **10**, No. 1, pp 108 - 114, 1971.

Koyama, K., and Takeuchi, Y., Clinoptilolite: the distribution of potassium atoms and its role in thermal stability, *Zeitschrift fur Kristallographie*, **145**, pp 216 - 239, 1977.

Labrousse, M., Non - Cryogenic Oxygen Production Largest in Europe, *Int. Symp. on Gas Sep. Tech.*, Antwerp, Belgium, 1989.

Langer, G., Roethe, A., Roethe, K. P., and Gelbin, D., Heat and Mass Transfer in Packed Beds III - Axial Mass Dispersion, *Int. J. Heat Mass Transfer*, **21**, pp 751 - 759, 1978.

Lee, H., and Chi, C. W., Carbon Dioxide Removal from Air by Sodium X Molecular Sieve under Nonisothermal Conditions, *AIChE Symp. Ser.*, **67**, No. 117, pp 84 - 89, 1971.

Lee, H., and Stahl, D. E., Oxygen Rich Gas from Air by Pressure Swing Adsorption Process, *AIChE Symp. Ser.*, **69**, No. 134, pp 1 - 8, 1973.

Lewis, W. K., Gilliland, E. R., Chertow, B., and Cadogan, W. P., Adsorption Equilibria: Hydrocarbon Gas Mixtures, *Ind. Eng. Chem.*, **42**, No. 7, pp 1319 - 1326, 1950.

Loughlin, K. F., Holborow, K. A., and Ruthven, D. M., Multicomponent Sorption Equilibria of Light Hydrocarbons in 5A Zeolite, *AIChE Symp. Ser.*, **71**, No. 152, pp 24 - 29, 1975.

Loughlin, K. F., and Ruthven, D. M., The sorption and diffusion of ethane in type A zeolites, *Chem. Eng. Sci.*, **27**, pp 1401 - 1408, 1972.

Ma, Y. H., and Lee, T. Y., Diffusion of Binary Gas Mixtures in Zeolite X Pellets, *Ind. Eng. Chem. Fundam.*, **16**, No. 1, pp 44 - 48, 1977.

Ma, Y. H., and Mancel, C., Diffusion of Hydrocarbons in Mordenites by Gas Chromatography, *Adv. Chem. Ser.*, pp 392 - 402, 1973.

Ma, Y. H., and Mancel, C., Diffusion Studies of CO_2, NO, NO_2, and SO_2 on Molecular Sieve Zeolites by Gas Chromatography, *AIChE J.*, **18**, No. 6, pp 1148 - 1153, 1972.

Ma, Y. H., and Roux, A. J., Multicomponent Rates of Sorption of SO_2 and CO_2 in Sodium Mordenite, *AIChE J.*, **19**, No. 5, pp 1055 - 1059, 1973.

MacDonald, W. R., and Habgood, H. W., A Gas Chromatographic Method for the Determination of Mass Transfer Resistances in Zeolite Catalysts, *Can. J. Chem. Eng.*, **50**, pp 462 - 469, 1972.

Meier, W. M., and Olson, D. H., *Atlas of Zeolite Structure Types*, Third Edition, Butterworth - Heinemann, Boston, 1992.

Michele, H., Purification of flue gases by dry sorbents - possibilities and limits, *Int. Chem. Eng.*, **27**, No. 2, pp 183 - 187, 1987.

Miller, G. W., Adsorption of Nitrogen, Oxygen, Argon, and Ternary Mixtures of these Gases in 13X Molecular Sieve, *AIChE Symp. Ser.*, **83**, No. 259, pp 28 - 39, 1987.

Miller, G. W., Knaebel, K. S., and Ikels, K. G., Equilibria of Nitrogen, Oxygen, Argon, and Air in Molecular Sieve 5A, *AIChE J.*, **33**, No. 2, pp 194 - 201, 1987.

Minato, H., Chemical Treatment of Natural Zeolites, and Properties and Utilizations of the Reacted Materials, *Zeolites*, Eds. Drzaj, B., Hocevar, S. and Pejnovik, S., Elsevier Science Publishers, Amsterdam, pp 513 - 522, 1985.

Minato, H., and Utada, M., Clinoptilolite from Japan, *Molecular Sieve Zeolites - I*, Am. Chem. Soc., pp 311 - 316, 1971.

Myers, A. L., and Ou, J. D. Y., Adsorption from Gas Mixtures on Heterogeneous Surfaces, *AIChE Symp. Ser.*, **79**, No. 230, pp 1 - 6, 1983.

Myers, A. L., and Prausnitz, J. M., Thermodynamics of Mixed Gas Adsorption, *AIChE J.*, **11**, 1965.

Neuzil, R. W., and Rosback, D. H., Olefin Separation Process; Adsorption using a Sodium Aluminum Silicate zeolite, U. S. Patent 4036744, 1977.

Nolan, J. T., McKeehan, T. W., and Danner, R. P., Equilibrium Adsorption of Oxygen, Nitrogen, Carbon Monoxide, and their Binary Mixtures on Molecular Sieve Type 10X, *J. Chem. Eng. Data*, **26**, pp 112 - 115, 1981.

Oberholtzer, J. E., and Rogers, L. B., Effects of Micropores on Peak Shape and Retention Volume in Gas - Solid Chromatography, *Anal. Chem.*, **41**, No. 12, pp 1590 - 1594, 1969 a.

Oberholtzer, J. E., and Rogers, L. B., Precise Gas Chromatographic Measurements, *Anal. Chem.*, **41**, No. 10, pp 1233 - 1239, 1969 b.

Rees, L. V. C., Bruckner, P., and Hampson, J., Sorption of N_2, CH_4, and CO_2 in Silicalite - 1, *Gas Sep. Purif.*, **5**, pp 67 - 75, 1991.

Reich, R., Ziegler, W. T., and Rogers, K. A., Adsorption of Methane, Ethane and Ethylene Gases and Their Binary and Ternary Mixtures and Carbon Dioxide on Activated Carbon at 212 - 301 K and Pressure to 35 Atmospheres, *Ind. Eng. Chem. Process Des. Dev.*, **19**, pp 336 - 344, 1980.

Reid, R. C., Prausnitz, J. M., and Sherwood, T. K., The Properties of Gases and Liquids, 3rd Ed., McGraw - Hill, New York, 1977.

Rosback, D. H., Process for Separating Olefins by Adsorption; Zeolites, U. S. Patent 3888939, 1975.

Rosback, D. H., Olefin Separation Process Using Copper - Exchanged Type X Zeolite, U. S. Patent, 1973.

Ruthven, D. M., Comparison of performance of PSA and membrane systems for N_2 production, *Gas Sep. Purif.*, **5**, pp 9 - 10, 1991.

Ruthven, D. M., Intracrystalline Diffusion in Zeolites and Carbon Molecular Sieves, *AIChE Symp. Ser.*, **80**, No. 233, pp 21 - 33, 1984 a.

Ruthven, D. M., *Principles of Adsorption and Adsorption Processes*, John Wiley & Sons Inc., New York, 1984 b.

Ruthven, D. M., Sorption of Oxygen, Nitrogen, Carbon Monoxide, Methane, and Binary Mixtures of these Gases in 5A Molecular Sieve, *AIChE J.*, **22**, No. 4, pp 753 - 759, 1976.

Ruthven, D. M., and Derrah, R. I., Diffusion of Monatomic and Diatomic Gases in 4A and 5A Zeolites, *J. Chem. Soc. Faraday Trans. 1*, **71**, pp 2031 - 2044, 1975.

Ruthven, D. M., and Derrah, R. I., Sorption in Davison 5A Molecular Sieve, *Can. J. Chem. Eng.*, **50**, pp 743 - 747, 1972 a.

Ruthven, D. M., and Derrah, R. I., Transition State Theory of Zeolitic Diffusion: Diffusion of CH_4 and CF_4 in 5A Zeolite, *J. Chem. Soc. Faraday Trans. 1*, **68**, pp 2332 - 2343, 1972.b.

Ruthven, D. M., Eic, M., and Xu, Z., Diffusion of Hydrocarbons in A and X Zeolites and Silicalite, *Catalysis and Adsorption by Zeolites*, Eds. Ohlmann, G. et al., Elsevier Science Publishers, Amsterdam, pp 233 - 246, 1991.

Ruthven, D. M., and Kumar, R., A Chromatographic Study of the Diffusion of N_2, CH_4 and Binary N_2 - CH_4 Mixtures in 4A Molecular Sieve, *Can. J. Chem. Eng.*, **57**, pp 342 - 348, 1979.

Ruthven, D. M., and Kumar, R., An Experimental Study of Single - Component and Binary Adsorption Equilibria by a Chromatographic Method, *Ind. Eng. Chem. Fundam.*, **19**, pp 27 - 32, 1980.

Ruthven, D. M., and Loughlin, K. F., The sorption and diffusion of n - butane in Linde 5A molecular sieve, *Chem. Eng. Sci.*, **26**, No. 8, pp 1145 - 1154, 1971.

Ruthven, D. M., Loughlin, K. F., and Derrah, R. I., Sorption and Diffusion of Light Hydrocarbons and Other Simple Nonpolar Molecules in Type A Zeolites, *Adv. Chem.*, **121**, pp 330 - 344, 1973.

Ruthven, D. M., Loughlin, K. F., and Holborow, K. A., Multicomponent sorption equilibrium in molecular sieve zeolites, *Chem. Eng. Sci.*, **28**, pp 701 - 709, 1973.

Ruthven, D. M., Tezel, F. H., Devgun, J. S., and Sridhar, T. S., Adsorptive Separation of Kr from N_2 - Part 1. Adsorbent Screening Studies, *Can. J. Chem. Eng.*, **62**, No. 4, pp 526 - 534, 1984.

Sand, L. B., and Mumpton, F. A., Eds., *Natural Zeolites*, Pergamon Press, Oxford, U. K., 1978.

Sarma, P. N., and Haynes, H. W., Application of Gas Chromatography to Measurement of Diffusion in Zeolites, *Adv. Chem. Ser.*, **133**, pp 205 - 217, 1974.

Schalles, D. G., and Danner, R. P., Adsorption of Oxygen and Nitrogen on Carbon Molecular Sieve Type 3A, *AIChE Symp. Ser.*, **84**, No. 264, pp 83 - 88, 1988.

Schneider, P., and Smith, J. M., Chromatographic Study of Surface Diffusion, *AIChE J.*, **14**, No. 6, pp 886 - 895, 1968 a.

Schneider, P., and Smith, J. M., Adsorption Rate Constants from Chromatography, *AIChE J.*, **14**, No. 5, 762 - 771, 1968 b.

Schoellner, R., and Mueller, U., Influence of mono- and bivalent cations in 4A zeolites on the adsorptive separation of ethene and propene from crack - gases, *Adsorption Sci. Tech.*, **3**, pp 167 - 171, 1986.

Shah, D. B., and Ruthven, D. M., Measurement of Zeolitic Diffusivities by Chromatography, *AIChE J.*, **23**, No. 6, pp 804 - 810, 1977.

Sircar, S., Separation of Methane and Carbon Dioxide Gas Mixtures by Pressure Swing Adsorption, *Sep. Sci. Tech.*, **23**, pp 519 - 529, 1988 a.

Sircar, S., High Efficiency Separation of Methane and Carbon Dioxide Mixtures by Adsorption, *AIChE Symp. Ser.*, **84**, No. 264, pp 70 - 72, 1988 b.

Sircar, S. and Myers, A. L., Surface potential theory of multilayer adsorption from gas mixtures, *Chem. Eng. Sci.*, **28**, pp 489 - 499, 1973.

Sirkecioglu, A., Altay, Y., Erdem - Senatalar, A., in preparation, 1992.

Strem Chemicals Inc., Type X Molecular Sieve Data Sheet, Strem Chemicals Inc., Newburyport, MA.

Sundaresan, B. B., Harding, C. I., May, F. P., and Hendrickson, E. R., Adsorption of Nitrogen Oxides from Waste Gas, *Env. Sci. Tech.*, **1**, No. 2, pp 151 - 156, 1967.

Suwanayuen, S. and Danner, R. P., A Gas Adsorption Isotherm Equation Based on Vacancy Solution Theory, *AIChE J.*, **26**, No. 1, pp 68 - 76, 1980 a.

Suwanayuen S., and Danner, R. P., Vacancy Solution Theory of Adsorption from Gas Mixtures, *AIChE J.*, **26**, No. 1, pp 76 - 83, 1980 b.

Suzuki, M., and Smith, J. M., Kinetic studies by chromatography, *Chem. Eng. Sci.*, **26**, No. 2, pp 221 - 235, 1971.

Talu, O., and Kabel, R. L., Isosteric Heat of Adsorption and the Vacancy Solution Model, *AIChE J.*, **33**, No. 3, pp 510 - 514, 1987.

Tezel, F. H., PhD Thesis dissertation, *Development of a Chromatographic Process for Krypton - Nitrogen Separation,* University of Ottawa, Ottawa, Canada, 1986.

Tezel, F. H., Tezel, H. O., and Ruthven, D. M., Determination of Pure and Binary Isotherms for Nitrogen and Krypton, *J Colloid Interface Sci.*, **149**, No. 1, 1992.

Tezel, F. H., and Apolonatos, G., Chromatographic study of adsorption for N_2, CO and CH_4 in molecular sieve zeolites, *Gas Sep. Purif.*, **7**, No. 1, pp 11 - 17, 1993.

Thorogood, R. M., Bennet, D. I., Allam, R. J., and Prentice, A. L., Air Separation Process Using Packed Columns for O_2 and Ar Recovery, US Patent 4,871,382, 1989.

Tsitsishvili, G. V., and Andronikashvili, T. G., Influence of Zeolite Cation Nature on Adsorption and Chromatographic Properties, *Adv. Chem. Ser.*, 102, pp 217 - 227, 1971.

UOP, Adsorbents Product Information - Molecular Sieve 5A, UOP, Danbury, CT.

Van Deemter, J. J., Zuiderweg, F. J., and Klinkenberg, A., Longitudinal diffusion and resistance to mass transfer as causes of nonideality in chromatography, *Chem. Eng. Sci.*, **5**, 271 - 289, 1956.

Van der Vlist, E., and Van der Meijden, J., Determination of the Adsorption Isotherms of the Components of Binary Gas Mixtures by Gas Chromatography, *J. Chromatography*, **79**, pp 1 - 13, 1973.

Wakao, N., and Funazkri, T., Effect of Fluid Dispersion Coefficients on Particle - to - Fluid Mass Transfer Coefficients in Packed Beds: Correlation of Sherwood Numbers, *Chem. Eng. Sci.*, **33**, pp 1375 - 1384, 1978.

Yang, R. T., *Gas Separation by Adsorption Processes, Butterworth Publishers,* Mass., U. S. A., 1987.

Yeh, Y. T., and Yang, R. T., Diffusion in Zeolites Containing Mixed Cations, *AIChE J.*, **35**, No. 10, pp 1659 - 1665, 1989.

Yucel, H. Y., and Ruthven, D. M., Diffusion in 4A Zeolite: Study of the Effect of Crystal Size, *J. Chem. Soc. Faraday Trans. 1*, **76**, pp 60 - 70, 1980 a.

Yucel, H. Y., and Ruthven, D. M., Diffusion in 5A Zeolite: Study of the Effect of Crystal Size, *J. Chem. Soc. Faraday Trans. 1*, **76**, pp 71 - 83, 1980 b.

9. Appendix

Appendix A - Calculation of Bed Density / Column Porosity

The porosity of the column was determined from the experimentally measured bulk density (total mass of column contents / total volume of column interior) using the following equation:

$$\rho_p = \frac{\rho_b}{0.3560\left(\log 2R_p - 1\right)}$$

The sample case presented is that for the 5A zeolite column with a diameter of 0.51 cm, for which the bed volume is:

$$V_b = \pi r_b^2 l$$

$$V_b = 2.04\ cm^3$$

The bed density was calculated from the experimentally measured zeolite mass, assuming the mass of the air in the column was neglible:

$$M_z = 1.901\ g$$

$$\rho_B = \frac{(M_Z + M_{Air})}{V_c}$$

$$\rho_B = \frac{1.901\ g}{2.04\ cm^3}$$

$$\rho_B = 0.932\ \frac{g}{cm^3}$$

Given a mean particle size of .5325 mm (taken from the 24 - 42 mesh sizes used in screening), the pellet density may be calculated as:

$$\rho_p = \frac{\rho_B}{.3560\left(\log\left(2R_p\right) - 1\right)}$$

where R_p is in μm. Then

$$\rho_p = 1.517\ \frac{g}{cm^3}$$

and the porosity may be calculated as:

$$\varepsilon = \frac{\rho_p - \rho_B}{\rho_p}$$

$$\varepsilon = .385$$

Calculated porosities for the various packed columns ranged from .355 to .385. The sensitivity of the calculation to potential error in the mean particle size was minimal. This is comforting since the mean particle size, taken from the aperture sizes of the screens used, is the most likely source of error in this calculation.

Appendix B - Calculation of Henry's Law Constant and Diffusivity

The sample case chosen for this calculation is Run ID# ND04209.dat, which is shown in figure B1. The column was packed with clinoptilolite, held at 393 K, and exposed to a pulse of N_2. The length of the column and the gas interstitial velocity are measured experimentally, and the porosity was calculated as shown above. The statistical mean, μ, and variance, σ^2 may be calculated as:

$$\mu = \frac{\int_0^\infty Ctdt}{\int_0^\infty Cdt}$$

$$\sigma^2 = \frac{\int_0^\infty \left(t-\mu\right)^2 Cdt}{\int_0^\infty Cdt}$$

The individual integrals in the two relationships were solved using Simpson's rule. Given the mean of the response curve, calculation of the Henry's law constant is trivial with equation 13. For the sample run selected, the mean was solved to be 47.43 s. This mean was then corrected for extra - column dead time. K_p was then calculated using the values of column length, interstitial velocity, and porosity (as determined above) listed at the head of the response curve plot. The value of the dimensionless Henry's law constant may be converted to more conventional units using the following relationship:

$$K_p(\dim) = K_p\left(\frac{cm^3(STP)}{g \bullet torr}\right) \bullet \left(\frac{760\left(\frac{atm}{g \bullet torr}\right) \bullet \rho\left(\frac{g}{cm^3}\right) \bullet RT\left(\frac{cm^3 \bullet atm}{mol}\right)}{22{,}400\left(\frac{cm^3}{mol}\right)}\right)$$

Where ρ is the density of the sorbent and R_g is the ideal gas constant expressed as cm^3 atm / g mol K.

Calculation of the micropore diffusivity was more complex. Experiments were done at constant temperature with varying interstitial velocities, and the (σ^2 L/2μ^2v) vs. ($1/v^2$) relationship was plotted. For N_2 on clinoptilolite at 393 K, The equation of the resultant line was:

temp (K)	mean (s)	variance (min^2)	int vel (cm/s)	diam (cm)	length (cm)	poros	V flow (ml/min)	Kp
393	47.16	0.06766	4.178	0.43	10	0.37	10.12	10.818

93-04-20

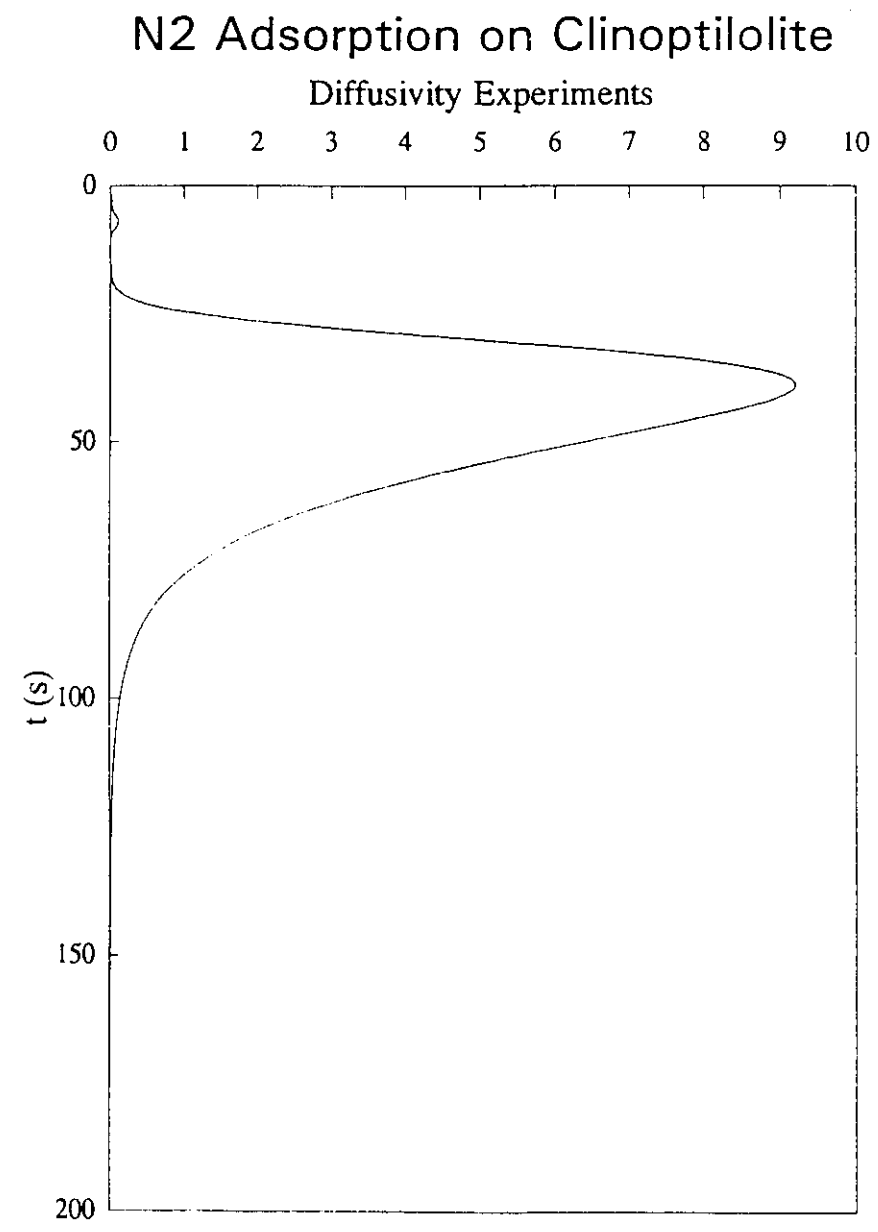

Figure B1 : Response peak resulting from sending a pulse of N_2 through clinoptilolite column at 393 K

$$\frac{\sigma^2 L}{2\mu^2 \upsilon} = \frac{1.21 \frac{cm^2}{s}}{\upsilon^2} + .1051$$

From equation 43, the axial dispersion, D_L, is equal to the slope (1.21 cm^2 / s). The intercept represents contributions from the other mass transfer mechanisms:

$$.1051\ s = \frac{\varepsilon}{1-\varepsilon}\left(\frac{R_p^2}{3D_M} + \frac{R_p^2}{15\theta D_p} + \frac{r_c^2}{15 D_c K_p}\right)$$

As discussed in section 2.5, the value of D_M may be determined empirically [Reid et al. (1977)], and D_p is calculated as a combination of the molecular diffusivity and the Knudsen diffusivity as per equations 45 and 46. Given R_p= .5325 mm (see section 5.2), and given D_M= 1.1 cm^2 / s and D_p = .13 cm^2 / s, it is clear that the first two terms in the brackets are small contributors to the total mass transfer resistance. The value of the micropore diffusivity can then be calculated by difference from the above relationship:

$$\frac{D_c}{r_c^2} = .0348\ s^{-1}$$

Such a method was used for calculation of N_2 and CO diffusivities in clinoptilolite at four different temperatures. Checking the condition for successful chromatographic measurement of micropore diffusivities (equation 47) yields the following inequality:

$$15 \bullet K_p \bullet \frac{D_c}{r_c^2} << \frac{D_M}{R_p^2}$$

$$5.66 << 387.9$$

Thus this criterion is easily met. Other criteria for successful chromatographic determination of micropore diffusivity have been given [Habgood & MacDonald (1970)]. These criteria were also tested and met by the experiments conducted here. Thus it is reasonable to conclude that in the range of conditions studied that micropore diffusion is clearly the dominant mechanism, and that it can therefore be accurately measured by chromatographic techniques.

Appendix C - Sample Curve Fitting / VST Calculation Programs

The FORTRAN program used to do all curve fittings, and specifically that involved in solving the VST, is presented here. The step by step method of calculation is fully documented in the articles by Suwanayuen & Danner [Suwanayuen & Danner, Suwanayuen & Danner], and the program was written on the University of Ottawa mainframes using IMSL subroutines. The program used to derive the binary isotherms from the pure isotherm VST coefficients is also supplied. The first program, program ISO, calculates the best fit coefficients for the VST equation (either Flory - Huggins or Wilson) given raw data and initial guesses of the coefficients. The second program, BINVAC, predicts the binary adsorption equilibrium from the pure gas coefficients. The programs are well commented, but should not be reviewed without copies of the articles from which the equations came [Cochran et al.(1985 a, b), Suwanayuen & Danner (1980 a, b)].

```
FILE: VSTISO   FORTRAN  *                    VM/SP CONVERSATIONAL MONITOR SYSTEM

      PROGRAM ISO                                                          VST00010
                                                                           VST00020
C*************************************************************************VST00030
C     A PROGRAM FOR THE CALCULATION OF THE VACANCY SOLUTION THEORY       *VST00040
C     COEFFICIENTS. THE ROUTINE IS A SIMPLE NON - LINEAR REGRESSION      *VST00050
C     USING IMSL SUBROUTINES. AND MAY BE USED FOR ANY CURVE FITTING      *VST00060
C     APPLICATIONS. NOT JUST THE VST.                                    *VST00070
C*************************************************************************VST00080
                                                                           VST00090
      INTEGER LDR, NOBS, NPARM                                             VST00100
      PARAMETER (NOBS=22, NPARM=3, LDR=NPARM)                              VST00110
                                                                           VST00120
      INTEGER IDERIV, IRANK, NOUT, IPARAM(6), IWK(NPARM)                   VST00130
      DOUBLE PRECISION DFE, R(LDR,NPARM), SSE, THETA(NPARM)                VST00140
      DOUBLE PRECISION RPARAM(7), WK(48)                                   VST00150
      EXTERNAL ISOTH, DRNLIN, UMACH, WRRRN, DR8LIN, DR2LIN                 VST00160
                                                                           VST00170
C*************************************************************************VST00180
C     THE INITIAL GUESSES OF THE COEFFICIENT VALUES ARE ENTERED          *VST00190
C     IN THE ARRAY THETA(N).                                             *VST00200
C*************************************************************************VST00210
                                                                           VST00220
      DATA THETA/30., 350., 4./                                            VST00230
      CALL UMACH(2,NOUT)                                                   VST00240
      IDERIV=0                                                             VST00250
                                                                           VST00260
      CALL DR8LIN (IPARAM, RPARAM)                                         VST00270
                                                                           VST00280
C*************************************************************************VST00290
C     THIS SUBROUTINE ALLOWS USER ADJUSTED VALUES OF THE REGRESSION      *VST00300
C     SUBROUTINE. IF NO VALUES ARE SPECIFIED, DEFAULT VALUES ARE USED.   *VST00310
C     THE VALUES OF THE REGRESSION PARAMETERS MAY THEN BE PRINTED AT     *VST00320
C     USER'S DISCRETION.                                                 *VST00330
C*************************************************************************VST00340
                                                                           VST00350
C     IPARAM(3)=20000                                                      VST00360
C     RPARAM(1)=0.6D-9                                                     VST00370
C     RPARAM(2)=0.3D-15                                                    VST00380
C     RPARAM(3)=0.37D-20                                                   VST00390
C     RPARAM(4)=0.5D-41                                                    VST00400
C     RPARAM(6)=10.                                                        VST00410
C     WRITE (*,*) '# OF ITERATIONS =' , IPARAM(3)                          VST00420
C     WRITE (*,*) 'MAX STEP SIZE =' , RPARAM(6)                            VST00430
C     WRITE (*,*) 'ABSOLUTE FUNCTION TOLERANCE = ' , RPARAM(4)             VST00440
C     WRITE (*,*) 'RELATIVE FUNCTION TOLERANCE = ' , RPARAM(3)             VST00450
C     WRITE (*,*) 'SCALED GRADIENT TOLERANCE = ' , RPARAM(1)               VST00460
C     WRITE (*,*) 'SCALED STEP TOLERANCE = ' , RPARAM(2)                   VST00470
                                                                           VST00480
      CALL DR2LIN (ISOTH, NPARM, IDERIV, THETA, R, LDR, IRANK, DFE, SSE,VST00490
     &             IPARAM, RPARAM, SCALE, IWK, WK)                         VST00500
                                                                           VST00510
C*************************************************************************VST00520
C     THIS IS THE IMSL SUBROUTINE WHICH USES A MODIFIED LEVENBERG -      *VST00530
C     MARQUARDT ALGORITHM FOR CURVE FITTING.                             *VST00540
C*************************************************************************VST00550
```

```
FILE: VSTISO   FORTRAN  *                    VM/SP CONVERSATIONAL MONITOR SYSTEM

      CALL WRRRN ('R', NPARM, NPARM, R, LDR, 0)                                 VST00560
      END                                                                       VST00570
                                                                                VST00580
C*************************************************************************     VST00590
C     THIS SUBROUTINE DEFINES THE FUNCTION TO BE FIT, AND THE DATA      *VST00600
C     TO FIT IT TO.                                                     *VST00610
C*************************************************************************     VST00620
                                                                                VST00630
      SUBROUTINE ISOTH (NPARM, THETA, IOPT, IOBS, FRQ, WT, E, DE, IEND)         VST00640
      INTEGER NPARM, IOT, IOBS, IEND                                            VST00650
      DOUBLE PRECISION THETA(NPARM), FRQ, WT, E, DE(1)                          VST00660
      INTEGER NOBS                                                              VST00670
      PARAMETER (NOBS=22)                                                       VST00680
      DOUBLE PRECISION DEXP, XDATA(NOBS), YDATA(NOBS), V1, V2, V3               VST00690
      INTRINSIC DEXP                                                            VST00700
                                                                                VST00710
      DATA XDATA/0, 7.97, 9.18, 9.99, 10.61, 11.13, 11.98, 12.96,               VST00720
     &     13.51, 14.21, 15.17, 15.96, 16.62, 17.19, 17.69, 18.12, 18.51,       VST00730
     &     18.85, 19.16, 19.68, 20.11, 20.43/                                   VST00740
      DATA YDATA/0, .01, .02, .03, .04, .05, .075, .1, .125, .15, .2,           VST00750
     &     .25, .3, .35, .4, .45, .5, .55, .6, .7, .8, .895/                    VST00760
      IF (IOBS .LE. NOBS) THEN                                                  VST00770
        WT = 1.0D0                                                              VST00780
        FRQ = 1.0D0                                                             VST00790
        IEND = 0                                                                VST00800
                                                                                VST00810
C*************************************************************************     VST00820
C        THE EQUATIONS FOR BOTH THE FLORY - HUGGINS AND THE WILSON FORMS*VST00830
C        OF THE VST ARE PROVIDED BELOW. ONE EQUATION FORM CAN BE        *VST00840
C        COMMENTED OUT TO RUN THE OTHER, OR BOTH MAY BE REMOVED TO      *VST00850
C        FIT DATA TO ANY FUNCTION.                                      *VST00860
C*************************************************************************     VST00870
                                                                                VST00880
        V1 = XDATA(IOBS)/THETA(1)                                               VST00890
C       V2 = (1.0-THETA(4))*V1                                                  VST00900
C       V3 = (1.0-THETA(3))*V1                                                  VST00910
        E =YDATA(IOBS)-(THETA(1)/THETA(2))*(V1/(1-V1))                          VST00920
C     &      *THETA(3)*((1.0-V2)/(THETA(3)+V3))                                VST00930
C     &      *DEXP((-THETA(4)*V2/(1-V2))-(V3/(THETA(3)+V3)))                   VST00940
     &      *DEXP(((THETA(3)**2)*V2)/(1+(THETA(3)*V2)))                        VST00950
C       WRITE (*,*) 'IOBS= ', IOBS, '  THETA(1)= ', THETA(1)                    VST00960
C       WRITE (*,*) 'THETA(2)=', THETA(2), 'THETA(3)= ', THETA(3)               VST00970
      ELSE                                                                      VST00980
        IEND = 1                                                                VST00990
      END IF                                                                    VST01000
      RETURN                                                                    VST01010
      END                                                                       VST01020
                                                                                VST01030
```

```
FILE: BINVAC   FORTRAN  *                    VM/SP CONVERSATIONAL MONITOR SYSTEM

      PROGRAM BINVAC                                                          BIN00010
                                                                              BIN00020
C*************************************************************************BIN00030
C     THIS PROGRAM CALCULATES THE VST BINARY ADSORPTION ISOTHERMS      *BIN00040
C     FROM THE EXPERIMENTALLY DETERMINED VST PURE ISOTHERM             *BIN00050
C     COEFFICIENTS. EQUATIONS FOR THE WILSON AND FLORY - HUGGINS       *BIN00060
C     FORMS OF THE VST ARE PROVIDED.                                   *BIN00070
C*************************************************************************BIN00080
                                                                              BIN00090
      INTEGER NITER, NIT                                                      BIN00100
      PARAMETER (NC=3)                                                        BIN00110
      DOUBLE PRECISION B(NC), NS(NC), NSINF(NC), NMS, NMSINF,                 BIN00120
     &                 P, X(NC), XS(NC), Y(NC), ACT(NC), A1, A2, A12,       BIN00130
     &                 THETA, W13, W23, W31, W32, FUG, W12, W21,            BIN00140
     &                 LACT(NC), PART(NC), CP, EQU(NC), DIFF, INC           BIN00150
                                                                              BIN00160
C*************************************************************************BIN00170
C     THE VALUES OF THE PURE COMPONENT ISOTHERMS COEFFICIENTS ARE      *BIN00180
C     ENTERED HERE.                                                    *BIN00190
C*************************************************************************BIN00200
      DATA B/131.3, 349., .1/                                                 BIN00210
      DATA NSINF/24.07, 19.3, .1/                                             BIN00220
      W13 = 0.2164                                                            BIN00230
      W31 = 4.62                                                              BIN00240
      W23 = 2.5                                                               BIN00250
      W32 = 0.00162                                                           BIN00260
                                                                              BIN00270
      P = 1.                                                                  BIN00280
      W12 = 1.                                                                BIN00290
      W21 = 1.                                                                BIN00300
      X(1) = 0.05                                                             BIN00310
                                                                              BIN00320
      A1 = 3.62                                                               BIN00330
      A2 = -.99                                                               BIN00340
      A12= ((A1+1)/(A2+1))-1                                                  BIN00350
                                                                              BIN00360
C*************************************************************************BIN00370
C     AFTER THE PURE GAS WILSON OR FLORY - HUGGINS COEFFICIENTS HAVE   *BIN00380
C     BEEN ENTERED, THE ITERATIONS BEGIN.                              *BIN00390
C*************************************************************************BIN00400
                                                                              BIN00410
      NITER = 8000                                                            BIN00420
 50   NIT = 1                                                                 BIN00430
      X(1) = .01 + X(1)                                                       BIN00440
      X(2) = 1.-X(1)                                                          BIN00450
                                                                              BIN00460
C*************************************************************************BIN00470
C     MAKE INITIAL GUESS AT THE SURFACE COVERAGE, NMS                  *BIN00480
C*************************************************************************BIN00490
                                                                              BIN00500
      NMS = .1*((NSINF(1)+NSINF(2))/2.)                                       BIN00510
      INC = .00'                                                              BIN00520
      NMSINF = (X(1)*NSINF(1)) + (X(2)*NSINF(2))                              BIN00530
100   XS(1) = X(1)*NMS/NMSINF                                                 BIN00540
      XS(2) = X(2)*NMS/NMSINF                                                 BIN00550
```

```
FILE: BINVAC   FORTRAN  *                    VM/SP CONVERSATIONAL MONITOR SYSTEM

      XS(3) = 1.-(NMS/NMSINF)                                                  BIN00560
C*****************************************************************************BIN00570
C     ACTIVITY EQUATIONS ARE PROVIDED FOR BOTH WILSON AND FLORY -              *BIN00580
C     HUGGINS FORMS. ONE SET SHOULD BE COMMENTED OUT WHILE THE OTHER           *BIN00590
C     IS USED                                                                  *BIN00600
C*****************************************************************************BIN00610
                                                                               *BIN00620
      LACT(1) = 1 - DLOG(XS(1)+(XS(2)*W12)+(XS(3)*W13)) -                      BIN00630
     &     (XS(1)/(XS(1)+(XS(2)*W12)+(XS(3)*W13)))-                            BIN00640
     &     ((XS(2)*W21)/((XS(1)*W21)+XS(2)+(XS(3)*W23)))-                      BIN00650
     &     ((XS(3)*W31)/((XS(1)*W31)+(XS(2)*W32)+XS(3)))                       BIN00660
                                                                               BIN00670
C     LACT(1) = -DLOG(XS(1)+(XS(2)/(1+A12))+(XS(3)/(1+A1)))+                   BIN00680
C    &     (1-(XS(1)+(XS(2)/(1+A12))+(XS(3)/(1+A1)))**(-1))                    BIN00690
                                                                               BIN00700
      LACT(2) = 1 - DLOG(XS(2)+(XS(1)*W21)*(XS(3)*W23))-                       BIN00710
     &     (XS(2)/(XS(2)+(XS(1)*W21)+(XS(3)*W23)))-                            BIN00720
     &     ((XS(1)*W12)/((XS(2)*W12)+XS(1)+(XS(3)*W13)))-                      BIN00730
     &     ((XS(3)*W32)/((XS(2)*W32)+(XS(1)*W31)+XS(3)))                       BIN00740
                                                                               BIN00750
C     LACT(2) = -DLOG((1+A12)*XS(1)+XS(2)+(XS(3)/(1+A2)))+                     BIN00760
C    &     (1-((1+A12)*XS(1)+XS(2)+(XS(3)/(1+A2)))**(-1))                      BIN00770
                                                                               BIN00780
C     LACT(3) = -DLOG((1+A1)*XS(1)+(1+A2)*XS(2)+XS(3))+                        BIN00790
C    &     (1-((1+A1)*XS(1)+(1+A2)*XS(2)+XS(3))**(-1))                         BIN00800
                                                                               BIN00810
      LACT(3) = 1 - DLOG((XS(1)*W31)+(XS(2)*W32)+XS(3)) -                      BIN00820
     &     ((XS(1)*W13)/(XS(1)+(XS(2)*W12)+(XS(3)*W13)))-                      BIN00830
     &     ((XS(2)*W23)/((XS(1)*W21)+XS(2)+(XS(3)*W23)))-                      BIN00840
     &     (XS(3)/((XS(1)*W31)+(XS(2)*W32)+XS(3)))                             BIN00850
                                                                               BIN00860
      ACT(1) = DEXP(LACT(1))                                                   BIN00870
      ACT(2) = DEXP(LACT(2))                                                   BIN00880
      ACT(3) = DEXP(LACT(3))                                                   BIN00890
                                                                               BIN00900
      PART(1) = -(1 + ((NMSINF-NSINF(1))/NMS)) * DLOG(ACT(3)*XS(3))            BIN00910
      PART(2) = -(1 + ((NMSINF-NSINF(2))/NMS)) * DLOG(ACT(3)*XS(3))            BIN00920
C     PART(1) = DEXP((((NSINF(1)-NMSINF)/NMS)-1)*DLOG(ACT(3)*XS(3)))           BIN00930
C     PART(2) = DEXP((((NSINF(2)-NMSINF)/NMS)-1)*DLOG(ACT(3)*XS(3)))           BIN00940
                                                                               BIN00950
C     EQU(1) = ACT(1)*X(1)*(NMS/NMSINF)*(NSINF(1)/B(1))*                       BIN00960
C    &          (DEXP(A1)/(1+A1))*PART(1)                                     BIN00970
C     EQU(2) = ACT(2)*X(2)*(NMS/NMSINF)*(NSINF(2)/B(2))*                       BIN00980
C    &          (DEXP(A2)/(1+A2))*PART(2)                                     BIN00990
      EQU(1) = ACT(1)*X(1)*NMS * (NSINF(1)*W13/(NMSINF*B(1))) *                BIN01000
     &          DEXP(W31-1) * DEXP(PART(1))                                   BIN01010
      EQU(2) = ACT(2)*X(2)*NMS * (NSINF(2)*W23/(NMSINF*B(2))) *                BIN01020
     &          DEXP(W32-1) * DEXP(PART(2))                                   BIN01030
                                                                               BIN01040
C*****************************************************************************BIN01050
C     THE PRESSURES FROM THE TWO EQUATIONS ARE ADDED AND COMPARED TO           *BIN01060
C     THE TOTAL PRESSURE. IF SO, THE VALUE OF X1 IS INCREASED AND              *BIN01070
C     THE EQUILIBRIUM IS PREDICTED AT THE NEXT SURFACE CONCENTRATION.          *BIN01080
C     OTHERWISE A THE VALUE OF NMS IS MODIFIED AND THE CALCULATION             *BIN01090
```

```
FILE: BINVAC   FORTRAN  *                    VM/SP CONVERSATIONAL MONITOR SYSTEM

C       REPEATED UNTIL THE CALCULATED PRESSURE, CP, EQUALS THE PRE      *BIN01110
C       DEFINED TOTAL SYSTEM PRESSURE.                                  *BIN01120
C*******************************************************************************BIN01130
                                                                         BIN01140
        CP = (EQU(1) + EQU(2))                                           BIN01150
C       WRITE (*,*) 'P1= ', EQU(1), 'P2= ', EQU(2)                       BIN01160
        Y(1) = EQU(1)/CP                                                 BIN01170
        DIFF = ABS(P-CP)                                                 BIN01180
C       WRITE (*,*) 'CP= ', CP, 'NMS= ', NMS, 'Y1= ', Y(1)               BIN01190
        NMS = NMS + INC                                                  BIN01200
        NIT = NIT + 1                                                    BIN01210
        ACC = 2.*INC                                                     BIN01220
        IF (NIT.GT.NITER) GOTO 200                                       BIN01230
        IF (DIFF.LT..002) GOTO 200                                       BIN01240
C       IF (DIFF.GT.ACC) GOTO 100                                        BIN01250
        GOTO 100                                                         BIN01260
                                                                         BIN01270
 200    WRITE (6,*) 'Y1= ', Y(1), 'X1= ', X(1)                           BIN01280
        NMS = NMS - INC                                                  BIN01290
        WRITE (6,*) 'CP= ', CP, 'NMS= ', NMS                             BIN01300
        IF (X(1).LT..49) GOTO 50                                         BIN01310
                                                                         BIN01320
        END                                                              BIN01330
```

Appendix D - Raw Data

The complete data obtained and analysed in this study is given in this section. The results of the Henry's law experiments are given first, followed by the diffusion and isotherm measurement raw data.

Methane Adsorption on Clinoptilolite

Cor mean (s)	mean (s)	temp (K)	diam (cm)	int vel (cm/s)	Kp	1/temp (1/K)	log Kp
12.60629	16.43	523	0.51	5.868311	3.693346	0.001912	0.56742
12.27629	16.1	523	0.51	5.868311	3.581552	0.001912	0.554071
11.75629	15.58	523	0.51	5.868311	3.405391	0.001912	0.532167
9.202169	11.21	498	0.51	11.1756	5.359518	0.002008	0.729126
8.952169	10.96	498	0.51	11.1756	5.198229	0.002008	0.715855
16.40434	20.42	498	0.51	5.587799	4.714365	0.002008	0.673423
13.25605	15.37	473	0.51	10.61457	7.545562	0.002114	0.877692
12.35605	14.47	473	0.51	10.61457	6.994073	0.002114	0.84473
19.54808	21.78	448	0.51	10.05355	10.768	0.002232	1.032135
17.08808	19.32	448	0.51	10.05355	9.340266	0.002232	0.970359
29.34617	31.71	423	0.51	9.492526	15.50416	0.002364	1.190448
27.22617	29.59	423	0.51	9.492526	14.34242	0.002364	1.156622
47.98769	50.5	398	0.51	8.931502	24.16536	0.002513	1.383193
49.52769	52.04	398	0.51	8.931502	24.95939	0.002513	1.397234
79.0693	81.75	373	0.51	8.370478	37.63033	0.002681	1.575538

Ethane Adsorption on Clinoptilolite

Cor mean (s)	mean (s)	temp (K)	diam (cm)	int vel (cm/s)	Kp	1/temp (1/K)	log Kp
17.66217	19.67	498	0.51	11.1756	10.81751	0.002008	1.034127
18.51217	20.52	498	0.51	11.1756	11.36589	0.002008	1.055603
27.98605	30.1	473	0.51	10.61457	16.5716	0.002114	1.219364
28.47605	30.59	473	0.51	10.61457	16.87185	0.002114	1.227163
47.66808	49.9	448	0.51	10.05355	27.08824	0.002232	1.432781
46.84808	49.08	448	0.51	10.05355	26.61233	0.002232	1.425083
68.15617	70.52	423	0.51	9.492526	36.7717	0.002364	1.565514
73.34617	75.71	423	0.51	9.492526	39.61577	0.002364	1.597868
61.15617	63.52	423	0.51	9.492526	32.93576	0.002364	1.517668
112.0877	114.6	398	0.51	8.931502	57.21558	0.002513	1.757514
89.97769	92.49	398	0.51	8.931502	45.81557	0.002513	1.661013
132.7193	135.4	373	0.51	8.370478	63.55492	0.002681	1.803149
105.3193	108	373	0.51	8.370478	50.31477	0.002681	1.701696
147.8267	150.7	348	0.51	7.809454	66.06738	0.002874	1.819987

* The last five data points (348, 373 and 398 K) were not used in the regression due to severe tailing

Nitrogen Adsorption on Clinoptilolite

Cor mean (s)	mean (s)	temp (K)	diam (cm)	int vel (cm/s)	Kp	1/temp (1/K)	log Kp
13.60806	15.01	423	0.51	9.492526	6.879811	0.002364	0.837577
13.42806	14.83	423	0.51	9.492526	6.781173	0.002364	0.831305
11.48806	12.89	423	0.51	9.492526	5.71807	0.002364	0.757249
11.27806	12.68	423	0.51	9.492526	5.602992	0.002364	0.74842
24.09	25.58	398	0.51	8.931502	11.84361	0.002513	1.073484
24.73	26.22	398	0.51	8.931502	12.1736	0.002513	1.085419
51.01013	52.6	373	0.51	8.370478	24.07167	0.002681	1.381506
50.79013	52.38	373	0.51	8.370478	23.96536	0.002681	1.379584
125.0959	126.8	348	0.51	7.809454	55.81966	0.002874	1.746787
126.7959	128.5	348	0.51	7.809454	56.58607	0.002874	1.75271
366.164	368	323	0.51	7.24843	152.6413	0.003096	2.183672
380.164	382	323	0.51	7.24843	158.4995	0.003096	2.200028
373.164	375	323	0.51	7.24843	155.5704	0.003096	2.191927

Carbon Monoxide Adsorption on Clinoptilolite

Cor mean (s)	mean (s)	temp (K)	diam (cm)	int vel (cm/s)	Kp	1/temp (1/K)	log Kp
14.13626	15.39	473	0.51	10.61457	8.084925	0.002114	0.907676
26.02629	27.35	448	0.51	10.05355	14.52781	0.002232	1.1622
25.68629	27.01	448	0.51	10.05355	14.33048	0.002232	1.156261
49.86806	51.27	423	0.51	9.492526	26.74997	0.002364	1.427323
123.11	124.6	398	0.51	8.931502	62.89873	0.002513	1.798642
307.9101	309.5	373	0.51	8.370478	148.2101	0.002681	2.170878
1036.296	1038	348	0.51	7.809454	466.6156	0.002874	2.668959
4101.164	4103	323	0.51	7.24843	1715.524	0.003096	3.234397

Nitric Oxide Adsorption on Clinoptilolite

Cor mean (s)	mean (s)	temp (K)	diam (cm)	int vel (cm/s)	Kp	1/temp (1/K)	log Kp
10.34626	11.6	473	0.51	10.61457	5.762544	0.002114	0.760614
16.87629	18.2	448	0.51	10.05355	9.21735	0.002232	0.964606
32.29806	33.7	423	0.51	9.492526	17.12177	0.002364	1.233549
63.51	65	398	0.51	8.931502	32.16873	0.002513	1.507434
130.0101	131.6	373	0.51	8.370478	62.2458	0.002681	1.79411
142.9101	144.5	373	0.51	8.370478	68.4793	0.002681	1.835559

Carbon Monoxide Adsorption on Activated Carbon

Cor mean (s)	mean (s)	temp (K)	diam (cm)	int vel (cm/s)	Kp	1/temp (1/K)	log Kp
8.908061	10.31	423	0.43	6.676598	2.856159	0.002364	0.455782
8.968061	10.37	423	0.43	6.676598	2.879285	0.002364	0.459285
13.84164	15.39	383	0.43	6.045241	4.253225	0.002611	0.628718
13.61164	15.16	383	0.43	6.045241	4.172959	0.002611	0.620444
17.30634	18.94	363	0.43	5.729563	5.146961	0.002755	0.711551
17.19634	18.83	363	0.43	5.729563	5.110577	0.002755	0.70847
24.17108	25.9	343	0.43	5.413884	6.977058	0.002915	0.843672
23.34108	25.07	343	0.43	5.413884	6.717653	0.002915	0.827218
35.43402	37.27	323	0.43	5.098206	9.851401	0.003096	0.993498
54.82284	56.78	303	0.43	4.782528	14.5587	0.0033	1.163123
55.38284	57.34	303	0.43	4.782528	14.71331	0.0033	1.16771

Carbon Dioxide Adsorption on Activated Carbon

Cor mean (s)	mean (s)	temp (K)	diam (cm)	int vel (cm/s)	Kp	1/temp (1/K)	log Kp
21.41806	22.82	423	0.43	6.676598	7.677905	0.002364	0.885243
30.29849	31.77	403	0.43	6.360919	10.54855	0.002481	1.023193
30.56849	32.04	403	0.43	6.360919	10.6477	0.002481	1.027256
45.11164	46.66	383	0.43	6.045241	15.16595	0.002611	1.18087
71.46634	73.1	363	0.43	5.729563	23.06094	0.002755	1.362877
72.14634	73.78	363	0.43	5.729563	23.28585	0.002755	1.367092
124.6711	126.4	343	0.43	5.413884	38.38698	0.002915	1.584184
228.764	230.6	323	0.43	5.098206	66.7509	0.003096	1.824457
454.7428	456.7	303	0.43	4.782528	124.9723	0.0033	2.096814

Nitric Oxide Adsorption on Activated Carbon

Cor mean (s)	mean (s)	temp (K)	diam (cm)	int vel (cm/s)	Kp	1/temp (1/K)	log Kp
10.75849	12.23	403	0.43	6.360919	3.373311	0.002481	0.528056
13.19164	14.74	383	0.43	6.045241	4.026385	0.002611	0.604915
17.09634	18.73	363	0.43	5.729563	5.077501	0.002755	0.70565
17.06634	18.7	363	0.43	5.729563	5.067578	0.002755	0.7048
22.57108	24.3	343	0.43	5.413884	6.477	0.002915	0.811374
32.84402	34.68	323	0.43	5.098206	9.089131	0.003096	0.958522
34.53402	36.37	323	0.43	5.098206	9.58652	0.003096	0.981661
41.84284	43.8	303	0.43	4.782528	10.97507	0.0033	1.040407
41.14284	43.1	303	0.43	4.782528	10.7818	0.0033	1.032691

Nitrogen Adsorption on Activated Carbon

Cor mean (s)	mean (s)	temp (K)	diam (cm)	int vel (cm/s)	Kp	1/temp (1/K)	log Kp
7.918486	9.39	403	0.43	6.360919	2.330442	0.002481	0.367438
8.238486	9.71	403	0.43	6.360919	2.447948	0.002481	0.388802
7.128486	8.6	403	0.43	6.360919	2.040348	0.002481	0.309704
9.081645	10.63	383	0.43	6.045241	2.592061	0.002611	0.413645
9.121645	10.67	383	0.43	6.045241	2.606021	0.002611	0.415978
11.33634	12.97	363	0.43	5.729563	3.172322	0.002755	0.501377
11.19634	12.83	363	0.43	5.729563	3.126016	0.002755	0.494991
11.87634	13.51	363	0.43	5.729563	3.350933	0.002755	0.525166
15.10108	16.83	343	0.43	5.413884	4.142352	0.002915	0.617247
14.52108	16.25	343	0.43	5.413884	3.961081	0.002915	0.597814
21.84402	23.68	323	0.43	5.098206	5.85169	0.003096	0.767281
21.33402	23.17	323	0.43	5.098206	5.70159	0.003096	0.755996
32.44284	34.4	303	0.43	4.782528	8.379828	0.0033	0.923235
31.84284	33.8	303	0.43	4.782528	8.214174	0.0033	0.914564

Methane Adsorption on H-Mordenite

Cor mean (s)	mean (s)	temp (K)	diam (cm)	int vel (cm/s)	Kp	1/temp (1/K)	log Kp
43.48542	46.53	323	0.51	7.24843	17.61886	0.003096	1.245978
57.77815	60.92	313	0.51	7.02402	22.85103	0.003195	1.358906
77.63446	80.88	303	0.51	6.79961	29.89678	0.0033	1.475624
107.3437	110.7	293	0.51	6.575201	40.168	0.003413	1.60388
152.1251	155.6	283	0.51	6.350791	55.19526	0.003534	1.741902
223.6978	227.3	273	0.51	6.126382	78.53749	0.003663	1.895077
341.6608	345.4	263	0.51	5.901972	115.8311	0.003802	2.063825
548.213	552.1	253	0.51	5.677563	179.1041	0.003953	2.253106
876.3531	880.4	243	0.51	5.453153	275.3017	0.004115	2.439809
1436.779	1441	233	0.51	5.228743	433.1126	0.004292	2.636601

Ethylene Adsorption on H-Mordenite

Cor mean (s)	mean (s)	temp (K)	diam (cm)	int vel (cm/s)	Kp	1/temp (1/K)	log Kp
7785.214	129.8	353	0.51	7.921658	3559.656	0.002833	3.551408
6561.133	109.4	343	0.51	7.697249	2914.877	0.002915	3.46462
1765.333	29.47	343	0.51	7.697249	783.8523	0.002915	2.894234
3551.955	59.25	323	0.51	7.24843	1485.712	0.003096	3.171935
5137.658	85.68	313	0.51	7.02402	2082.679	0.003195	3.318622
10394.75	173.3	303	0.51	6.79961	4079.704	0.0033	3.610629
19928.64	332.2	293	0.51	6.575201	7563.894	0.003413	3.878745

* The first two data points (means of 129.8 and 109.4) are not used in the regression due to faulty baselines (see raw data).

Carbon Monoxide Adsorption on H-Mordenite

Cor mean (s)	mean (s)	temp (K)	diam (cm)	int vel (cm/s)	Kp	1/temp (1/K)	log Kp
9.155335	10.78	373	0.51	8.370478	3.846725	0.002681	0.585091
11.48058	13.15	363	0.51	8.146068	4.821592	0.002755	0.68319
19.07324	20.84	343	0.51	7.697249	7.897948	0.002915	0.897514
27.15384	29.03	323	0.51	7.24843	10.78503	0.003096	1.032821
49.39	51.39	303	0.51	6.79961	18.8099	0.0033	1.274387

Methane Adsorption on 5A Zeolite

Cor mean (s)	mean (s)	temp (K)	diam (cm)	int vel (cm/s)	Kp	1/temp (1/K)	log Kp
6.280911	8.476	448	0.51	10.05355	3.068018	0.002232	0.486858
9.889146	12.36	398	0.51	8.931502	4.521596	0.002513	0.655292
14.01354	16.65	373	0.51	8.370478	6.194291	0.002681	0.791992
22.26294	25.13	343	0.51	7.697249	9.315302	0.002915	0.969197
21.99294	24.86	343	0.51	7.697249	9.195327	0.002915	0.963567
32.79542	35.84	323	0.51	7.24843	13.14571	0.003096	1.118784
32.47542	35.52	323	0.51	7.24843	13.01181	0.003096	1.114338
47.87446	51.12	303	0.51	6.79961	18.215	0.0033	1.260429
49.02446	52.27	303	0.51	6.79961	18.66642	0.0033	1.271061
161.7608	165.5	263	0.51	5.901972	54.53677	0.003802	1.736689
335.4531	339.5	243	0.51	5.453153	105.0245	0.004115	2.021291

Ethylene Adsorption on 5A Zeolite

Cor mean (s)	mean (s)	temp (K)	diam (cm)	int vel (cm/s)	Kp	1/temp (1/K)	log Kp
114.1209	116.2	473	0.51	10.61457	69.35209	0.002114	1.84106
213.4049	215.6	448	0.51	10.05355	123.2783	0.002232	2.090887
444.1752	446.5	423	0.51	9.492526	242.8268	0.002364	2.385297
1010.529	1013	398	0.51	8.931502	520.4556	0.002513	2.716384
2574.364	2577	373	0.51	8.370478	1243.399	0.002681	3.09461
11045.13	11048	343	0.51	7.697249	4907.352	0.002915	3.690847

Ethane Adsorption on 5A Zeolite

Cor mean (s)	mean (s)	temp (K)	diam (cm)	int vel (cm/s)	Kp	1/temp (1/K)	log Kp
163.4531	2.77	358	0.51	8.033863	75.22972	0.002793	1.876389
243.0129	4.098	343	0.51	7.697249	107.4061	0.002915	2.031029
384.6018	6.46	328	0.51	7.360634	162.8477	0.003049	2.211782
634.0581	10.62	313	0.51	7.02402	256.5254	0.003195	2.40913
1125.9	18.82	298	0.51	6.687406	434.0824	0.003356	2.637572
2126.525	35.5	283	0.51	6.350791	779.0557	0.003534	2.891568
3396.598	56.67	273	0.51	6.126382	1200.691	0.003663	3.079431
5420.861	90.41	263	0.51	5.901972	1846.382	0.003802	3.266321
12608.03	210.2	248	0.51	5.565358	4050.144	0.004032	3.60747
22759.78	379.4	233	0.51	5.228743	6869.43	0.004292	3.836921

Carbon Monoxide Adsorption on 5A Zeolite

Cor mean (s)	mean (s)	temp (K)	diam (cm)	int vel (cm/s)	Kp	1/temp (1/K)	log Kp
30.37058	32.04	363	0.51	8.146068	13.70484	0.002755	1.136874
54.52324	56.29	343	0.51	7.697249	23.65023	0.002915	1.373835
113.6238	115.5	323	0.51	7.24843	46.96775	0.003096	1.6718
233.5	235.5	303	0.51	6.79961	91.0791	0.0033	1.959419
594.1587	596.3	283	0.51	6.350791	217.2549	0.003534	2.33697
1825.198	1829	263	0.51	5.901972	621.2918	0.003802	2.793296

Nitric Oxide Adsorption on 5A Zeolite

Cor mean (s)	mean (s)	temp (K)	diam (cm)	int vel (cm/s)	Kp	1/temp (1/K)	log Kp
12.21775	13.8	383	0.51	8.594887	5.484817	0.002611	0.739162
15.81058	17.48	363	0.51	8.146068	6.857827	0.002755	0.836187
22.49324	24.26	343	0.51	7.697249	9.417632	0.002915	0.973942
32.95384	34.83	323	0.51	7.24843	13.212	0.003096	1.120969
33.32384	35.2	323	0.51	7.24843	13.36682	0.003096	1.126028
55.14	57.14	303	0.51	6.79961	21.06697	0.0033	1.323602
99.95866	102.1	283	0.51	6.350791	36.06985	0.003534	1.557144
211.0958	213.4	263	0.51	5.901972	71.34585	0.003802	1.853369
444.9062	447.4	243	0.51	5.453153	139.4807	0.004115	2.144514

Methane Adsorption on 4A Zeolite

Cor mean (s)	mean (s)	temp (K)	diam (cm)	int vel (cm/s)	Kp	1/temp (1/K)	log Kp
30.89542	33.94	323	0.51	7.24843	12.35067	0.003096	1.09169
44.05446	47.3	303	0.51	6.79961	16.71553	0.0033	1.22312
44.99446	48.24	303	0.51	6.79961	17.08451	0.0033	1.232602
72.51509	76.93	283	0.51	6.350791	26.00841	0.003534	1.415114
104.9608	108.7	263	0.51	5.901972	35.18426	0.003802	1.546348
199.3531	203.4	243	0.51	5.453153	62.17976	0.004115	1.793649
200.0901	204.5	223	0.51	5.004334	57.2275	0.004484	1.757605

Ethylene Adsorption on 4A Zeolite

Cor mean (s)	mean (s)	temp (K)	diam (cm)	int vel (cm/s)	Kp	1/temp (1/K)	log Kp
758.1635	12.68	373	0.51	8.370478	365.7801	0.002681	2.56322
2559.133	42.7	343	0.51	7.697249	1136.579	0.002915	3.0556
11816.86	197	313	0.51	7.02402	4791.012	0.003195	3.680427

Ethane Adsorption on 4A Zeolite

Cor mean (s)	mean (s)	temp (K)	diam (cm)	int vel (cm/s)	Kp	1/temp (1/K)	log Kp
117.4109	2.002	363	0.51	8.146068	54.6366	0.002755	1.737484
224.1129	3.783	343	0.51	7.697249	99.0078	0.002915	1.995669
382.1554	6.42	323	0.51	7.24843	159.3328	0.003096	2.202305
782.7545	13.1	303	0.51	6.79961	306.6794	0.0033	2.486685
1780.925	29.74	283	0.51	6.350791	652.3508	0.003534	2.814481
4266.461	71.17	263	0.51	5.901972	1453.062	0.003802	3.162284

Carbon Monoxide Adsorption on 4A Zeolite

Cor mean (s)	mean (s)	temp (K)	diam (cm)	int vel (cm/s)	Kp	1/temp (1/K)	log Kp
20.73058	22.4	363	0.51	8.146068	9.171516	0.002755	0.962441
37.08324	38.85	343	0.51	7.697249	15.90073	0.002915	1.201417
57.78384	59.66	323	0.51	7.24843	23.60193	0.003096	1.372947
111.3	113.3	303	0.51	6.79961	43.1116	0.0033	1.634594
244.1587	246.3	283	0.51	6.350791	88.93688	0.003534	1.949082
630.6958	633	263	0.51	5.901972	214.3091	0.003802	2.331041
1826.506	1829	243	0.51	5.453153	574.4132	0.004115	2.759224

Methane Adsorption on 13X Zeolite

Cor mean (s)	mean (s)	temp (K)	diam (cm)	int vel (cm/s)	Kp	1/temp (1/K)	log Kp
4.22993	6.309	473	0.51	10.61457	2.014669	0.002114	0.304204
4.67093	6.75	473	0.51	10.61457	2.284898	0.002114	0.358867
6.115177	8.44	423	0.51	9.492526	2.773776	0.002364	0.443071
6.205177	8.53	423	0.51	9.492526	2.823096	0.002364	0.450726
7.909146	10.38	398	0.51	8.931502	3.5007	0.002513	0.544155
10.56354	13.2	373	0.51	8.370478	4.527193	0.002681	0.655829
10.46354	13.1	373	0.51	8.370478	4.478871	0.002681	0.651169
15.16414	17.99	348	0.51	7.809454	6.259156	0.002874	0.796516
15.13414	17.96	348	0.51	7.809454	6.245631	0.002874	0.795576
23.47542	26.52	323	0.51	7.24843	9.245825	0.003096	0.965946
23.27542	26.32	323	0.51	7.24843	9.162136	0.003096	0.961997

Ethylene Adsorption on 13X Zeolite

Cor mean (s)	mean (s)	temp (K)	diam (cm)	int vel (cm/s)	Kp	1/temp (1/K)	log Kp
48.94093	51.02	473	0.51	10.61457	29.41203	0.002114	1.468525
48.79093	50.87	473	0.51	10.61457	29.32012	0.002114	1.467166
143.9752	146.3	423	0.51	9.492526	78.31985	0.002364	1.893872
144.4752	146.8	423	0.51	9.492526	78.59384	0.002364	1.895389
612.7635	615.4	373	0.51	8.370478	295.5204	0.002681	2.470587
611.9635	614.6	373	0.51	8.370478	295.1338	0.002681	2.470019
4359.955	4363	323	0.51	7.24843	1823.813	0.003096	3.26098
4361.955	4365	323	0.51	7.24843	1824.65	0.003096	3.26118

Methane Adsorption on CaX Zeolite

Cor mean (s)	mean (s)	temp (K)	diam (cm)	int vel (cm/s)	Kp	1/temp (1/K)	log Kp
7.45093	9.53	473	0.43	7.465794	2.633994	0.002114	0.420615
7.29093	9.37	473	0.43	7.465794	2.565035	0.002114	0.409093
10.13518	12.46	423	0.43	6.676598	3.329128	0.002364	0.522331
19.12354	21.76	373	0.43	5.887402	5.92227	0.002681	0.772488
18.42354	21.06	373	0.43	5.887402	5.68436	0.002681	0.754682
43.29542	46.34	323	0.43	5.098206	12.16511	0.003096	1.085116

Ethylene Adsorption on CaX Zeolite

Cor mean (s)	mean (s)	temp (K)	diam (cm)	int vel (cm/s)	Kp	1/temp (1/K)	log Kp
473.8419	478	473	0.43	7.465794	203.6441	0.002114	2.308872
232.8419	237	473	0.43	14.93159	200.128	0.002114	2.301308
24968.73	24974	373	0.43	5.887402	8485.596	0.002681	3.928682

Nitrogen / Clinoptilolite Isotherm

Temp =	303	K	Dead Vol =	1.56	cc
Length =	10	cm	Porosity =	0.67	
Diameter	0.43	cm			

% N2	Vol Flow (cc/min)	Int Vel (cm/s)	Raw Mean (s)	Cor Mean (s)	Kp	Integrand
0	15.31	4.874	1435	1428.886	403.2009	403.2009
0	15.31	4.874	1427	1420.886	400.9403	400.9403
0	15.31	4.874	1243	1236.886	348.9448	348.9448
0	15.46	4.921	1515	1508.946	429.9362	429.9362
0.02	15.62	4.972	245	239.0077	68.31802	69.70608
0.04	15.96	5.081	150.5	144.6353	42.02771	43.76624
0.075	15.46	4.921	99.9	93.84567	26.19525	28.29462
0.11	15.08	4.8	93.7	87.4931	23.76901	26.66931
0.155	15.71	5.001	73.5	67.54201	19.00385	22.43419
0.2	14.86	4.73	60.4	54.10121	14.25669	17.74511
0.21	14.93	4.753	64.18	57.91074	15.37862	19.38606
0.3	15.38	4.896	40.9	34.81417	9.302563	13.15952
0.37	15	4.775	35.8	29.56	7.603741	11.89148
0.47	14.71	4.683	29.8	23.43698	5.783606	10.64377
0.49	15.38	4.896	25.79	19.70417	5.013442	9.539162
0.6	15.38	4.896	21.73	15.64417	3.860972	9.19793
0.68	14.78	4.705	20.11	13.77712	3.178425	9.288704
0.78	14.85	4.727	16.11	9.80697	2.107934	8.507243
0.89	14.85	4.727	13.73	7.42697	1.455667	10.78179

CO / Clinoptilolite Isotherm

Temp =	303	K	Dead Vol =	1.56	cc
Length =	10	cm	Porosity =	0.67	
Diameter	0.43	cm			

% CO	Vol Flow (cc/min)	Int Vel (cm/s)	Raw Mean (s)	Cor Mean (s)	Kp'	Integrand
0	15.47	4.877	6328	22100	6248.375	6248.375
0.01	15.6	4.918	1074	1068	265	267.6755
0.03	16.19	5.104	449	443.2187	123	126.8001
0.04	16.17	5.097	279	273.2115	80.15785	83.49238
0.05	15.46	4.873	330.5	324.4457	91.08463	95.87177
0.08	16.94	5.34	166.4	160.8746	52.4	56.9453
0.1	15.91	5.015	167	161.1169	47.4	52.65233
0.12	15.06	4.747	153	146.7849	39.4	44.75514
0.13	15.21	4.796	116	109.8462	29.96425	34.4224
0.15	14.6	4.602	141	134.589	35.5	41.74194
0.2	15.42	4.861	91	84.92996	23.6	29.46775
0.27	15.13	4.769	62.5	56.31362	14.99074	20.48755
0.3	15.42	4.861	64.2	58.12996	15.7	22.37329
0.38	15.37	4.845	41.6	35.51021	9.4	15.08223
0.4	15.39	4.851	49.7	43.61813	11.3	18.74733
0.56	15.29	4.82	27.3	21.17835	5.81	13.04036
0.73	14.94	4.71	17.3	11.03494	2.55	9.095667
0.87	14.95	4.713	12.04	5.77913	0.98	6.675154

CO / N2 / Clinoptilolite Isotherm

Temp =	303	K	Dead Vol =	1.56	cc
Length =	10	cm	Porosity =	0.67	
Diameter =	0.43	cm			

Sample	% CO	Vol Flow (cc/min)	Int Vel (cm/s)	Raw Mean (s)	Cor Mean (s)	% N2	Kp'
CO	0	14.93	4.706	959	952.7307	1	259.367
CO	0	14.93	4.706	884	877.7307	1	238.9037
CO	0.01	15.03	4.738	793	786.7725	0.99	215.546
CO	0.02	15.29	4.82	533.6	527.4784	0.98	146.8258
CO	0.02	15.2	4.792	429	422.8421	0.98	116.8984
CO	0.02	15.2	4.792	556	549.8421	0.98	152.1829
CO	0.02	15.2	4.792	485	478.8421	0.98	132.4569
CO	0.02	15.2	4.792	504	497.8421	0.98	137.7357
CO	0.12	14.97	4.719	166	159.7475	0.88	43.12676
CO	0.2	15.47	4.877	111	104.9496	0.8	29.09557
CO	0.2	15.47	4.877	109	102.9496	0.8	28.53005
CO	0.36	15.67	4.94	71.9	65.9268	0.64	18.30237
CO	0.36	15.67	4.94	69.8	63.8268	0.64	17.7009
N2	0.36	15.67	4.94	80.1	74.1268	0.64	20.65093
N2	0.36	15.67	4.94	77.2	71.2268	0.64	19.82034
CO	0.48	16.35	5.154	55.1	49.37523	0.52	14.17443
CO	0.48	16.35	5.154	60.7	54.97523	0.52	15.84781
N2	0.48	16.35	5.154	69.7	63.97523	0.52	18.53717
N2	0.48	16.35	5.154	59.4	53.67523	0.52	15.45935
CO	0.66	16.04	5.056	51.9	46.06459	0.34	12.92342
CO	0.66	16.04	5.056	46.3	40.46459	0.34	11.28186
N2	0.66	16.04	5.056	52.7	46.86459	0.34	13.15793
N2	0.66	16.04	5.056	55.1	49.26459	0.34	13.86145
CO	0.72	16.45	5.186	42.3	36.61003	0.28	10.42788
N2	0.72	16.45	5.186	42.6	36.91003	0.28	10.51808
CO	0.9	15.04	4.741	31	24.7766	0.1	6.230642
N2	0.9	15.04	4.741	33.7	27.4766	0.1	6.972799
N2	1	13.68	4.312	30.5	23.65789	0	5.33471